

THE ASEAN JOURNAL OF RADIOLOGY

ISSN 0859 144X Volume XIX Number II May-August 2013



May-August 2013
Volume XIX Number II
ISSN 0859 144X

Published by

Royal College of Radiologists of Thailand

and

Radiological Society of Thailand

Bangkok, Thailand



THE ASEAN JOURNAL OF RADIOLOGY

May-August 2013, Volume XIX No.II



Letter from editorial board

On behalf of the editorial staffs of The Asean Journal of Radiology, I would like to express my appreciation to all authors and all peer reviewers for participating in our Asean Journal of Radiology. We encourage all members and readers to submit scientific works in all branches of Radiology, including original article of research works, article reviews, case reports and any innovations in related medical sciences. Your contributions and responses will help to promote our journal and our society. If you have any suggestions, please e-mail to us at thercrt@gmail.com

Anchalee Churojana, MD

Editor in Chief, Asean Journal of Radiology
Royal College of Radiologists of Thailand and
Radiological Society of Thailand

Contents

Original Articles

<p>1. A Comparison of Bone Scan Using between F-18 NaF PET/CT and Tc-99m MDP</p> <p style="text-align: right;">77-87</p> <table style="width: 100%; border-collapse: collapse;"> <tr> <td style="width: 50%;">Pawana Pusuwan</td> <td style="width: 50%;">Tawatchai Ekjeen</td> </tr> <tr> <td>Chiraporn Tocharoenchai</td> <td>Kobkun Maungsomboon</td> </tr> <tr> <td>Kanyalak Wiyaporn</td> <td>Chulalak Komoltri</td> </tr> <tr> <td>Ananya Ruangma</td> <td>Ruentip Tiparoj</td> </tr> </table> <p>2. Diagnostic Efficacy of CT/MR Imaging and Adrenal Vein Sampling for Localization of Aldosterone-producing Adrenal Adenomas in Primary Aldosteronism</p> <p style="text-align: right;">88-99</p> <table style="width: 100%; border-collapse: collapse;"> <tr> <td style="width: 50%;">Nontika Boontankan</td> <td style="width: 50%;">Kewalee Sasiwimonphan</td> </tr> </table> <p>3. Unsatisfactory Ultrasound-Guided Fine Needle Aspiration of Thyroid Nodule: Which Factors Limit Cytology Result?</p> <p style="text-align: right;">100-107</p> <table style="width: 100%; border-collapse: collapse;"> <tr> <td style="width: 50%;">Pratirop Poonotoke</td> <td style="width: 50%;"></td> </tr> </table> <p>4. Computed Tomography Analysis of the Ethmoid Roof: A Region at Risk in Endoscopic Sinus Injury</p> <p style="text-align: right;">108-115</p> <table style="width: 100%; border-collapse: collapse;"> <tr> <td style="width: 50%;">Pra Urusopone</td> <td style="width: 50%;"></td> </tr> </table>	Pawana Pusuwan	Tawatchai Ekjeen	Chiraporn Tocharoenchai	Kobkun Maungsomboon	Kanyalak Wiyaporn	Chulalak Komoltri	Ananya Ruangma	Ruentip Tiparoj	Nontika Boontankan	Kewalee Sasiwimonphan	Pratirop Poonotoke		Pra Urusopone		
Pawana Pusuwan	Tawatchai Ekjeen														
Chiraporn Tocharoenchai	Kobkun Maungsomboon														
Kanyalak Wiyaporn	Chulalak Komoltri														
Ananya Ruangma	Ruentip Tiparoj														
Nontika Boontankan	Kewalee Sasiwimonphan														
Pratirop Poonotoke															
Pra Urusopone															

Case Reports

<p>5. Two Case Reports of Madelung's Disease: CT Finding</p> <p style="text-align: right;">116-121</p> <table style="width: 100%; border-collapse: collapse;"> <tr> <td style="width: 50%;">Chanpen Buranachokpaisan</td> <td style="width: 50%;"></td> </tr> </table> <p>6. Cerebral Hemorrhage and Femoral Neck Fracture as Initial Presentations of Hepatocellular Carcinoma</p> <p style="text-align: right;">122-128</p> <table style="width: 100%; border-collapse: collapse;"> <tr> <td style="width: 50%;">Patanee O'Charoen</td> <td style="width: 50%;"></td> </tr> </table> <p>7. Reports of Four Cases of Hypertrophic Olivary Degeneration in King-Chulalongkorn Memorial Hospital from August 2010 to November 2011</p> <p style="text-align: right;">129-142</p> <table style="width: 100%; border-collapse: collapse;"> <tr> <td style="width: 50%;">Pra Urusopone</td> <td style="width: 50%;">Sasitorn Petcharunpaisan</td> </tr> <tr> <td>Sukalaya Lerdlum</td> <td></td> </tr> </table>	Chanpen Buranachokpaisan		Patanee O'Charoen		Pra Urusopone	Sasitorn Petcharunpaisan	Sukalaya Lerdlum		
Chanpen Buranachokpaisan									
Patanee O'Charoen									
Pra Urusopone	Sasitorn Petcharunpaisan								
Sukalaya Lerdlum									

8. Blunt Traumatic Diaphragmatic Hernia: Case Report	143-147
Siwipan Changtham	
9. Tumefactive Multiple Sclerosis Clinically Mimicking Acute Stroke and Lesional Migration Along the Biopsy Tract: A Case Report	148-153
Oranan Tritanon	Arunee Singhsnaeh
Jiraporn Laothamatus	Atthaporn Boongird
Disya Ratanakorn	Prawat Nitayanant
10. Reversible Cerebral Vasoconstriction Syndrome: A Commonly Missed Diagnosis in Acute Severe Headaches	154-163
Siriporn Hirunpat	Nuttha Sanghan
Adchara Wan-ai	Natee Ina
Pornrujee Hirunpat	
11. Kartagener's Syndrome: A Case Report in the Samutsakhon Hospital	164-170
Luckana Girapongsa	Thanapat Puangpatch
Orawan Autravisitkul	Pariyanoot Deesuwun
The Committee of Royal College of Radiologists of Thailand and Radiological Society of Thailand: Apr 2013-Mar 2015	171
The Journal of the Royal College of Radiologists & Radiological Society of Thailand (2013 - 2015)	172
Instructions for Authors	173



Original Article

A Comparison of Bone Scan Using between F-18 NaF PET/CT and Tc-99m MDP

**Pawana Pusuwan, MD¹, Tawatchai Ekjeen, MSc², Chiraporn Tocharoenchai, PhD²,
Kobkun Maungsomboon, MD¹, Kanyalak Wiyaporn, MSc², Chulalak Komoltri, PhD³,
Ananya Ruangma, PhD⁴, Ruentip Tiparoj, MSc¹.**

¹ Department of Radiology, Faculty of Medicine Siriraj Hospital, Mahidol University, Bangkok, Thailand

² Department of Radiological Technology, Faculty of Medical Technology, Mahidol University, Bangkok, Thailand

³ Department of Research Development, Faculty of Medicine Siriraj Hospital, Mahidol University, Bangkok, Thailand

⁴ Oncology Imaging & Nuclear Medicine Department, Wattanosoth Hospital, Bangkok Hospital Group, Bangkok, Thailand

Abstract

Objective: To study bone scintigraphy using between F-18 NaF PET/CT and Tc-99m MDP scan for detecting bone metastases.

Material and Methods: Thirteen patients (5 males, mean age 55.4 years, range 34-74 years) who were suspected bone metastases with single or two equivocal lesions on Tc-99m MDP bone scan were recruited between October 2010 and October 2012. All these patients underwent F-18 NaF PET/CT scan within one week after Tc-99m MDP bone scan. The sensitivity, specificity and accuracy of Tc-99m MDP bone scan and F-18 NaF PET/CT in differentiating metastatic bone lesion from benign lesion by patient-based and lesion-based analyses were studied.

Results: F-18 NaF PET/CT could identify all seven patients with malignant bone metastases that Tc-99m MDP bone scan was interpreted as malignancy in only three patients (42.9%) and equivocal in the rest of these patients. For lesion-based analysis of the overall 75 lesions, the sensitivity, specificity and accuracy of Tc-99m MDP bone scan were 48%, 83.3% and 70.7% and F-18 NaF PET/CT were 100% for all parameters. Besides the ability of F-18 NaF PET/CT to accurately identify malignancy from benign lesion, unenhanced CT portion of PET/CT can show extra-osseous findings that may change patient management.

Conclusion: F-18 NaF PET/CT provides an excellent bone image quality and higher accuracy than Tc-99m MDP bone scan. Then F-18 NaF PET/CT is a good choice for evaluating bone metastases.

Keywords: Bone scan, F-18 NaF PET/CT, Tc-99m MDP, bone metastases.

Correspondence to: Pusuwan P. Division of Nuclear Medicine, Department of Radiology, Faculty of Medicine Siriraj Hospital, Mahidol University, 2 Prannok Road, Bangkoknoi, Bangkok 10700, Thailand.

Phone: 0-2419-6220-1, Fax: 0-2412-7165 E-mail: pawana.pus@mahidol.ac.th

Introduction

Bone metastases are the most common malignant bone tumor and occur in 30%-70% of all cancer patients⁽¹⁾. In 1971, Subramanian and McAfee developed Tc-99m MDP for bone imaging and this technique has been the method of choice for routine skeletal surveys^(2,3). Although F-18 NaF (511 keV; half-life, 110 minutes) was introduced as a radiopharmaceutical for bone imaging by Blau et al in 1962, the image quality of a gamma camera was poor because it performed best at lower energy levels^(4,5). In the early 1990s, Phelps et al used F-18 NaF as a model for the development of whole body PET because of the favorable skeletal kinetics of F-18 NaF⁽⁶⁾.

For the past few years, there was a problem with Tc-99m shortage that affected nuclear medicine services around the world. Reimbursement for F-18 NaF was approved by Centers for Medicare and Medicaid Services and many nuclear medicine centers in the USA started to use this radiopharmaceutical for routine PET bone scan.

The aim of this study was to prospectively compare the detection of bone metastases by Tc-99m MDP planar bone scan and F-18 NaF PET/CT in patients with a known primary tumor.

Materials and Methods

Subjects

Descriptive prospective study was performed at Division of Nuclear Medicine, Faculty of Medicine Siriraj Hospital between October 2010 and October 2012. Thirteen patients (5 male and 8 female; mean age 55.4±10.6 years; range 34-74 years) were referred for evaluation of suspected (11 patients) or progression (2 patients) of bone metastases in the course of the disease. The patients had various

oncologic diseases including cancer of the breast (n = 6) and one patient in each of the following cancers of thyroid, prostate, ovary, colon, pyriform sinus, kidney and nasopharynx. The study was approved by the Siriraj Ethics Committee for Human Experiment and a written informed consent was obtained from each subject.

Planar whole body bone images were performed 3 hours after intravenous injection of 20 mCi Tc-99m MDP using a dual-head gamma camera (Infinia Hawk Eye: GE Healthcare). F-18 NaF PET/CT study was studied within 1 week after Tc-99m MDP bone scan. Imaging was performed 60 minutes after intravenous injection of 10 mCi F-18 NaF using a Discovery PET/CT system (GE Healthcare). Low-dose CT acquisition was performed first with 140 kV, 80 mA, 0.8 seconds per CT rotation, a pitch of 6 and a table speed of 22.5 mm/second. A PET emission scan was performed immediately after acquisition of the CT without changing patient's positioning. Five to 7 bed positions were performed with an acquisition time of 3 minutes per bed from skull to midthigh. PET images were reconstructed using an ordered-subsets expectation maximization algorithm. CT data were used for attenuation correction. Studies were interpreted on a Xeleris workstation.

Image interpretation

Whole body bone scan and F-18 NaF PET/CT were interpreted blindly and separately. Interpretation of PET/CT was done as a consensus reading of a nuclear medicine physician and a radiologist. Each area of abnormal increased uptake of Tc-99m MDP or F-18 NaF was categorized as normal, benign, equivocal or malignant. Lesions on bone scan were classified as benign when they appeared as

hot osteophytes or located around joints. Vertebral lesions were categorized as malignant when they involved the posterior aspect of the vertebral body and pedicle or involved the vertebra extensively⁽⁷⁾. Rib lesions were considered malignant when they appeared as elongated uptake. When they involved vertically several ribs, they were categorized as benign. CT data of PET/CT were used to categorize as benign when they appeared at the corresponding areas as degenerative changes, fractures or benign bone lesions. The osteoblastic metastases were classified as malignancy. Lesions not classified as benign or malignant were categorized as equivocal. Lesions on F-18 NaF PET/CT that were not visible on bone scan were classified as normal on bone scan. Patients were monitored for 6 months and the final diagnosis was concluded from their medical records.

Statistical analysis

Both patient-based and lesion-based analyses were performed. The sensitivity, specificity, accuracy, positive predictive value and negative predictive value with 95% confidence intervals were

analyzed for the diagnosis of bone metastases from benign lesion.

Results

Patient-based analysis

From 13 patients, seven patients (53.8%) had bone metastases according to definite F-18 NaF PET/CT findings and follow-up imaging. A lesion with abnormal increased uptake on F-18 NaF PET scan was identified as bony metastasis if CT data of the corresponding area also showed osteoblastic metastasis. Thus F-18 NaF PET/CT could identify all 7 patients with malignant bone metastases. The rest of patients had benign bone lesions which were determined by benign findings at the corresponding location on CT part of F-18 NaF PET/CT. Follow-up for at least 6 months of these patients with benign bone lesions had no clinical or imaging evidence of bone metastasis.

In 7 patients with bone metastases on F-18 NaF PET/CT, Tc-99m MDP bone scan was interpreted as equivocal (n=4; 57.1%) and malignancy (n=3; 42.9%) (Table 1). In 6 patients with benign PET/CT findings, planar bone scan was interpreted

Table 1 Assessment of bone metastases by Tc-99m MDP planar bone scan (BS) and F-18 NaF PET/CT (PET/CT) in 13 patients

Modality	Final diagnosis						
	Bone metastases (n=7)			No bone metastases (n=6)			
	Metastases	Equivocal	Benign	Metastases	Equivocal	Benign	
BS	3	4	0	0	3	3	
PET/CT	7	0	0	0	0	6	

Table 2 Location and diagnosis of 74 lesions seen on F-18 NaF PET/CT

Site of increased F-18 NaF uptake	Number of lesions	Diagnosis	
		Malignant	Benign
Skull	5	1	4
Spine	30	4	25
Thorax	17	10	6
Pelvis	15	9	7
Long bones	8	2	6
Total	75	27 (36%)	48 (64%)

as equivocal (n=3; 50%) and benign lesion. Among 7 patients with equivocal results on planar bone scan, PET/CT accurately identified the presence of bony metastases in 4 patients (57.1%) and excluded bone metastases in 3 patients (42.9%).

Lesion-based analysis

Seventy-five lesions with increased F-18 NaF uptake were studied. Location and final diagnosis of these lesions were shown in Table 2. Twenty-seven lesions (36%) showed osteoblastic metastases on the CT part of the PET/CT images. Forty-eight lesions (64%) showed benign abnormalities on the CT part in the corresponding location with increased F-18 NaF uptake.

In 27 bone metastatic lesions on PET/CT, bone scan was interpreted as benign/normal (n=14; 51.9%), equivocal (n=8; 29.6%) and malignancy (n=5; 18.5%) (Table 3). In 48 benign bone lesions on PET/CT findings, bone scan was interpreted as benign/normal (n=40; 83.3%), equivocal (n=7; 14.6%) and malignancy (n=1; 2.1%). Among 15 equivocal lesions on bone scan, PET/CT accurately confirmed

the presence of bony metastases in 8 lesions (53.3%) and excluded bone metastases in 7 lesions (46.7%). There were 3 equivocal lesions on bone scan that PET/CT demonstrated no abnormality in one lesion (Fig 1) and extra-osseous abnormalities in 2 lesions (Fig 2).

Additional extra-osseous findings on unenhanced CT images of F-18 NaF PET/CT scan

The unenhanced CT images of F-18 NaF PET/CT scan were analyzed. From 13 patients, 6 patients (46.2%) showed additional extra-osseous findings which four of them were previously known before their participation in this study (Table 4). The other two patients showed clinically significant new extra-osseous findings. In one patient, there was progression of right mastoiditis (patient no. 2) while the other patient (patient no. 4) showed multiple new abnormal lesions as followed: a mass in descending colon with pericolic nodes, a nodule at right peri-renal and right buttock and a mass at left lateral aspect of urinary bladder (Fig 2).

Table 3 Assessment of bone metastases by Tc-99m MDP bone scan (BS) and F-18 NaF PET/CT (PET/CT) (lesion-based)

		Diagnosis		Sensitivity(%)	Specificity(%)	Accuracy(%)	PPV(%)	NPV(%)
		Malignant	Benign	(95% CI)	(95% CI)	(95% CI)	(95% CI)	(95% CI)
BS	+	13	8	48.1	83.3	70.7	61.9	74.1
	-	14	40	(28.7, 68.1)	(69.8, 92.5)	(59.0, 80.6)	(38.4, 81.9)	(60.4, 85.0)
PET/CT	+	27	0	100	100	100	100	100
	-	0	48	(87.2, 100)	(92.6, 100)	(95.2, 100)	(87.2, 100)	(92.6, 100)

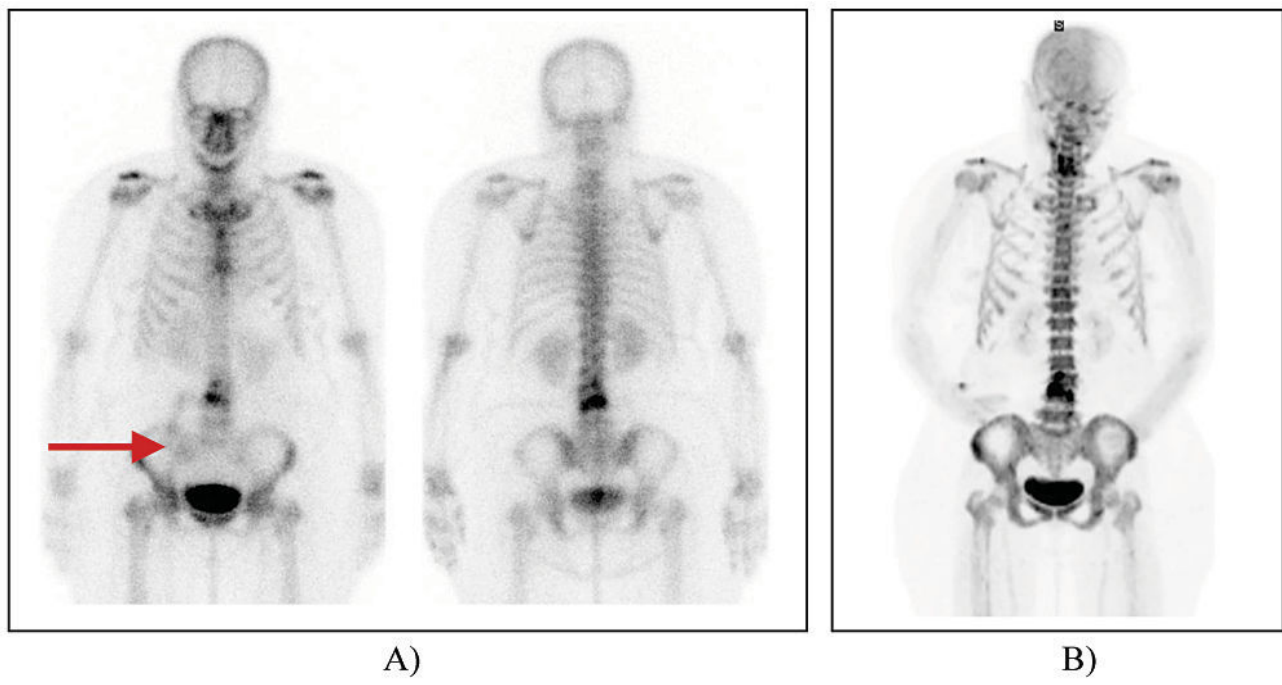


Fig 1 A) Planar bone scan anterior and posterior show equivocal lesion at right iliac bone (arrow) from artifact as compared with normal appearance on F-18 NaF PET (B).

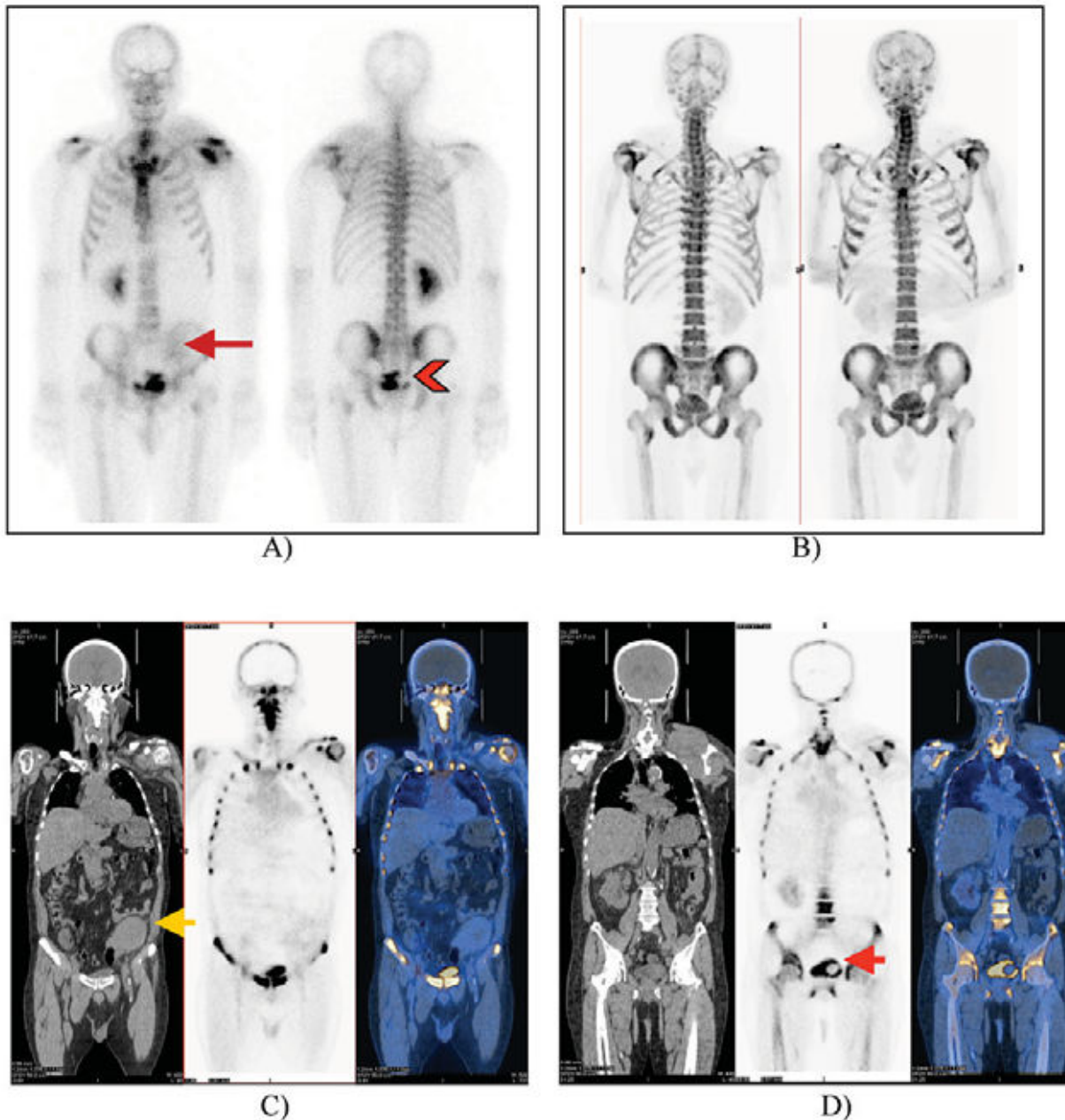


Fig 2 A) Anterior and posterior planar bone scan show two equivocal lesions at left iliac bone (arrow) and sacrum (arrow head) B) PET/CT clearly demonstrated false-positive lesions from C) colonic mass in the left lower abdomen superimposed left iliac bone (arrow) and D) recurrent mass in left lateral aspect of urinary bladder (arrow) mimics lesion in sacrum.

Table 4 Additional extra-osseous findings on unenhanced CT of F-18 NaF PET/CT

Patient no.	Age (years)	Sex	Type of cancer	Incidental findings on CT
1	48	M	Cancer of pyriform sinus	- A large mass at right oropharynx - Cervical metastatic lymph nodes - Active chronic lung disease
2	54	M	Naopharyngeal cancer	- Right mastoiditis
3	65	F	Thyroid cancer	- Pulmonary nodule and right paratracheal node
4	57	M	Renal carcinoma	- Pulmonary metastases - Mediastinal and abdominal lymphadenopathy - A mass in descending colon with pericolic nodes - A nodule at right perirenal and right buttock - A mass at left lateral aspect of urinary bladder
5	49	F	Breast cancer	- Atelectasis and pleural thickening post radiation fibrosis with pulmonary metastases
6	49	F	Breast cancer	- Right pleural mass and effusion

Discussion

Tc-99m MDP bone scan is a well-accepted imaging for the detection of bone metastases due to its high sensitivity and cost-effectiveness but its main drawback is lack of specificity⁽⁸⁾. The uptake mechanism of F-18 NaF in the skeleton is dependent on regional blood flow and new bone formation resembles that of Tc-99m MDP but has better pharmacokinetic characteristics including faster blood clearance and twice higher uptake in the bone⁽⁹⁾. At the beginning, imaging of 511-keV annihilation photons produced by the decay of F-18 was not suitable by gamma-camera but the use of PET/CT machine has significantly improved the specificity of F-18 NaF imaging as the CT component can demonstrate morphologic characterization of abnormal uptake and accurately differentiate between benign and metastatic lesion^(9,10).

In this study, most of the equivocal lesions on planar bone scan were found in ribs (n = 6). Four patients in this group have their rib lesions as a single bone scan abnormality. This is an especially difficult group which was found around 7% of patients with bone metastases⁽¹¹⁾. The probability of a malignant cause for a solitary increased uptake in patients with a known primary cancer varies with the site of the abnormality on bone scan. Tumeh et al reported that solitary rib lesions were rare in cancer patient and were usually due to benign disease⁽¹²⁾. McNeil estimated the frequency of a malignant cancer in a solitary rib lesions vary between 1% and 17%⁽¹³⁾. In our four patients with a single rib abnormality, three patients had rib fracture and only one patient had osteoblastic bony metastasis. The rest of equivocal ribs on bone scan (n = 2) were osteoblastic bony metastases. Other equivocal lesions on bone scan were found in the spines

(n = 5), pelvis (n = 3) and skull (n = 1). Two lesions in lumbar spines were degenerative changes as clearly demonstrated on CT part of PET/CT (Fig 3). These two lesions were confirmed on follow-up MRI scan. Bony destruction was clearly identified in other three equivocal spine lesions on CT part of PET/CT (Fig 4). All three equivocal lesions in the pelvis were false-positive which were clearly identified on CT part of PET/CT as shown in Fig 1 and Fig 2. Therefore all equivocal bone scan abnormalities should be correlated with the results of other more specific investigations. In clinical practice, a radiograph of the area showing abnormal uptake should be obtained. If standard radiographs were normal, CT of bone can be used in evaluating the significance of a scan abnormality^(14,15). Thus the use of hybrid PET/CT or SPECT/CT systems can significantly improved the specificity of bone imaging by the combination of cross-sectional functional and anatomic imaging for definite diagnosis.

This study showed that the sensitivity, specificity, accuracy, positive predictive value and negative predictive value of Tc-99m MDP bone scan were 48%, 83.3%, 70.7%, 61.9% and 70.7%, respectively and F-18 NaF PET/CT were 100% for all parameters. The similar result were published by Even-Sapir, et al who reported the sensitivity, specificity, positive predictive value and negative predictive value of Tc-99m MDP bone scan of 70%, 57%, 64%, and 55% and F-18 NaF PET/CT of 100% for all parameters⁽⁷⁾. Besides the ability of F-18 NaF PET/CT to accurately identify malignancy from benign lesion, unenhanced CT portion of PET/CT can show extra-osseous findings that may change patient management.

Many research showed that NaF-18 bone scan with PET/CT has undoubtedly superiority than Tc-

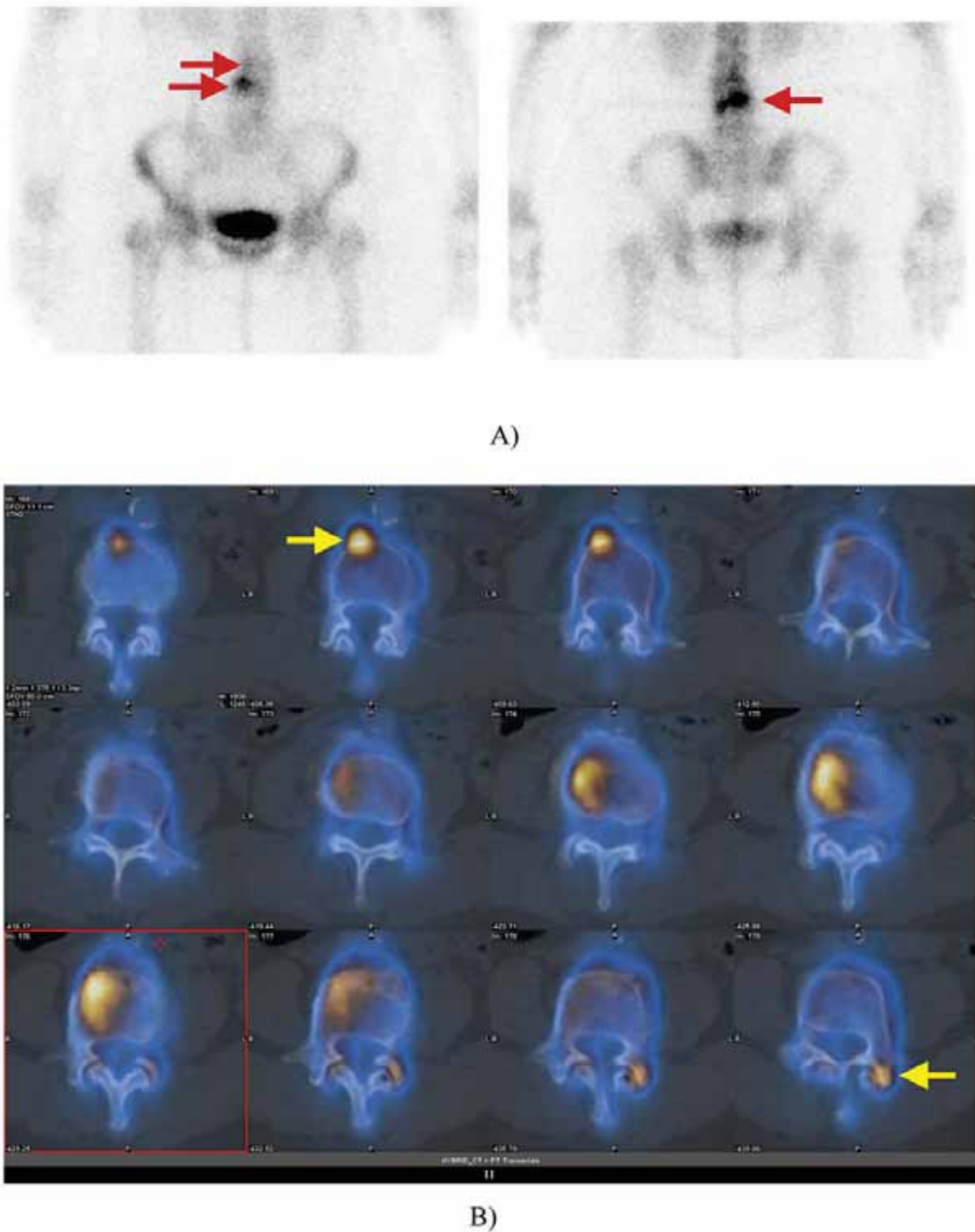


Fig 3 A) Anterior and posterior spot images of Tc-99m bone scan show increased radioactivity uptake at L3 and L4 (arrows) B) Fusion PET/CT image shows degenerative change at L3 and L4 (arrow)

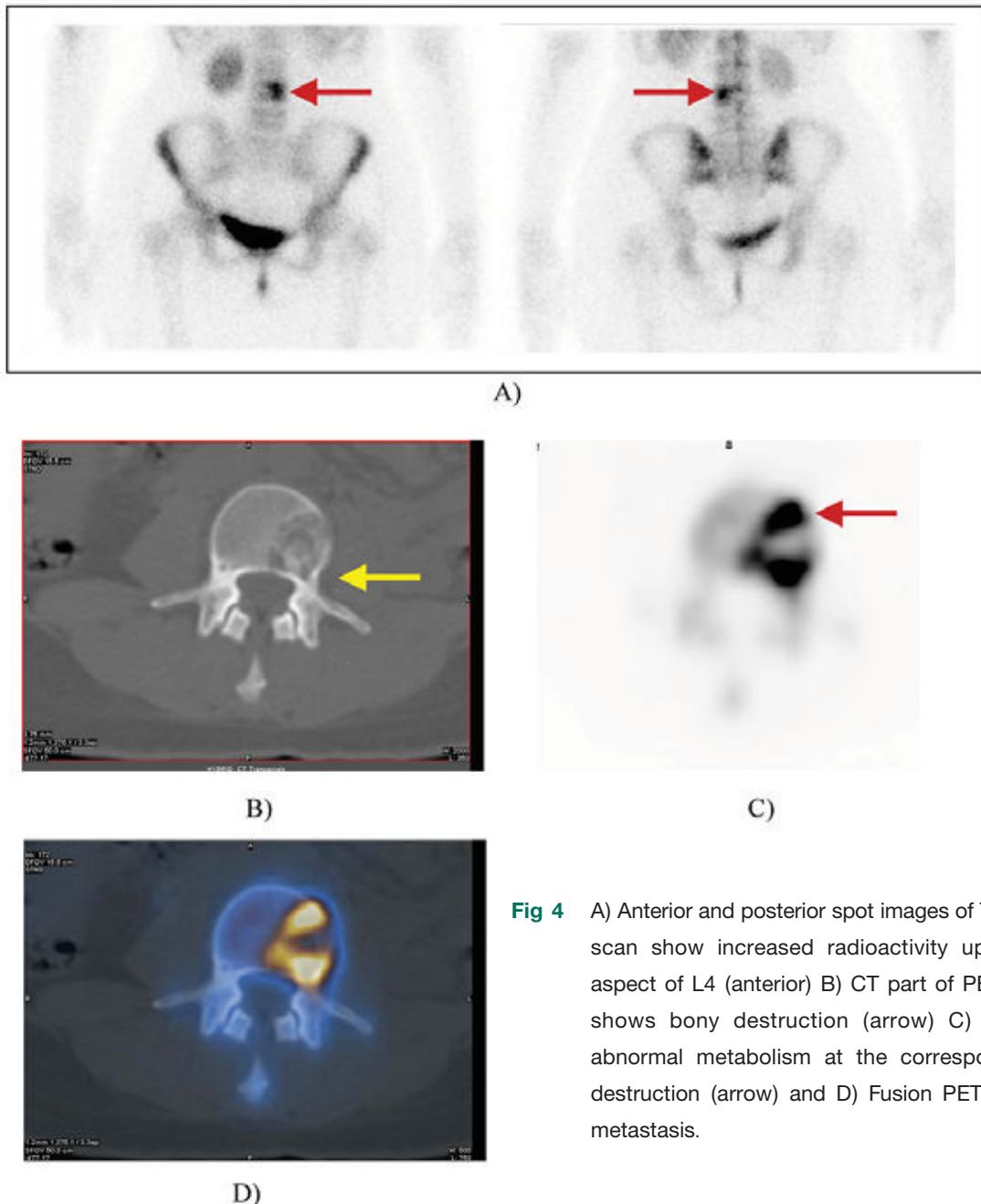


Fig 4 A) Anterior and posterior spot images of Tc-99m bone scan show increased radioactivity uptake at left aspect of L4 (anterior) B) CT part of PET/CT image shows bony destruction (arrow) C) PET shows abnormal metabolism at the corresponding bony destruction (arrow) and D) Fusion PET/CT of bony metastasis.

99m MDP with gamma camera and similarly to this study. At present, PET/CT seems to be underused in Thailand due to the cost of the study. Bone imaging with NaF-18 PET/CT may be a good option for the patient who can afford the cost but rewarding in terms of higher accuracy in identifying malignancy. This study would like to introduce the new option for bone metastases imaging.

Conclusion

Tc-99m MDP bone scan is good for screening abnormal bone lesions but specificity is poor while F-18 NaF PET/CT is superb in characterization of abnormal bone lesions. Even though the cost of PET/CT is relatively high, higher accuracy in identifying malignancy is rewarded. Then F-18 NaF PET/CT is a good choice for evaluating bone metastases.

Acknowledgements

This study is supported by Siriraj Grant for Research Development and Medical Education, Faculty of Medicine Siriraj Hospital, Mahidol University and the Grant of Strategic Scholarships for Frontier Research Network for the Ph.D. Program from the Office of the Higher Education Commission, Thailand. The author Pawana Pusuwan is supported by "Chalermphrakiat" Grant, Faculty of Medicine Siriraj Hospital, Mahidol University.

References

- Even-Sapir E. Imaging of malignant bone involvement by morphologic, scintigraphic, and hybrid modalities. *J Nucl Med* 2005;46:1356-67.
- Subramanian G, McAfee JG. A new complex of Tc-99m for skeletal imaging. *Radiology* 1971;99:192-6.
- Schirrmeister H, Guhlmann A, Elsner K, Kotzerke J, Glatting G, Rentschler M, et al. Sensitivity in detecting osseous lesions depends on anatomic localization: Planar bone scintigraphy versus 18F PET. *J Nucl Med* 1999;40:1623-9.
- Blau M, Nagler W, Bender MA. A new isotope for bone scanning. *J Nucl Med* 1962;3:332-4.
- Bridges RL, Wiley CR, Christian JC, Strohm AP. An introduction to Na18F bone scintigraphy: basic principles, advanced imaging concepts, and case examples. *J Nucl Med Technol* 2007;35:64-76.
- Grant FD, Fahey FH, Packard AB, Davis RT, Alavi A, Treves TS. Skeletal PET with 18F-fluoride: Applying new technology to an old tracer. *J Nucl Med* 2008;49:68-78.
- Even-Sapir E, Metser U, Mishani E, Lievshitz G, Lernan H, Leibovitch I. The detection of bone metastases in patients with high-risk prostate cancer: 99mTc-MDP planar bone scintigraphy, single- and multi-field-of-view SPECT, 18F-fluoride PET, and 18F-fluoride PET/CT. *J Nucl Med* 2006;47:287-97.
- Chua S, Gnanasegaran G, Cook GJR. Miscellaneous cancer (lung, thyroid, renal cancer, myeloma, and neuroendocrine tumors): role of SPECT and PET in imaging bone metastases. *Semin Nucl Med* 2009;39:416-30.
- Segall G, Delbeke D, Stabin MG, Even-Sapir E, Fair J, Sajdak R, et al. SNM practice guideline for sodium 18F-fluoride PET/CT bone scan 1.0. *J Nucl Med* 2010;51:1813-20.
- Chen CJ, Ma SY. Prevalence of clinically significant extraosseous findings on unenhanced CT portions of 18F-fluoride PET/CT bone scan. *The scientific World Journal* [Online]. 2012 [cited 2012 Dec 5]; Available from: <http://www.hindawi.com/journals/tswj/2012/979867.pdf>.
- Mckillop JH. Bone scanning in metastatic disease. In: Fogelman I, editor. *Bone scanning in clinical practice*. London: Springer-Verlag; 1987, p. 41-60.
- Tumeh SS, Beadle G, Kaplan WD. Clinical significance of solitary rib lesions in patients with extraskeletal malignancy. *J Nucl Med* 1985;26:1140-3.
- McNeil BJ. Value of bone scanning and malignant disease. *Semin Nucl Med* 1984;14:277-86.
- Durning P, Best JJK, Sellwood RA. Recognition of metastatic bone disease in cancer of the breast by computed tomography. *Clin Oncol* 1983;9:943-6.
- Muindi J, Coombes RC, Golding S, Parboo TJ, Khan O, Husband J. The role of computed tomography in the detection of bone metastases in breast cancer patients. *Br J Radiol* 1983;56:233-6.



Diagnostic Efficacy of CT/MR Imaging and Adrenal Vein Sampling for Localization of Aldosterone-producing Adrenal Adenomas in Primary Aldosteronism

Nontika Boontakan, MD., Kewalee Sasiwimonphan, MD.

*Division of Diagnostic Radiology, Department of Radiology, King Chulalongkorn Memorial Hospital,
Thai Red Cross Society, Faculty of Medicine, Chulalongkorn University*

Abstract

Objective: To test the sensitivity, specificity, accuracy, positive predictive value (PPV) and negative predictive value (NPV) of CT/MR imaging and adrenal vein sampling (AVS) for diagnosis of aldosterone-producing adrenal adenoma (APA).

Material and method: Retrospective study of 14 patients with primary hyperaldosteronism (PAL) who underwent both CT/MR imaging and AVS between June 2007 and June 2012 were performed. The study included 7 male and 7 female patients. Review CT/MR findings of these cases and compared with AVS results were done.

Results: Five of fourteen patients (35%) had unilateral adrenal nodules on CT, and one of fourteen patients (7.1%) had bilateral adrenal nodules on CT[D1]. The remaining eight patients had no significant nodules in both adrenal glands.

Among 5 patients who had unilateral adrenal nodule detected from CT, 4 patients (80%) with nodule greater than 10 mm also presented with lateralization from AVS and finally pathological proven APA. The last patient with unilateral nodule showed small size less than 10 mm and had AVS results of bilateral lesion. Medical therapy was applied for this patient instead of surgical treatment.

In other group (8 of 14 patients, 57.1%), there was no significant nodule from CT or MRI and AVS results indicated bilateral lesions in two patients (25%). The rest of six patients found unilateral lesion on AVS which underwent adrenalectomy and histological revealed adrenal hyperplasia of all cases. Two of six patients concluded to be primary adrenal hyperplasia (PAH) or unilateral adrenal hyperplasia (UAH), which showed clinical cure after adrenalectomy. The remaining four patients who showed no improvement of hypertension after adrenalectomy concluded to be bilateral adrenal hyperplasia (BAH).

The sensitivity, specificity, accuracy, PPV and NPV for detected adrenal adenoma by CT/MRI of our study were 66.67%, 87.50%, 78.57%, 80.00%, and 77.78%, respectively. The sensitivity, specificity, accuracy, PPV and NPV for detected adrenal adenoma by AVS at cut point AVS ratio at 2 were 100%, 50%, 71.43%, 60% and 100%, respectively.

Conclusion: In patient with suspected PAL who presented with unilateral adrenal nodule at least 10 mm in size detected by CT, these patient should be referred for adrenalectomy without need to performing AVS. The differentiation of subtype in patients with PAL is most reliably achieved with AVS which may reserve for patient who had no significant adrenal nodule from CT/MRI.

Contact: kewalees@hotmail.com

Keywords: Primary aldosteronism, aldosterone-producing adenoma, bilateral adrenal hyperplasia, unilateral adrenal hyperplasia, computed tomography, magnetic resonance imaging, adrenal venous sampling.

Introduction

Primary aldosteronism (PAL) is defined as secondary hypertension accompanied by aldosterone hypersecretion leading to suppressed plasma renin, resulting in hypertension and usually hypokalemia. It is accounted for 3-15% of all hypertensive patients⁽¹⁾. Two most common causes of PAL include aldosterone-producing adrenal adenoma (APA, or Conn's syndrome) and bilateral adrenal hyperplasia (BAH) which account for over 95% of all cases⁽²⁾. It is important to differentiate between APA and BAH because of different in treatment techniques. APA should be treated surgically, whereas bilateral adrenal hyperplasia is best managed medically⁽³⁾. The rare entity of PAL is primary adrenal hyperplasia (PAH) or unilateral adrenal hyperplasia (UAH) which physiologically and biochemically mimics APA and also still has benefit from surgery⁽⁴⁾.

Several techniques have been used as the pre-operative identification of unilateral disease including APA and PAH, included computed tomography, MR imaging and adrenal venous sampling.

Computed tomography (CT) is the modality of choice for the detection of APA. It is a fast, easily accessible and non-invasive investigation with sensitivity, specificity and accuracy varying from 53-100%, 33-100% and 37-86%, respectively. The CT characteristics of adrenal adenoma is low density on CT scan (<10 Hounsfield units) due to high intracellular lipid content⁽²⁾. Many studies employ CT attenuation and washout value to differentiate adrenal adenoma and non adenoma⁽⁵⁾. However, up to 20% of APA has been reported as being smaller than 1 cm and CT scan might miss these nodules. In contrast, CT scan may indentify a non secreting nodule in patients with BAH as an APA⁽⁶⁾.

Magnetic resonance imaging (MRI) has the

advantage of superior soft-tissue contrast resolution and lack of ionizing radiation. Disadvantages include higher cost, longer scanning time, poorer spatial resolution compared with CT⁽²⁾. Chemical shift imaging quantitatively assesses lipid content in tissue that has close relationship between lipid content and the functional aspect of adrenocortical lesions. It has been suggested that chemical shift image may enable better differentiation between APAs and nonfunctional adenomas from MRI than Hounsfield unit measurement from CT scan⁽⁷⁾. However, some studies⁽⁸⁾ suggested that chemical shift imaging could not help in the differentiation among functional and non functional adrenal adenoma, because both were found to contain lipid without significant differences in appearance⁽²⁾. Adrenal vein sampling (AVS) was initially described in 1967 to aid determination of the sub-type of primary aldosteronism and to differentiate between unilateral and bilateral production of aldosterone, with sensitivity approaching 100%^(1,2). However, this procedure is invasive, difficult technique especially the right renal vein catheterization and this procedure also requires long fluoroscopy time, which exposes patient to high radiation exposure. The success rate depends on the angiographer's experience and failure rate is as high as 30%⁽⁹⁾. And there are reported complications of AVS such as venous extravasations, hemorrhage and adrenal vein thrombosis⁽²⁾.

Aim of this study is try to compare efficacy of CT and/or MRI and AVS in differentiation of PAL.

Material and Methods

Retrospective analysis of all patients with secondary hypertension who were biochemically suspected to be PAL and underwent both CT/MR imaging and adrenal vein sampling in our hospital

from June 2007 to June 2012. Five patients were excluded from the study due to failure to identify right adrenal vein and three patients were excluded due to unavailability of CT or MRI. Total fourteen patients were included in this study.

Computed tomography was performed in all cases with standard, contiguous 5 mm slice thickness obtained using 16-channel (Sensation16, Siemens, Cleveland, OH) and 320-channel (Aquilion One Dynamic Volume CT, Toshiba Medical System, Tochigi-ken, Japan) CT scanners. All cases had pre contrast and post contrast enhanced CT imaging of adrenal glands. Two-mm slice thickness was generated in most of cases. Pre contrast studies were reviewed in which low density (<10 Hounsfield units) nodule indicated lipid rich adenoma. If adrenal adenoma was not diagnosed with pre contrast CT, contrast enhanced CT would be used to determine their enhancement. If relative washout value is more than 40% or absolute washout value is more than 60%, lipid poor adrenal adenoma is suggested. Morphology of both adrenal glands were analyzed and described as "normal" if the adrenal glands were normal, "plump" if its edges lose concavity and "nodule" if a circular adrenal lesion was detected. Size of nodule was recorded in millimeter (mm). A macronodule was a nodule that size is at least 10 mm.

One case underwent MR imaging for adrenal gland using 3 Tesla system (Achieva 3T, Philips Medical System, Best, the Netherlands) generally consists of axial T1 gradient echo in-phase and out-of-phase and axial T2-weighted with fat suppression sequences. Chemical shift imaging sequence was used to differentiate adrenal mass.

AVS was performed in all cases. Blood samples were obtained from bilateral adrenal veins and infe-

rior vena cava (IVC) for cortisol and aldosterone measurements. Successful AVS was determined by at least double elevation in adrenal vein cortisol levels compared with IVC level. Lateralization criteria or unilateral aldosterone hypersecretion were defined as followed (1) the ratio of adrenal vein aldosterone concentration to the homolateral cortisol concentration on the side with higher ratio over the contralateral aldosterone to cortisol ratio (AVS ratio) was greater than 2. (2) The aldosterone/cortisol (A/C) ratio of the non-dominant adrenal vein was less than that of the IVC⁽¹⁰⁾.

Definition of primary aldosteronism sub-type

1. Aldosterone-producing adenoma (APA) was defined by concordant results between the unilateral adrenal nodule detected by CT or MRI and lateralized aldosterone production as assessed by AVS which are finally pathological proven.
2. Primary adrenal hyperplasia (PAH)/Unilateral adrenal hyperplasia (UAH) was defined by normal, unilateral or bilateral plump on CT, and lateralized aldosterone production as assessed by AVS.
3. Bilateral adrenal hyperplasia (BAH) was defined by normal or bilateral CT abnormalities and bilateral aldosterone secretion or unilateral aldosterone secretion on AVS that clinical is not improvement after adrenalectomy⁽¹²⁾.

A final diagnosis of APA and PAH/UAH was considered proven, providing that all the following conditions were satisfied:

- 1) Histological proven of adenoma
- 2) Normalization of hypokalemia if present
- 3) Cure or improvement of hypertension. Cure of hypertension was defined as normal blood pressure level without treatment; improvement was defined as achievement of normal blood pressure with

a reduced number of drugs, compared with the number before adrenalectomy.

Patient characteristics were reported descriptive analysis. Efficacy of CT/MRI and AVS were evaluated and reported as sensitivity, specificity, accuracy, NPV and PPV.

Results

The medical records of 14 included patients were reviewed. There are 7 men and 7 women with mean age of 58 years for men (43-69 years) and 43 years for women (13-65 years).

Five of 14 patients (35%) had unilateral adrenal nodules on CT, and one of fourteen patients (7.1%) had bilateral adrenal nodules on CT. The remaining patients had no significant nodules in both adrenal glands (Fig 1).

In five patients who had unilateral adrenal nodules on CT, 4 patients (80%) had nodule greater than 10 mm and also had lateralization from AVS. These patients underwent adrenalectomy, which were pathological proven adrenal adenoma. Two of them had unilateral lipid rich adenoma (Fig 2). Other two had unilateral lipid poor adenoma. The last patient in this group who had unilateral nodule less than 10 mm from CT, AVS result indicates bilateral lesions (Fig 3). Medical therapy was applied for this patient instead of surgical treatment.

In other 8 patients (57.1%) which CT scan/MRI showed no detectable nodule, 2/8 patients had AVS result of bilateral diseases and received medical therapy with clinical improvement later. The other six patients found unilateral disease on AVS which underwent adrenalectomy and histological revealed adrenal hyperplasia. Two of 6 patients showed improvement of hypertension after adrenalectomy which diagnosis of UAH/PAH (Fig 4). The remaining

four patients were not improved after adrenalectomy.

The result of 4 of 8 patients (50%) may have inappropriate treatment from AVS when AVS cutoff ratio is at 2 (Fig 5).

The sensitivity, specificity, accuracy, positive predictive value(PPV) and negative predictive value(NPV) of CT/MRI to detect APA were 66.67%, 87.50%, 78.57%, 80.00%, and 77.78%, respectively. The sensitivity, specificity, accuracy, PPV and NPV of AVS at ratio cut point 2 to detect APA were 100%, 50%, 71.43%, 60% and 100%, respectively. When increased AVS ratio cut point to 4, the specificity, accuracy and PPV increased to 87.5%, 92.8%, and 85.7%, respectively (table 1).

Discussion

Patients with a bilateral source of excess aldosterone secretion should undergo pharmaceutical therapy⁽¹²⁾. AVS is a difficult procedure that may not be available in many general hospitals and typically require interpretation from experts so it may not always be the gold standard for diagnosing primary hyperaldosteronism. Our study showed that 22.7% of patients had incomplete AVS due to the difficulties in right adrenal vein catheterization similar to prior literatures^(9,10), the catheterization failure ranges from 10 to 30%.

To our understanding, CT is less sensitive in assessment of lesion localization compared to AVS, which can cause improper management in PAL. Two of 14 patients (14%) demonstrated no nodule from CT whereas AVS indicated lateralization. The patients were performed adrenalectomy and proven unilateral adrenal hyperplasia. However, our study showed lower percentage of inappropriate management in PAL than the prior literatures. Prior study

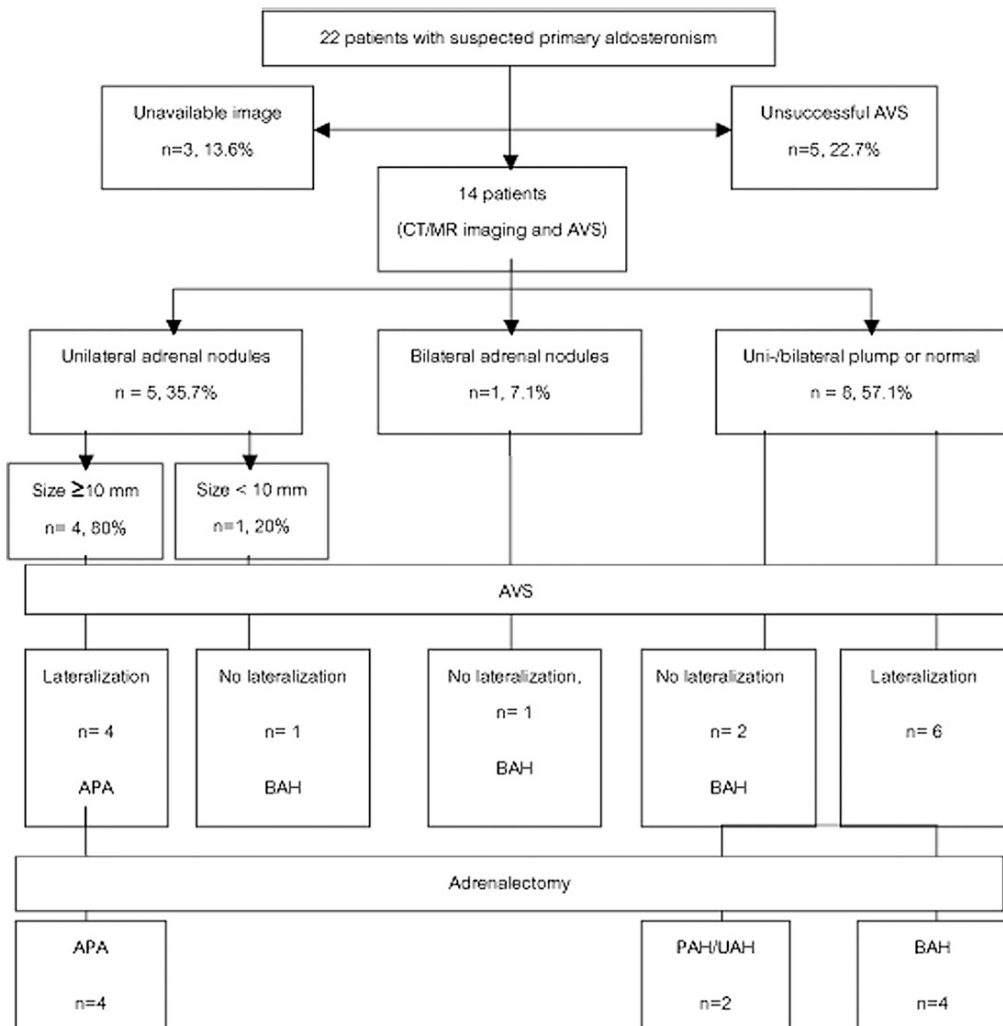


Fig.1 Summarized findings of computed tomography and adrenal venous sampling for causes of primary aldosteronism.

(APA, adenoma-producing aldosterone; AVS, adrenal venous sampling; BAH, bilateral adrenal hyperplasia; PAH, primary adrenal hyperplasia; UAH, unilateral adrenal hyperplasia)



Fig.2 A 65-years-old female with right adrenal adenoma. (A-C) Pre contrast axial CT reveals a 17x14-mm nodule at medial limb of right adrenal gland that attenuation is less than 10 HU, indicating lipid-rich adenoma. Coronal reformat (D) reveals right adrenal nodule.



Fig.3 A 50-years-old female had unilateral adrenal nodule and finally proven bilateral adrenal hyperplasia (A-B). Axial non contrast CT of adrenal gland reveals a nodule at medial limb of right adrenal gland which attenuation is less than 10 HU, indicating lipid-rich adenoma (C) Axial post contrast 15-min delayed phase of adrenal gland shows hypo enhancement of the right adrenal nodule that size less than 10 mm. (D) Coronal reformat in portovenous phase confirmed right adrenal nodule.

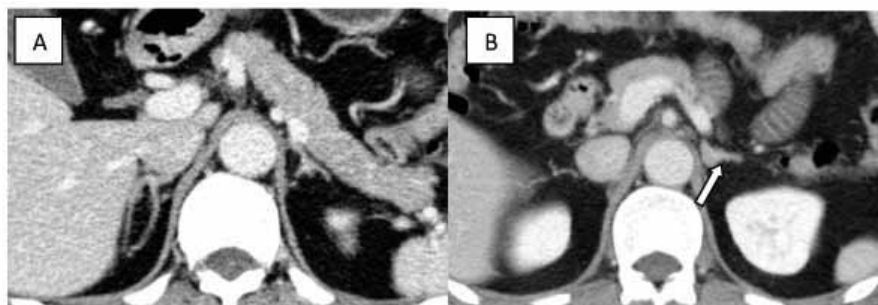


Fig.4 A 65-years-old male with left unilateral adrenal hyperplasia (UAH). (A-B) Post contrast axial CT of adrenal glands reveal normal appearance of right adrenal gland and plump (arrow) at left adrenal gland.

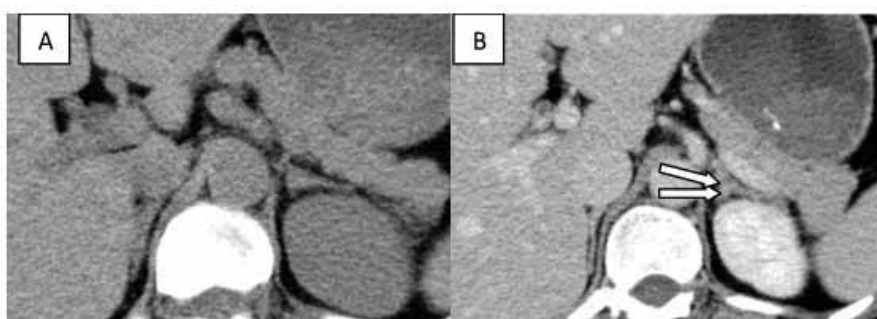


Fig.5 A 57-years-old male with BAH. (A) Pre contrast and (B) post contrast axial CT of adrenal gland reveal plumps (arrow) at left adrenal gland. He underwent left adrenalectomy due to lateralization from AVS ratio greater than 2 that is not cure after adrenalectomy.

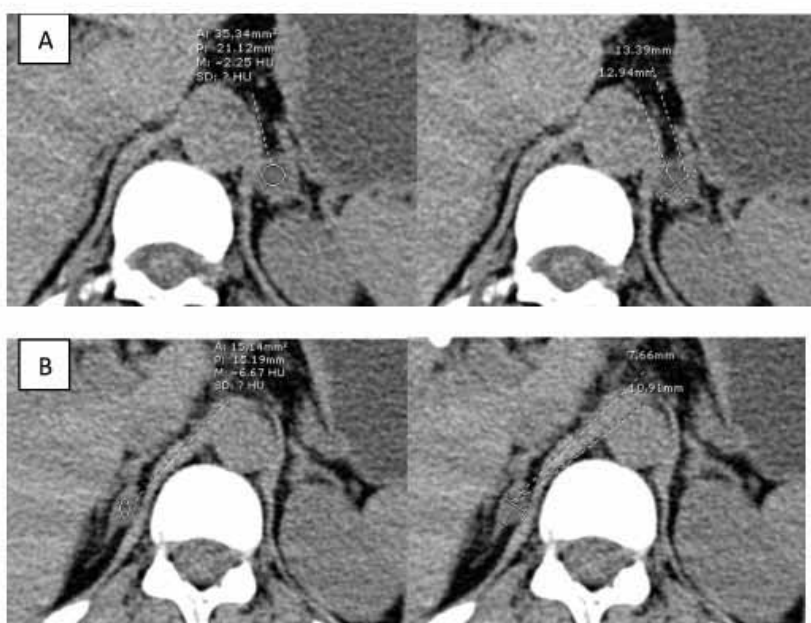


Fig.6 A 34-years-old female with BAH. Plain CT of adrenal glands reveals a 13x13-mm nodule at medial limb of left adrenal gland(A) and a 11x8-mm nodule at medial limb of right adrenal gland(B), which attenuation are less than 10 HU and AVS results indicated bilateral lesions.

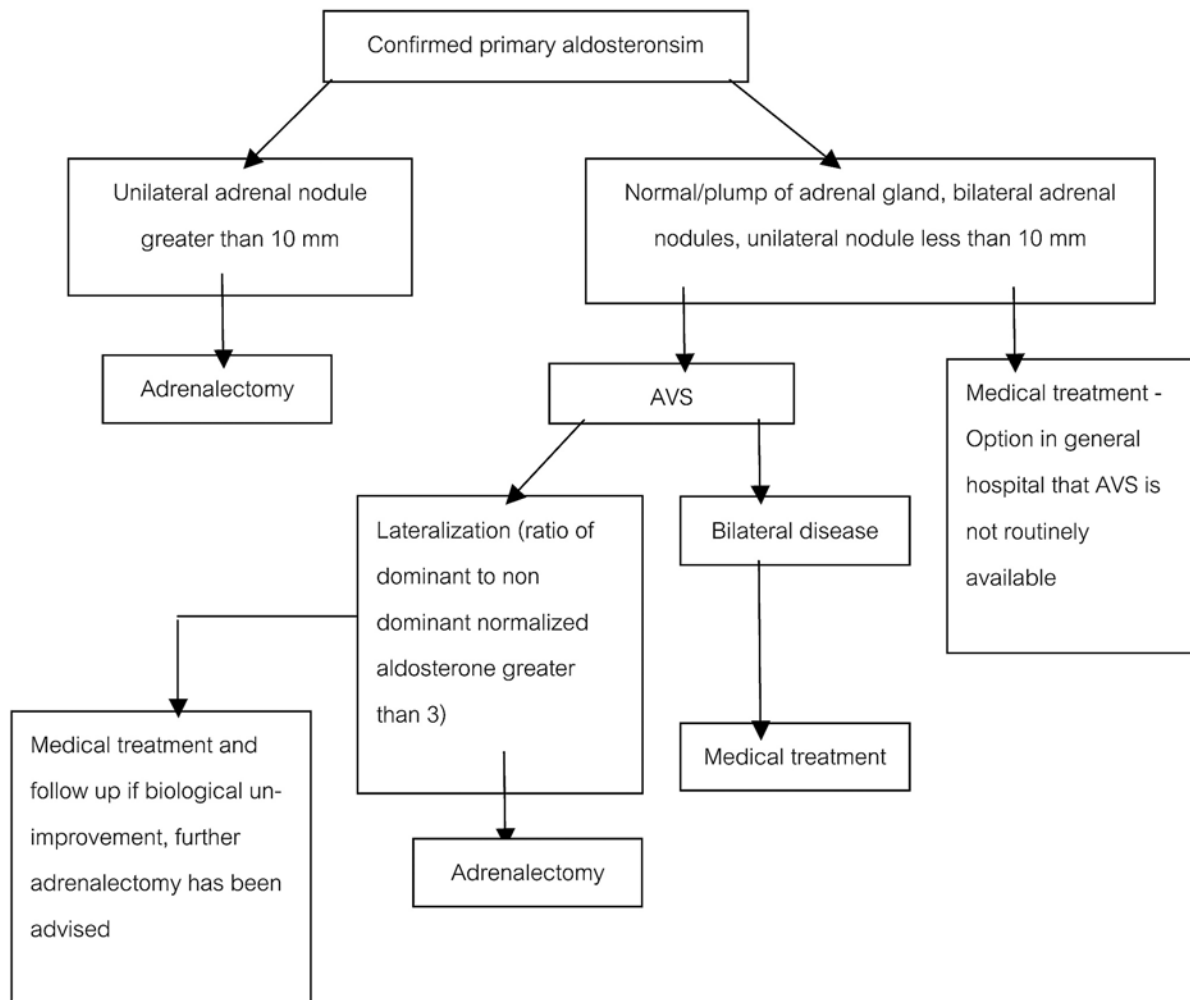


Fig.7 Flow chart for management of primary hyperaldosteronism.

Table.1 Sensitivity, specificity, accuracy, PPV and NPV to detect adrenal adenoma by AVS at cut point normalized aldosterone ratio (AVS ratio) at 2, 3 and 4.

	AVS ratio ≥ 2	AVS ratio ≥ 3	AVS ratio ≥ 4
Sensitivity	100%	100%	83.3%
Specificity	50%	75%	87.5%
Accuracy	71.43%	85.7%	85.7%
PPV	60%	75%	83.3%
NPV	100%	100%	87.5%

such as Sarlon-Bartol G, et al⁽¹¹⁾ and Oh EM, et al⁽¹³⁾ reported that many of patients (37% and 22.09%, respectively) had received inappropriate surgery and/or management if decision making is based solely on CT findings alone. And both studies recommended that AVS should be performed before an adrenalectomy regardless of the nodule size found by CT. In other prior studies showed superiorly of AVS over CT in differentiating subtype of PAL. Sensitivity of CT varies among previous literatures, approximately 53% in study of Happer R et al⁽³⁾ and 82% in study of Dunnick NR, et al⁽¹⁴⁾. Direct comparison between the two methods in study of Doppman JL, et al⁽¹⁵⁾ reported only 67% sensitivity for CT and 92% sensitivity for AVS.

Our study shows about 66.67% sensitivity and 77.78% NPV of CT/MRI to detect APA and 100% sensitivity and 100% NPV of AVS at cut point ratio = 2 to detect APA which similar to the study of Doppman JL, et al⁽¹⁵⁾ that the sensitivity and NPV of CT are lower than AVS. However, PPV of CT in our study is higher than PPV of AVS (80% vs 60%) and can reach 100% in case of macronodule. Similar results were also suggested by Happer R, et al⁽³⁾ who studies AVS and CT imaging in 34 patients. This study reported that PPV of CT scan is about 100% and also suggested that if CT imaging of patients with PAL showed a focal mass, ipsilateral adrenalectomy could be performed with the expectation of cure. However, if no mass was found on CT imaging, AVS could be used to detect an adenoma instead.

Some clinician recommended that for the patient aged below 40 years old, who has an adrenal macronodule and normal appearance of contralateral gland, no further imaging or evaluation is needed, and the patient should be referred for

adrenalectomy⁽¹⁶⁾. However, there is no patient under 40 years old with adrenal nodule had been included in our study.

AVS is a better alternative for detecting undemonstrable nodule because of its high NPV which sometimes reaches 100% compared to CT and MRI imaging which produce significantly lower NPV. If AVS showed no lateralization, patient should be treated medically. However, If AVS found lateralization; surgical treatment should be carefully considered. Due to low PPV of AVS, it may cause false positive in adrenal hyperplasia which cannot be cured by adrenalectomy. Cut point value for lateralization criteria vary between different institutions. Higher cut point raised specificity of AVS but decreased sensitivity. From our study, we can increase the cut point AVS ratio up to 3 without degrading sensitivity and NPV and also increase specificity to 75%. However, when the cut point AVS ratio is raised up to 4, the specificity can be as high as 87.5%, which equal to CT scan but decrease sensitivity and NPV.

Zarnegar et al⁽¹⁸⁾ concluded that a CT could be used to reliably diagnose adenomas larger than 10 mm and that AVS should be used when CT scan findings are normal or both adrenal glands are abnormal.

Our suggestion which similar to study of Zarnegar et al⁽¹⁸⁾ which suggested that if unilateral adrenal adenoma larger than 10 mm in case of suspected PAL is found, patient should be decided to adrenalectomy without performing AVS. AVS should be preserved when CT scan findings shows normal adrenal gland or both adrenal glands are abnormal. In case of unilateralization found on AVS and AVS ratio more than 3 should be decided to adrenalectomy and in case of bilateral disease, medical treatment is recommended which summa-

rized in diagram on Fig 7. However, our study is limited due to retrospective study with small number of cases. Further study with increase number of the patients should be considered.

Conclusion

The results of this study confirm that differentiation of subtype in patients with PAL is most reliably achieved with AVS. However, CT/MRI still has high PPV in case of detectable unilateral adrenal nodule, especially the nodule size is more than 10 mm. This patient groups should be referred to adrenalectomy without performing AVS. AVS is suitable for patient who had no adrenal nodule from CT/MRI imaging. If no lateralization is detected from AVS, medical treatment should be considered. And the cut point of AVS ratio at 3 is a proper value for differentiating APA from BAH due to increased PPV without degrading sensitivity and NPV.

References

- Ishibashi T, Satoh F, Yamada T, Sato A, Matsuhashi T, Takase K. Primary aldosteronism: a pictorial essay. *Abdominal Imaging* 2007;32:504-14.
- Simon DR, Palese MA. Noninvasive adrenal imaging in primary aldosteronism. *Current Urology Reports* 2008;9: 80-7.
- Harper R, Ferrett C.G., McKnight J.A., McIlrath E.M., Russell C.F., Sheridan B, et al. Accuracy of CT scanning and adrenal vein sampling in the pre-operative localization of aldosterone-secreting adrenal adenomas. *Q J Med* 1999; 92:643-50.
- Banks WA, Kastin AJ, Biglieri EG, Ruiz AE. Primary adrenal hyperplasia: a new subset of primary hyperaldosteronism. *J Clin Endocrinol Metab* 1984; 58:783-5.
- Caoili EM, Korobkin M, Francis IR, Cohan RH, Platt JF, Dunnick NR, et al. Adrenal masses: characterization with combined unenhanced and delayed enhanced CT. *Radiology* 2002;222(3):629-33.
- Mulatero P, Bertello C, Rossato D, Mengozzi G, Milan A, Garrone C, et al. Role of clinical criteria, computed tomography scan and adrenal vein sampling in differential diagnosis of primary aldosteronism subtypes. *J Clin Endocrinol Metab* 2008;93(4):1366-71.
- Tsushima Y. Different lipid contents between aldosterone-producing and non hyperfunctioning adrenocortical adenomas: in vivo measurement using chemical-shift magnetic resonance imaging. *J Clin Endocrinol Metab* 1994; 76(6):1759-62.
- Sohail SA, Peppercorn PD, Allan C, Monson JP, Grossman AB, Besser GM, et al. Primary hyperaldosteronism (Conn syndrome): MR imaging findings. *Radiology* 2000;214(2): 527-31.
- Sheaves R, Goldin J, Reznek RH, et al. Relative value of computed tomography scanning and venous sampling in establishing the cause of primary hyperaldosteronism. *Eur J Endocrinol* 134:308-13.
- Rossi GP, Sacchetto A, Chiesura-Corona M, De Toni R, Gallina M, Feltrin GP. Identification of the etiology of primary aldosteronism with adrenal vein sampling in patients with equivocal computed tomography and magnetic resonance findings: results in 104 consecutive cases. *J Clin Endocrinol Metab* 2001;86:1083-90.
- Sarlon-Bartoli , Michel N, Taieb D, Mancini J, Gonthier C, Silhol F, et al. Adrenal venous sampling is crucial before an adrenalectomy whatever the adrenal-nodule size on computed tomography. *Journal of hypertension* 2011;29: 1196-202.
- Oh EM, Lee KE, Yoon K, Kim SY, Kim HC, Youn YK. Value of adrenal venous sampling for lesion localization in primary aldosteronism. *World J Surgery* 2012;36:2522-7.
- Aloia JF, Beutow G. Malignant hypertension with aldosteronoma producing adenoma. *Am J Med Sci* 1974; 268:241-5.
- Dunnick NR, Leight GS, Roubidoux MA, Leder RA, Raulson L, Paulson E. CT in the diagnosis of primary aldosteronism: sensitivity in 29 patients. *AJR* 1993; 160:321-4.
- Doppman JL, Grill JR Jr, Miller DL, Chang R, Gupta R, Friedman TC, et al. Distinction between primary aldosteronism due to bilateral hyperplasia and unilateral aldosteronoma: reliability of CT. *Radiology* 1992;184(3): 677-82.

16. Zeigger MA, Thompson GB, Duh QY, Hamrahan AH, Angelos P, Elaraj D, et al. American Association of Clinical Endocrinologists and American Association of Endocrine Surgeons Medical Guidelines for the Management of Adrenal Incidentalomas. *Endocr Pract* 2009;15 Suppl 1: 1-20.
17. Magill SB, Raff H, Shaker JL, Brickner RC, Knechtges TE, Kehoe ME, et al. Comparison of adrenal vein sampling and computed tomography in the differentiation of primary aldosteronism. *J Clin Endocrinol Metab* 2001;86: 1066-71.
18. Zarnegar R, Bloom AI, Lee J, Kerlan RK Jr, Wilson MW, Laberge JM, et al. Is adrenal venous sampling necessary in all patients with hyperaldosteronism before adrenalectomy? *J Vasc Interv Radiol* 2008;19(1):66-71.



Unsatisfactory Ultrasound-Guided Fine Needle Aspiration of Thyroid Nodule: Which Factors Limit Cytology Result?

Pratirop Poonotoke, MD.

Department of Radiology, Lerdsin Hospital, Bangkok 10500, Thailand.

Abstract

Objective: The purpose of this study is to focus on which factors affect or limit fine-needle aspiration-cytology (FNAC) results of thyroid nodule, in order to increase the satisfactory cytologic results and to avoid unnecessary FNAC in patients with asymptomatic benign nodules and highly possible unsatisfactory results.

Materials and Methods: The records of 217 thyroid nodules in 179 patients referred to the radiology department at Lerdsin Hospital for US-guided FNAC between January 2010 and December 2013 were retrospectively reviewed. Cytologic specimens of the FNAC were classified as unsatisfactory (non-diagnostic) and satisfactory (diagnostic) results and analyzed by mean of Logistic regression analysis, based on patient's age, gender, nodule size, number and solid-cystic composition of nodule.

Results: The cytologic result was satisfactory for diagnosis in 154 specimens (71%) and unsatisfactory in 63 specimens (29%). Patient's age, gender, number and size of nodule of the unsatisfactory result group were not different from the satisfactory result group but the nodule composition was different. Percentage of the unsatisfactory aspiration increased as the cystic component increased, ranging from 15.3% in solid nodules to 59.3% in predominant cystic nodules (cystic $\geq 75\%$). Upon the binary logistic regression analysis, the predominant cystic nodule was the only significant predictor of unsatisfactory result (p -value < 0.001) while solid nodules, predominant solid nodules and solid-cystic nodules are not significant. Unsatisfactory FNAC result of the predominant cystic nodules was about 8 times higher than the solid nodule (crude odds ratio = 8.087, p -value < 0.001).

Conclusion: To optimize the usefulness of FNAC, we should realize that solid-cystic composition of the thyroid nodules influence the non-diagnostic and diagnostic cytology.

Introduction

Thyroid nodules represent a common problem, with an estimated prevalence of 4-10% in the adult population for palpable nodules¹⁻³. The prevalence of non-palpable thyroid nodules appears to be higher with ultrasonographic(US) examination, approximately 10-40%^{1,4}. Most of thyroid nodules are benign. Only 5-10% of these are malignant.^{1,3-5} Unfortunately,no specific sonographic characteristics of malignancy have been published and there is overlap of sonographic characteristic findings in benign and malignant nodules. Fine-needle aspiration cytology (FNAC) is minimally invasive procedure that is usually performed on an out-patient basis. Real-time ultrasonography guidance permits visualization of the needle tip within the nodule resulting in decreased needle misplacement and increased FNAC accuracy of the non-palpable nodules. It has become the standard of care for the initial diagnostic workup of a thyroid nodule. Although the majority of FNAC are adequate for diagnosis, 5-20% are inadequate^{1,4,6}. The achievement of FNAC results requires not only an US guidance aspiration technique skill to obtain adequate material for cytology but also awareness of limitation of FNAC. The purpose of this study is to focus on which factors affect or limit material adequacy for FNAC, based on nodule size,number and US features so we can decide which nodules should be subjected to US-guided fine needle aspiration and which thyroid nodules need not be subjected to fine-needle aspiration because of high possibility of inadequate specimen.

Materials and Methods

We reviewed the records of all patients referred to the radiology department at Lerdsin Hos-

pital for evaluation of thyroid nodule with US-guided FNAC between January 2010 and December 2013. For each thyroid nodule that FNAC was performed, gray-scale US was used to evaluate the US features, which included number, size and composition .

Maximum diameter of each nodule was reported and classified as ≤ 1 cm ,1.1-2.0 cm and >2 cm.

Number of nodules was classified as single nodule or multiple nodules on US examination.

In case of multiple nodules, FNAC was performed in the prominent nodule or suspicious nodule.

Composition was classified as a solid, a predominantly solid nodule ($\leq 25\%$ cystic), a solid-cystic ($25\% < \text{cystic} < 75\%$) and a predominantly cystic nodule ($\geq 75\%$ cystic,including 100% cystic).

US-guided FNAC was performed by the same interventional radiologist,using a high-resolution (11.5 MHz) linear-array transducer. A 21-gauge needle with 10 ml disposable syringe was used. A perpendicular puncture was done with limited local anesthesia. When the needle tip reached the target nodule, the needle was observed as a small echogenic spot within the nodule on the US monitor. After the needle tip was placed in the appropriate area of the target nodule, the needle was moved up and down with aspiration for a few seconds under US guidance. After a sample was obtained, it was smeared promptly onto a glass slide. The smears were quickly fixed in 95% ethyl alcohol. We obtained 4-6 slides by performing 2-3 punctures from each nodule. All specimens were processed using the Papanicolaou staining method. All slides were reviewed and interpreted by a cytopathologist at Lerdsin Hospital.

Cytologic specimens of the FNA were classi-

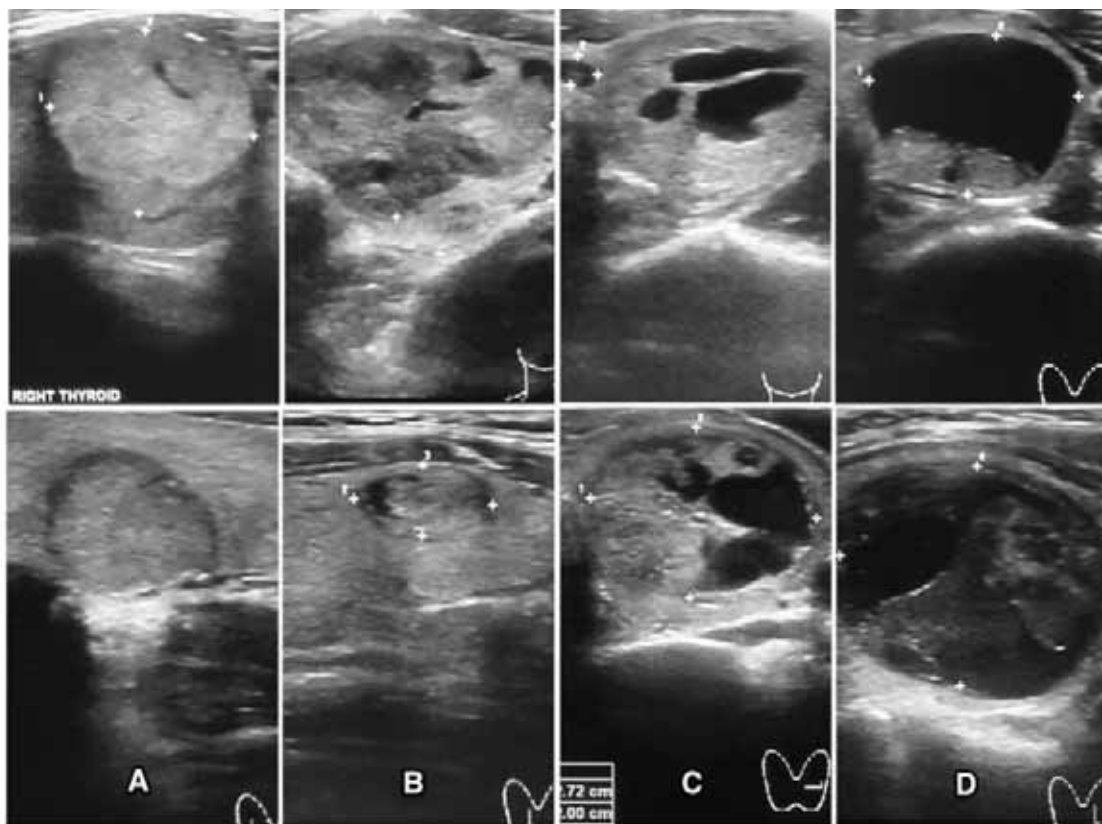


Fig. 1 US features of thyroid nodules. A - solid, B - predominantly solid, C -solid-cystic, D - predominantly cystic

fied as unsatisfactory (non-diagnostic) and satisfactory(diagnostic).

Specimens were considered unsatisfactory (non-diagnostic) if insufficient cellular material, air drying artifact or blood contamination was found. Satisfactory specimens (benign, intermediate and malignant/suspicious of malignancy) were including nodular goiter, follicular lesion, follicular lesion with cystic degeneration, Hashimoto thyroiditis, hemorrhagic cyst, presence of atypical cells, suspicious of papillary thyroid carcinoma.

Results of FNAC of thyroid nodules were retrospectively analysed. The Ethic Committee of Lerdsin Hospital has approved the study.

Statistics

Descriptive statistics were presented according to nodule or patient. Binary logistic regression analysis was performed using SPSS software (version 17.0, SPSS, Inc., Chicago, IL). Patient's age gender and number of nodule (single or multiple) were analyzed as dichotomous variables. Patient's age (10 year interval from 20-29 years to 60-69 years and more than 70 years) , nodule size (≤ 1 cm, 1.1-2.0 cm or > 2 cm.) and solid-cystic composition (solid , cystic $\leq 25\%$, 25<cystic< 75%, or cystic $\geq 75\%$) were analyzed as categorical variables. Significance was accepted at $P < 0.05$. Adjusted odds ratio and crude odds ratio were calculated.

Results

FNAC of 217 thyroid nodules were performed in 179 patients (16 men and 163 women), aged from 20 to 87 years (mean 49.88). The aspiration was performed twice in 16 patients and three times in 1 patient on follow-up, due to unsatisfactory cytological result or nodule growth. The indication was single nodule in 54 patients and dominant nodule of multiple nodules in 125 patients. In multiple nodules, FNAC of 2 nodules per patient were done in 18 patients and 3 nodules per patient in 1 patient. A total of 217 cytological diagnoses were reviewed. The maximum diameter of nodules vary from 0.4-4.8 cm (mean 2.05 cm. SD. = 0.9651). The cytologic result was satisfactory for diagnosis in 154 specimens (71%) and unsatisfactory in 63 specimens (29%). The demographic and US features were compared between these 2 groups (table 1). Patient's age, gender, nodule composition, nodule size and number of nodules were evaluated as possible predictors of an unsatisfactory FNAC. Gender, age, nodule size and number of the unsatisfactory result group were not different from the satisfactory result group but the nodule composition was different. Percentage of the unsatisfactory aspiration increased as the cystic component increased, ranging from 15.3% in solid nodules, 15.9% in predominant solid nodules, 23.8% in solid-cystic nodules to 59.3% in predominant cystic nodules (table 2). Upon the binary logistic regression analysis, the predominant cystic nodule was the only significant predictor of unsatisfactory result (p -value < 0.001) while solid nodules, predominant solid nodules and solid-cystic nodules are not significant. Unsatisfactory FNAC result of the predominant cystic nodules (cystic $\geq 75\%$) was about 8 times higher than the solid nodule (crude odds ratio = 8.087, p -value < 0.001).

Discussion

Thyroid nodules are very common in the general population, but malignancy is relatively rare. Ultrasonography (US) is increasingly able to detect thyroid nodules, and the differentiation between malignant and benign nodules has been raising issues among both physicians and patients. Thyroid FNAC is a well-established method and its main goal is to differentiate malignant from benign nodules. Its reliability depends on several factors, such as the skill of the interventional radiologist or the experience of the cytopathologist. Although use of ultrasonography in FNAC increases significantly the sensitivity, specificity and accuracy compared with conventional palpation-guided FNAC^{7,8,9}, unsatisfactory cytology is frequently troubled.

The aims of our study are to define to which factors unsatisfactory results are related, in order to increase the satisfactory cytologic results and to avoid unnecessary FNAC in patients with benign, asymptomatic and highly probable unsatisfactory result.

We used 2 categories (satisfactory and unsatisfactory). All patients were recorded for their demographic features, that is, age and gender and US features of nodules were recorded in the term of single vs. multiple, size and solid-cystic composition. In our study, unsatisfactory results were found in 29%. Almost all of unsatisfactory cytology were insufficient cellular material for diagnosis. The rests are limited by air-drying artifact and blood contamination.

We found that the patient's age, gender, nodule size and number with unsatisfactory cytology were not different from those with satisfactory cytology and were not the predictive factors for non-diagnostic specimens ($P > 0.05$) upon the binary

Table 1 Demographic and US features between satisfactory and unsatisfactory result groups.

Factors	Total	Satisfactory	Unsatisfactory
Number of nodules	217	154 (71%)	63 (29%)
Age (mean \pm SD.)	49.88 \pm 13.92	48.20 \pm 13.96	53.97 \pm 13.02
Female	201	147 (95.5%)	54 (85.7%)
Male	16	7 (4.5%)	9 (14.3%)
Single nodule	59	36 (23.4%)	23 (36.5%)
Multiple nodules	158	118 (76.6%)	40 (63.5%)
Size (mean \pm SD, cm)	2.05 \pm 0.96	1.98 \pm 0.89	2.23 \pm 1.10
solid	72	61 (39.6%)	11 (17.5%)
predominantly solid nodule (cystic \leq 25%)	44	37 (24.0%)	7 (11.1%)
solid-cystic (25% $<$ cystic $<$ 75%)	42	32 (20.8%)	10 (15.9%)
predominantly cystic nodule (cystic \geq 75%)	59	24 (15.6%)	35 (55.6%)

logistic regression analysis. The predominant cystic nodule was the only significant predictor of unsatisfactory result (p -value $<$ 0.001).

Cystic composition was a significant problem in our study, with unsatisfactory specimens reaching 59% in nodules more than 75% cystic. We found that the highest proportion of unsatisfactory specimens occurred in nodules with the greatest cystic content. In our study, 16 simple thyroid cysts were included in the predominant cystic nodule group and showed no satisfactory cytology, due to insufficient cellular materials in all cysts. It could be due to dilution effect of the sample and

scant thyroid follicular cell in the cystic content. In spite of US-guided FNAC, there is a risk of unsatisfactory cytology, especially the nodule with prominent cystic portion. We may assume that the unsatisfactory cytology is influenced more by lesion composition than by mistaken targeting. Aspiration is normally done when the US shows the tip of needle in the solid portion of the nodule to avoid aspiration of the cystic portion. However cystic content is usually contaminated in the samples, especially in the greater cystic nodule. It may dilute specimens, resulting in insufficient cellular material¹⁰. If the nodule has a large cystic portion, aspiration of the

Table 2 Binary logistic regression analysis of patient age, gender, nodule composition ,nodule size and number of nodules as possible predictors of an unsatisfactory FNAC.

Factors	NO.	Satisfactory	Unsatisfactory	p-value	Adjusted OR	Crude OR	95% CI
solid	72	61 (84.7%)	11 (15.3%)		1	1	
predominantly solid	44	37 (84.1%)	7 (15.9%)	0.978	0.984	1.049	0.374- 2.944
solid-cystic	42	32 (76.2%)	10 (23.8%)	0.110	2.378	1.733	0.665-4.514
predominantly cystic	59	24 (40.7%)	35 (59.3%)	<0.001	10.140	8.087	3.541- 18.469
size \leq 1.0 cm	30	20 (66.7%)	10 (33.3%)		1	1	
size 1.1-2.0 cm	91	69 (75.8%)	22 (24.2%)	0.292	0.557	0.638	0.260- 1.565
size \geq 2.1 cm	96	65 (67.7%)	31 (32.3%)	0.626	0.764	0.954	0.399- 2.280
Age 20-29	11	10 (90.9%)	1 (9.1%)		1	1	
Age 30-39	51		7 (13.7%)	0.744	1.484	1.591	0.175- 14.429
Age 40-49	47	33 (70.2%)	14 (29.8%)	0.218	4.246	4.242	0.495- 36.369
Age 50-59	44	26 (59.1%)	18 (40.9%)	0.086	7.658	6.923	0.813- 58.941
Age 60-69	44	29 (65.9%)	15 (34.1%)	0.056	9.953	5.172	0.604- 44.318
Age 70-79	17	10 (58.8%)	7 (41.2%)	0.052	12.028	7.000	0.722- 67.840
Age 80-89	3	2 (66.7%)	1 (33.3%)	0.080	20.994	5.000	0.212- 117.894
Number				0.374	0.686	0.531	0.281- 1.001
Gender				0.53	0.289	0.286	0.101- 0.805

cystic portion should be done to evacuate fluid. Then FNAC of the residual solid portion may be performed. In case of simple cysts, aspiration of the fluid content is inevitably done and satisfactory cytology is not expected. Insufficient cellular material does not reflect poor aspiration skill in the simple cyst aspiration. Most thyroid cysts are benign but a small number of papillary carcinoma are cystic so it is reasonable to perform FNAC in thyroid cysts. About 50-70% of benign cysts do not recur, in contrast, all cystic papillary carcinoma recur¹⁰. Repeated FNA is suggested if cyst recurs or shows progressive growth on follow-up.

In an ideal settings, slides are immediately reviewed by an on-site cytopathologist. This allows immediate feedback regarding specimen adequacy to the interventional radiologist performing the aspiration. In less ideal environment, the radiologist may require skill and training to produce high quality slides.

Any residual specimen can be dispersed into an appropriate rinse solution by flushing the needle to extract all of the specimen for cytologic examination as liquid-based technique. In the cytopathology laboratory this material will be spun in a centrifuge, and the resulting precipitant will be used to produce smears. Liquid-based technique appears to produce more satisfactory slides than the conventional smear¹¹.

In our study, we prepared specimens only with conventional smear technique which had some limitations related to the low cellularity and bloody background. No on-site cytopathologist was available during the procedure.

Besides insufficient cellular materials, air-drying artifact is one of the causes of unsatisfactory FNAC. This problem can be easily avoided with immediate fixation of the smears in 95% ethyl alcohol.

Blood contamination may limit the cytopathologist to evaluate the smears, resulting in unsatisfactory result. In our study, we used a 21-gauge needle for aspiration with suction technique. Some have suggested the use of 23-, 25- or 27 gauge needle and non-suction technique for FNA of markedly hypervascular nodules to produce specimens that are less bloody⁹. However conventional suction technique sometimes yields more material¹⁰. Liquid-based smear may also show cleaner background¹¹.

Not only FNA technique but also specimen preparation has influenced the diagnostic or non-diagnostic cytology. The interventional radiologist who performs the procedure should produce high quality specimens by improving his skill and technique for FNA and specimen preparation. Liquid-based smear may increase diagnostic result from increasing cellular material, particularly in case of predominant cystic nodule so liquid-based technique should be implemented.

Conclusion

To optimize the usefulness of FNAC, we should realize that solid-cystic composition of the thyroid nodules influence the non-diagnostic and diagnostic cytology. The appropriate technique of US guided FNAC and specimen preparation should be tailored especially in case of the predominant cystic nodule which has a high possibility of unsatisfactory cytology.

Acknowledgements We are thankful to the support of Radiological Department and Pathology Department of Lerdsin Hospital and indebted to Dr. Attasit Srisubat for helpful advice of statistic analysis.

References

1. Yeung MJ, Serpell JW. Management of the solitary thyroid nodule. *Oncologist* 2008;13:105-12.
2. Gupta M, Gupta S, Gupta VB. Correlation of fine needle aspiration cytology with histopathology in the diagnostic solitary thyroid nodule. *J Thyroid Res* 2010;1:1-5.
3. Gbalec F, Cap J, Ryska A, Vasatko T, Ceeova V. Benign fine-needle aspiration cytology of thyroid nodule:to repeat or not to repeat? *Eur J Endocrinol* 2009;161:933-7.
4. Alexander EK, Heering JP, Benson CB, Frates MC, Doubilet PM, Cibas ES, et al. Assessment of nondiagnostic ultrasound-guided fine needle aspirations of thyroid nodules. *J Clin Endocrinol Metab* 87(11):4924-7.
5. Flanagan MB, Ohori NP, Carty SE, Hunt JL. Repeat thyroid nodule fine-needle aspiration in patients with initial benign cytologic results. *Am J Clin Pathol* 2006;125:698-702.
6. Deandrea M, Mormile A, Veglio M, Motta M, Pellerito R, Gallone G, et al. Fine-needle aspiration biopsy of the thyroid : comparison between thyroid palpation and ultrasonography. *Endocr Pract* 2002;8:282-28.
7. Morris LF, Ragavendra N, Yeh MW. Evidence-based assessment of the role of ultrasonography in the management of benign thyroid nodules. *World J Surg* 2008;32:1253-63.
8. Al-Sindi KA, Bukhari MH, Saba K, Ali W, Arshad M, Zaidi NZ. Evaluation of non-palpable thyroid nodules by ultrasound guided fine needle aspiration cytology. *Natural science* 2013;5:214-20.
9. Kim MJ, Kim EK, Park SI, Kim BM, Kwak JY, Kim SJ, et al. US-guided fine-needle aspiration of thyroid nodules: indications, techniques, results. *Radiographics* 2008;28:1869-89.
10. Suen KC. Fine-needle aspiration biopsy of the thyroid. *CMCJ* 2002;167(5):491-5.
11. Kim DH, Kim MK, Chae SW, Lee KB, Han EM, Kang SH, Sohn JH. The useful of SurePath(TM) Liquid-based smear in sono-guided thyroid fine needle aspiration; a comparison of a conventional smear and SurePath(TM) Liquid-based cytology. *Korean J Cytopathol* 2007;18(2):143-52.



Computed Tomography Analysis of the Ethmoid Roof: A Region at Risk in Endoscopic Sinus Injury

Pra Urusopone, MD.

Department of Radiology, Lerdsin General Hospital, Bangkok Thailand.

Abstract

Objective: To determine the olfactory fossa depth according to the Keros classification and determine the incidence of asymmetry in height and configuration of the ethmoid roof.

Materials and Methods: Retrospective analysis of 75 coronal computed tomography studies of paranasal sinuses and facial bones were performed. Measurement of the depth of the lateral lamella, classification of the depth according to Keros type and determination of the asymmetries in the ethmoid roof depth and configuration were done.

Results: The mean height of the lateral lamella cribiform plate (LLCP) was 2.15 ± 1.29 mm. The cases were classified as 87.33% Keros type 1 and 12.67 % as Keros type 2. No Keros type 3 was found .There was asymmetry in the LLCP height of 33.33% of cases and a configuration asymmetry in 8% of the cases.

No significant difference between the mean height and distribution of Keros type between gender and laterality were also found.

Conclusion: As regards the olfactory fossa depth, the Keros type 1 was most frequently found. Asymmetry in the depth and configuration were detected in 33.33 and 8% respectively. Risk of inadvertent intracranial entry through the lateral lamella among Thai may be lower than other studies with majority of cases classified as Keros type 2 or 3.

Keyword: Ethmoid roof, Keros type

Introduction

Endoscopic sinus surgery (ESS) is now considered as the treatment of choice for chronic rhinosinusitis which is resistant to medical treatment as well as for other diseases such as mucocele, nasal polyposis, sellar and parasellar tumors, choanal atresia, and optic nerve decompression.⁽¹⁾ There may be intraoperative complications because this surgery is performed in a complex anatomy. The complications are categorized into minor and major types. Minor complications occur in 1.1-20.8% of the cases which are hemorrhage, infection, cohesions, narrowing in the ostium, insensitivity of the teeth or lips and the relapse of the disease. The major complications are cerebrospinal fluid leakage, ocular trauma, meningitis or intracranial penetration which occur in 0-1.5% of cases.⁽²⁻⁴⁾

Most of major complications are related to surgical manipulation of the ethmoid and frontal sinuses. The roof of the ethmoidal labyrinth is formed by the fovea ethmoidalis; an extension of the frontal bone orbital plate separating the ethmoidal cells from the anterior cranial fossa. It connects with the lateral lamella of the cribriform plate (LLCP), the thinnest bone of the skull base.^(5,6) The fovea ethmoidalis and the lateral lamella both are the most vulnerable skull base to be injured during ESS.^(6,7) In 1962, Keros determined the depth of the olfactory fossa

into 3 types according to the height of the lateral lamella as Table 1.

Depending on the Keros type, the greater the depth of olfactory fossa, the higher the risk of its penetration into the anterior cranial fossa is.⁽⁸⁾ Besides the depth of olfactory fossa, one factor which may cause surgical difficulties is the configuration of the ethmoid roof. Asymmetry of the height of the ethmoid roof between two sides must be determined as well as the variation in their contour. The shape of the contour is identified by the angle at which the fovea ethmoidalis joins with the cribriform plate. It may be straight or in the shape of a broken wing if the angle increases.⁽⁹⁾ This angulation may result in surgical difficulties. That is why the knowledge about the complex skull base anatomy and variation is essential for pre-operative evaluation in endoscopic nasal surgeries.

Computed tomography (CT) has become the potential investigation not only to evaluate of sinonasal disease, but also to be a road map in characterization of the paranasal sinus anatomy in the planning of ESS.⁽⁸⁾

The reasoning of this study are evaluation the depth of the olfactory fossa, characterization them according to Keros classification, and determination the asymmetry of the ethmoid roof. The end goal is to gather this knowledge for the surgeons in an effect to reduce the surgical complications.

Table 1 Three types of Keros classification according to the height of lateral lamella

Height of lateral lamella : Depth of olfactory fossa (mm)	Keros type
0-3	1
4-7	2
8-16	3

Materials and Methods

Retrospective analysis of all paranasal sinus and facial bone CT acquired in the period between June 2013-May 2014 in Lerdsin General hospital were done. The exclusion criteria were patients under the age of 16, previous history of trauma or surgery in the paranasal sinuses or skull base, sinonasal tumor and serious rhinosinusitis. Seventy five CT studies were included in this study. This study was approved by the Human Ethics Committee of Lerdsin General hospital.

All CT studies were performed using a 64 multi-slice CT equipment. (Somatom Definition AS Siemen) The technical parameter are shown in Chart 1.

Only coronal images were utilized in this study. The images were acquired perpendicular to the hard palate from the anterior margin of the frontal sinus to the anterior margin of the clivus. All images were evaluated by the same radiologist. The ethmoid roof measurement was performed manually using a digital screen. The standard anatomic points were determined such as the medial ethmoid roof point, the cribriform plate point and the infraorbital nerve point.

Measurements were performed using the distance measurement technique in the coronal plane.

The horizontal line crossing between both infraorbital neural foramen were performed. The vertical line drawn from the medial ethmoid roof to the horizontal plane was measured and defined as the medial ethmoid roof height (MEH). The length of a vertical line from the cribriform plate to the horizontal line was defined as the cribriform plate height (CPH). The height of the lateral lamellar (LLH) was the result of subtracting the CPH from MEH. (fig 1a)

Measurements were compared between the right and left side and categorized according to Keros classification (fig 1c, d) and their distributions were analyzed according to gender. Mean height of the lateral lamellar (LLH) with standard deviation were calculated. All differences in means were analyzed using standard T test. Difference in the distribution of Keros classification according to laterality and gender were tested by Fisher's exact test whichever was appropriate p-value less than 0.05 were considered significant.

The configuration of the ethmoid roof was evaluated a having straight or significant broken wing type. (fig 1b) The asymmetry of the roof was calculated in depth differences and divided into 3 categories; 1) right side deeper than left, 2) left side

Chart 1 : Technical parameter

KV	120
mAs	91
FOV	197 mm.
Pitch	0.8
Filter	Low/contrast B135 medium smooth
Slice thickness	2 mm.
Window	2500/800

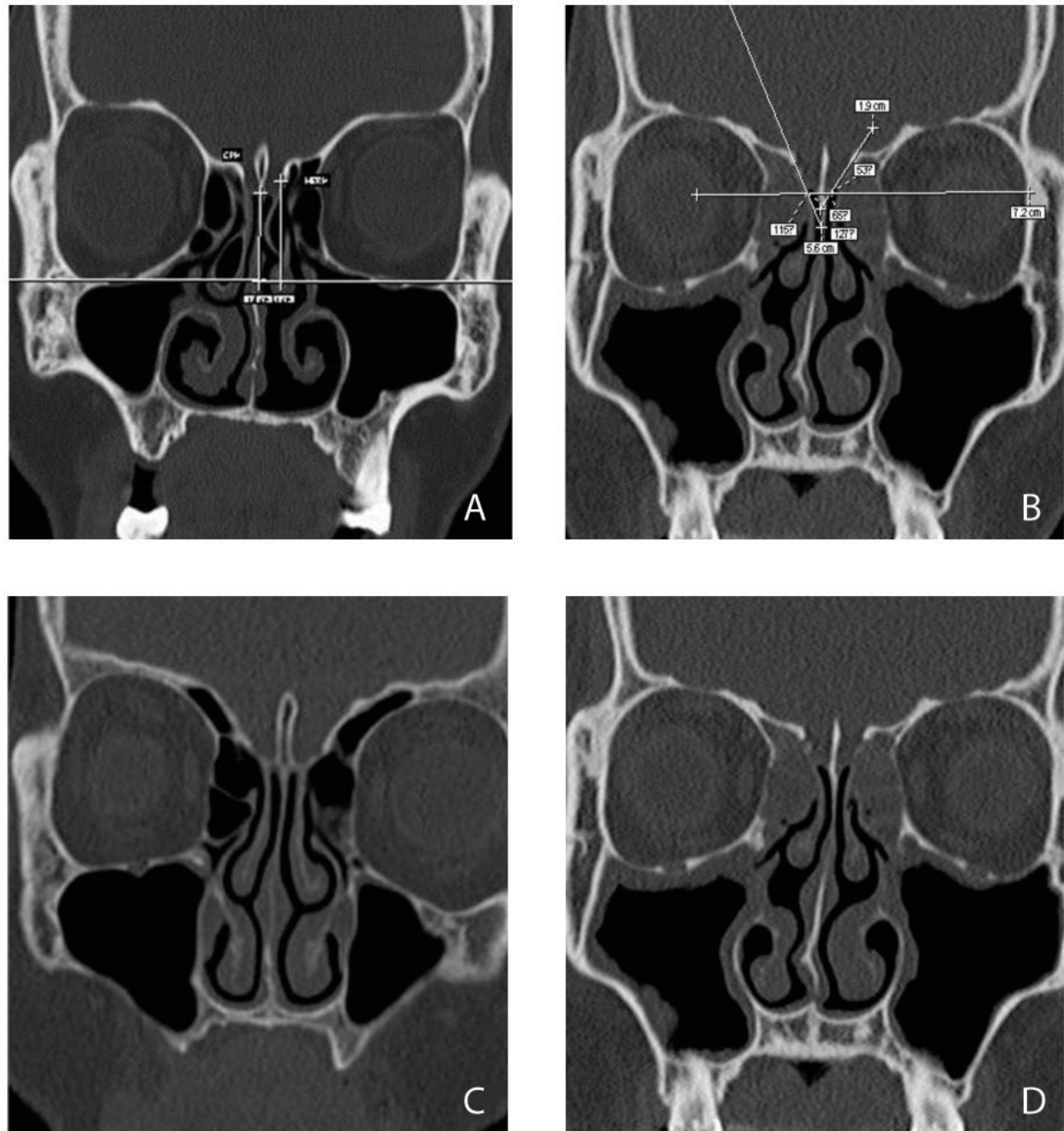


Fig 1: **a:** Measurement of the depth of the lateral lamella in a coronal paranasal sinus CT scan
b: Measurement of angulation
c: Example of Keros type 1 with angulation
d: Example of Keros type 2

deeper than right and symmetrical right and left side.

Results

CT scans of 75 patients (150 sides) were analyzed. There were 51 males (68%) and 24 females (32%). The average age of the patients was 40.91 (17-77) which of the male and female were 49.83 and 36.71 respectively.

The height of the lateral lamellar cribiform plate (LLCP) {N=150} range from 0-6 mm. The average height of LLCP was 2.15 ± 1.29 mm and 2.16 ± 1.35 and 2.13 ± 1.15 mm for the right and left side respectively. [Table 1]

There were no statistic difference between the average right and left LLCP height in both men, women and overall. ($p=0.243, 0.242$ and 0.741). Com-

parison between gender, there were also no statistic difference of average of LLCP height. ($p=0.078$)

When the LLCP height of right and left side were compared for each individual, asymmetrical height between two sides were found in 33 cases (30.67%). The average height difference was 0.39 mm. which was no statistic difference between the gender. The distribution of the difference between two sides according to gender is presented in Table 2.

According to Keros classification, the LLCP height were classified into Keros type1 in 131 sides (87.33%) and Keros type 2 in 19 sides (12.67%). There was no Keros type 3 found in our study. No significant difference between male and female in term of Keros classification type (Fisher exact test $p=0.80$). The distribution and percentage values of

Table 1 Average±standard deviation of LLCP height according to gender and laterality

	Right (mm)	Left (mm)	Overall (mm)
Male	2.33 ± 1.38	2.21 ± 1.19	2.28 ± 1.28
Female	1.79 ± 1.25	1.96 ± 1.33	1.88 ± 1.28
Overall	2.16 ± 1.35	2.13 ± 1.15	2.15 ± 1.29

Table 2 Distribution and percentage values of the right and left LLCP height difference according to gender

the LLCP height according to Keros type are shown as in Table 3.

The average LLCP height of each Keros type was calculated as in Table 4. There was only statistic difference in average height of Keros type 2 between gender. ($p=0.05$)

For each individual different Keros type were seen in 3 cases (4%), 2 male and 1 female. Configuration asymmetry in the fovea ethmoidalis were found in 6 cases (8%) which one case shown bilaterally. (Table 5)

Table 3 Distribution and percentage values of the LLCP height according to Keros classification

Keros type	Right		Left		Overall
	Male (%)	Female (%)	Male (%)	Female (%)	
1	42 (82.35)	22 (91.67)	46 (90.2)	21 (87.5)	131 (87.3)
2	9 (17.65)	2 (8.33)	5 (17.65)	3 (12.5)	19 (12.67)
3	0	0	0	0	0
Overall	51 (100)	24 (100)	51 (100)	24 (100)	150 (100)

Table 4 Average height of the LLCP according to Keros classification between gender

Type	Male		Female		Both sex		Overall
	Right	Left	Right	Left	Right	Left	
1	1.90 \pm 1.08	1.98 \pm 0.98	1.64 \pm 1.09	1.67 \pm 1.15	1.81 \pm 1.08	1.88 \pm 1.04	1.85 \pm 1.055
2	4.33 \pm 0.71	4.40 \pm 0.55	4.00	4.00	4.28 \pm 0.47	4.25 \pm 0.46	4.26 \pm 0.56

Table 5 Distribution and percentage of the LLCP height symmetry-asymmetry

	Male (%)	Female (%)	Overall (%)
No angulation	48 (94.12)	21 (87.5)	69 (92.00)
Right angulation	1 (1.96)	1 (4.17)	2 (2.67)
Left angulation	2 (3.92)	1 (4.17)	3 (4.00)
Bilateral angulation	-	1 (4.17)	1 (1.33)

Discussion

With advanced in ESS, CT study has been an important tool for preoperative evaluation together with the clinical examination and nasal endoscope. With CT study, determining the depth of the ethmoid roof is crucial for planning the upper limit of the dissection and providing a road map for the surgical procedure and assisting in avoidance surgical manipulation.

In anatomical study of 450 skulls by Keros, type 1 was found in 12%, type 2 in 70% and type 3 in 18 %.

As compared to Keros study, we find the difference in the distribution of the Keros type. Our study shows that Keros type 1 is the most frequent type, 89.33%, followed by type 2, 12.67%. There is no type 3 at all. Our finding is the same as Paber et al study in Philippine (109 patients) which classified 81.6% of the sides as Keros type 1 and 17.9% as type 2. Only 1 case (0.5%) was classified as type 3. Distribution and percentage of Keros type in different studies are seen in Table 6.

The average of the LLCP height in our study is 2.15 mm. The study from Philippines showed 2.11 mm.

Melani et al determined the mean LLCP height to be 5.9 mm. in subjects from Italy. Alazzawi et al found a mean height of 2.64 mm. in the study from Malaysia, China and India and Kaplanoglu et al reported a mean height of 4.92 mm. from Turkey.

Analysis the results from Table 6 and average values of LLCP height from many studies support and strengthen the hypothesis that the ethmoid roof configuration varies between populations.

Comparison between gender, our study shows no different regards to the mean LLCP height or in terms of the distribution of Keros classification. These findings are the same as Kaplanoglu et al study.

There is also no significant difference between the mean height or distribution of Keros type of the right and left side. Therefore the risk of intracranial entry through the lateral lamella during ESS is the same regardless of laterality.

About the ethmoid roof configuration, there

Table 6 Distribution and percentage of Keros classification in different studies.

Study	Country	Number of sides	Keros type		
			1 (%)	2 (%)	3 (%)
Present	Thailand	150	87.33	12.67	0
Paber et al (10)	Philippines	218	81.6	17.9	0.5
Alazzawi et al (12)	Malaysia, China, India	300	80.0	20.0	0
Elwany et al (12)	Egypt	600	42.5	56.8	1.4
Souza et al (11)	Brazil	400	26.3	73.3	0.5
Salaries et al (12)	USA	100	83.0	15.0	2.0
Keplanoglu et al (12)	Turkey	1000	13.4	76.1	10.5

are 36.7% of cases that show different in LLCP height. However there are only 8% of cases that show angulation of the ethmoid roof.

In conclusion, this study evaluates the height, classification and configuration of the ethmoid roof and analyzes the difference between gender and side. In this study, Keros type 1 is the most frequent type. Only 8% of cases showing angulation of the ethmoid roof is observed. That means there may be low risk of inadvertent intracranial entry during ESS procedure in Thai patients. However the sample size is not enough to represent Thai people. Further collection of cases is recommended. Moreover the careful pre-operative evaluation of the anatomy of each patient is still crucial for the surgeon. The LLCP height and presence of ethmoid roof asymmetry must be included in the routine description of CT reports.

References

1. Luong,Marple BF. Sinus surgery: indications and techniques. *Cli Rev Allergy Immunol* 2006;30:217-22.
2. Dessa P,Castro F,Trigia JM,Zanaret M, Cannoni M. Major complications of sinus surgery: a review of 1192 procedures. *J Laryngol Otol* 1994;108:212-5.
3. McMains KC.Safety in endoscopic sinus surgery. *Curr Opin Otolaryngol Head Neck Surg* 2008;16:247-51.
4. Ulualp SO.Complications of endoscopic sinus surgery : appropriate management of complications: *Curr Opin Otolaryngol Head Neck Surg* 2008;16:252-9.
5. Stammberger HR, Kennedy DW. Paranasal sinuses: anatomic terminology and nomenclature. The Anatomic Terminology Group. *Ann Otol Rhinol Laryngol Suppl* 1995;167:7-16.
6. Kainz J Stammberger H. The roof of the anterior ethmoid:a locus minoris resistentiae in the skull base.*Laryngol Rhinol Otol (Stuttg)*.1988;67:142-9.
7. Ohnishi T, Tachibana T,Kaneko Y,Esaki S. Higgh risk areas in endoscopic sinus surgery and prevention of complications *Laryngoscope* 1993;103:181-5.
8. Basak S, Karaman CZ, Akdilli A, et al. Evaluation of some important anatomical variations and dangerous areas of the paranasal sinuses by CT for safer endonasal surgery. *Rhinology*.1998;36:162-7.
9. Rei M, Rei G. Height of Right and Left ethmoid roofs: Aspects of Laterality in 644 Patients. *Int J Otolaryngol* 2011;508907
10. Paber J et al. Radiologic Analysis of the Ethmoid Roof based on KEROS classification among Filipinos. *Philippine Journal of Otolryngology-Head and neck Surgery*. 2008;23:15-9.
11. Solza S. et al. Computed tomography assessment of the ethmoid roof:a relevant region at risk in endoscopic sinus surgery. *Radiol.Bros*.2008;41(3):143-7.
12. Kaplinoglu H.et al.An analysis of the Anatomic Variations of the Paranasal sinuses and Ethmoid Roof Using Computed Tomography. *Eurasian j Med*.2013;45:115-25.



Two Case Reports of Madelung's Disease: CT Finding.

Chanpen Buranachokpaisan, MD.

Department of Radiology, Buddachinnaraj Hospital, Phitsanulok, Thailand.

Abstract

Madelung's disease or Benign symmetric lipomatosis is the rare disease that is the one of differential diagnosis of palpable neck mass that easily diagnosis by CT imaging. We report two cases of this condition and review the radiological findings.

Key words: Madelung's disease, Multiple symmetric lipomatosis (MSL), Launois-Bensaude Syndrome

Introduction

Madelung's disease is a rare condition characterized by the growth of fatty masses in different parts of the body in a very specific pattern or distribution. The disease frequently affects men with a Mediterranean origin between the ages of 30 and 70 with a history of alcohol abuse. Non-alcoholics and women are also affected. The signs and symptoms are varying greatly from person to person. The disease may cause cosmetic deformity, movement limitation, and peripheral neuropathy. The serious complication is airway obstruction. The disease is benign condition that unknown cause but most strongly associated with alcohol consumption. However, there is a reported case in which became liposarcoma. The treatment might include reduced alcoholic intake, correct metabolic conditions and surgery to remove lipomas in cases of mass effect or cosmetic concerned⁽¹⁾. We report two cases of the Madelung's disease in Asian countries and review the radiological findings.

Case report

Case 1

A 43-year old man presented with painless left neck mass with progressive growth for 1 year. The physical examination revealed an ill-defined mass at left upper neck and submandibular area approximately 6 cm and an ill-defined mass at right upper neck about 3 cm, other ENT examinations are within normal limits. No neurological deficit or muscular weakness is noted. Past history of heavy alcohol consumption for 20 years and was a nonsmoker. No other underlying disease was noted.

Laboratory test results were the following: Hb 12.8 g/dl ; Hct 40%; MCV 82.3 fl; MCH 26.2 pg; MCHC 31.8 g/dl; RDW 15.5%; WBC 8540/mm³ (Neu 67%, mono8%, lymph 23%, Eos 1%) ; platelet 222,000/mm³; Anti-HIV negative. A liver ultrasound showed mild liver enlargement with diffuse fatty infiltration.

Multi-Detector Computed Tomography (MDCT) scan showed excessive fat deposit diffusely in sub-

37270
10/2008 08:55:00Ring.25/50
Frame:1/1
11.09 : 1 (LY 100)
112%

Fig. 1A

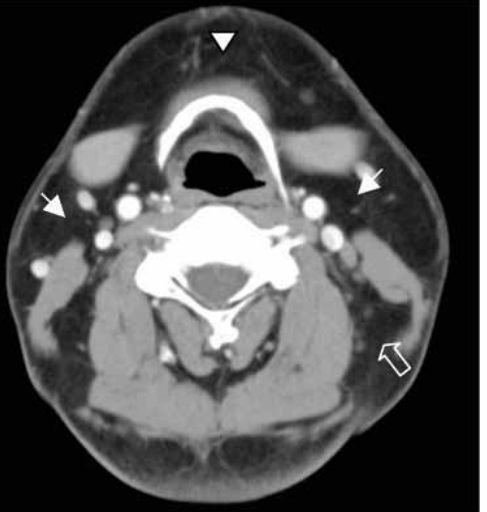


Fig. 1B

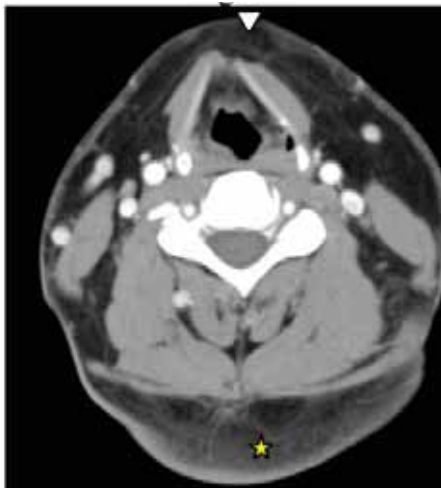


Fig. 1C



Fig. 1D



Fig. 1E



Fig. 1F

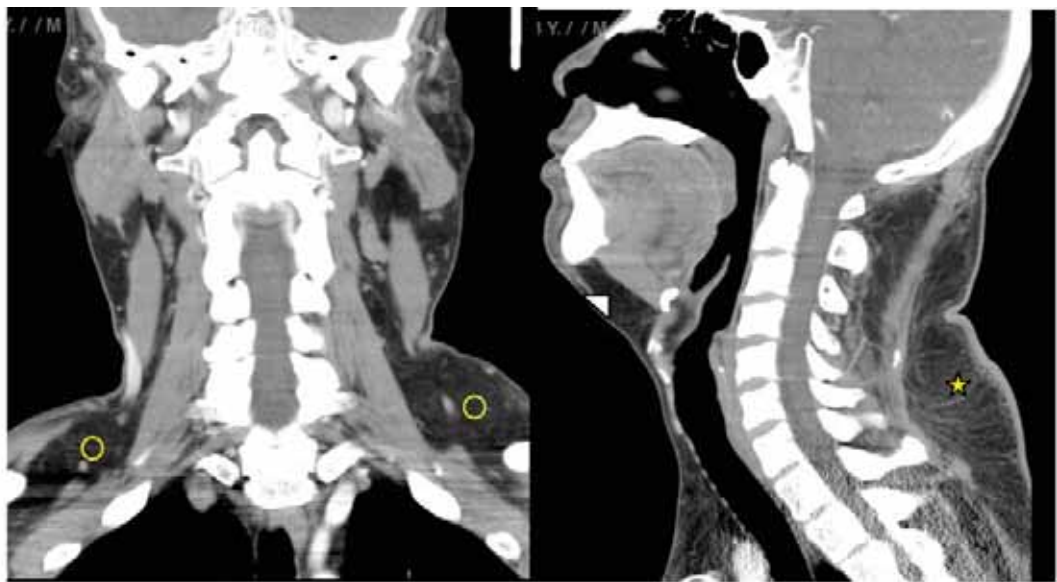


Fig. 1G

Fig 1H

Figure.1 1A - 1D axial views and Figure. 1E - 1H coronal reconstruction of CT study showed excessive fat deposit diffusely in subcutaneous tissue of both cheeks and bilateral carotid spaces (small white arrow), the anterior part of neck (arrow head) , above and below bilateral sternocleidomastoid muscles (blank arrow), paraspinal muscles, bilateral posterior triangles (yellow circle) and posterior aspect of the neck (star), predominately on the left sided.

cutaneous tissue of the anterior part of neck (suprahyoid, infrahyoid, interclavicular and superior mediastinal regions), both cheeks, bilateral carotid spaces, above and below bilateral sternocleidomastoid muscles, bilateral posterior triangles, paraspinal muscles and posterior aspect of the neck and bilateral supraclavicular regions, predominately at left sided. A clinical diagnosis of Madelung's disease type I was made. (Figure 1A-H)

Since our patient was asymptomatic, no surgical treatment was proposed. He was started on lipid-lowering therapy and referred to an alcohol detoxification program.

Case 2

A 47-year old man presented with bilateral cervical neck masses for 2 years. No dysphagia, odynophagia or weight loss was noted. The patient

had a history of longstanding alcohol consumption more than 10 years and was a nonsmoker. The physical examination showed generalized soft tissue masses at both cervical necks. The ENT examination was normal. Both lungs were clear. No neurological deficit or myelopathy.

The Laboratory results were only; BUN = 12 mg/dl, Cr = 0.75 mg/dl and eGFR = 118.84 cc/min.

Multi-Detector Computed Tomography (MDCT) scan revealed generalized excessive fat density deposition at chin, cervical paraspinal and surrounding all anterior, lateral and posterior necks without definite mass, cyst or calcification. The clinical diagnosis of Madelung's disease type I was also noted (Fig 2A-F). This patient was also asymptomatic, just reassuring and no surgical treatment was performed. He was started in a reduced lipid and alcohol intakes and exercise program.

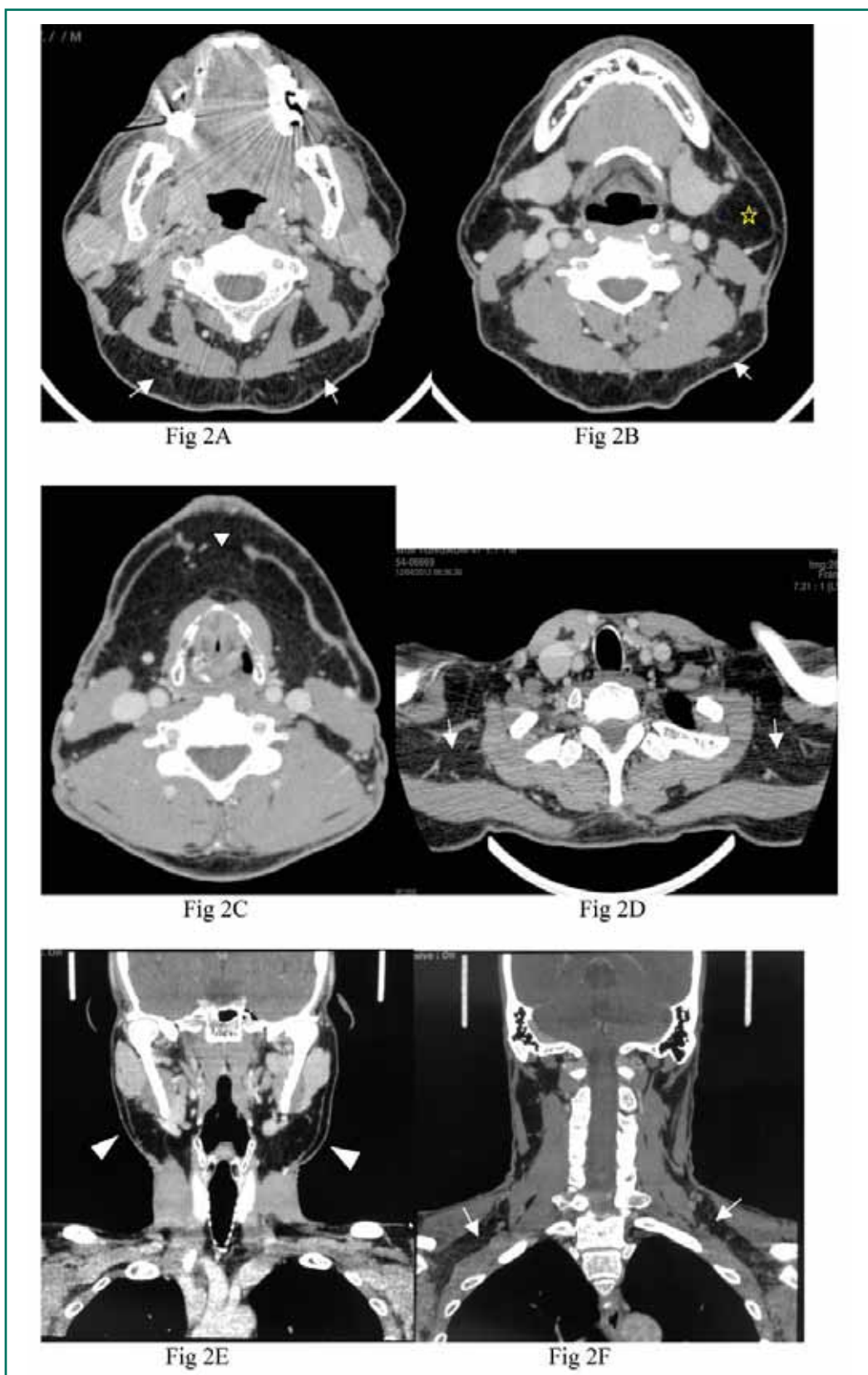


Figure 2. 2A - 2D Axial CT scan, Figure 2E and 2F Coronal reconstruction MDCT scan of the neck revealed generalized excessive fat density deposition at both cheeks (star), chin (arrow head), paraspinal region and surrounding all anterior, lateral and posterior necks (small white arrow)

Discussion

Multiple symmetric lipomatosis was first described in 1888 by the German surgeon Otto Madelung. Several years later, Lanois and Bensaude described a further case series of the same entity, which is now referred to as Madelung's disease, Launois-Bensaude syndrome, benign symmetric lipomatosis or cephalothoracic lipodystrophy^(2,3). This is a rare disorder of unknown cause. In reported case series, up to 90% of patients have a history of chronic alcoholism, and there is a strong male predominance⁽⁴⁾. There is a predilection for people from the Mediterranean^(2,5) and not much in oriental countries⁽⁶⁾. The signs and symptoms of Madelung's disease vary from person to person. The deposits present in the disease typically occur around the face, the back of the head, the neck, the upper arms, the abdomen, and the back and upper parts of the leg in a very specific pattern or distribution, rarely tongue, mediastinal or below knee involvement occurs. Often, the disease has a period of rapid growth following by a period of stabilization, without spontaneous resolution. Unlike the usual lipoma, these benign fatty masses are not enclosed within a membranous capsule with very distinct boundaries that are often dismissed as simple obesity. It has been divided into three types: Type I or diffuse lipomatosis of the neck (horsecollar lipomata); Type II or multiple symmetric lipomata of the shoulder girdle, the upper arms, the thorax, the thighs and sometimes the abdomen (pseudoathletic appearance); and Type III or a rare type with preponderance of the lipomatosis in the thigh girth (gynecomastoid type). Women tend to have Type II and III⁽⁷⁾. The most common complaint is the significant cosmetic deformities. However, some patients also complain of movement limitation and neurological dis-

turbances such as weakness, areas of paresthesia as well as autonomic nervous system manifestations such as unusual flushing and sweating (particularly after eating), wide fluctuations in blood pressure and heart rate, adult onset asthma, glucose intolerance, gastrointestinal problems (particularly nocturnal diarrhea), difficulty swallowing, hoarseness, sleep problems and foot problems such as ulcers on the plantar surface of the foot or spontaneous fractures of small bones. The only serious condition is laryngeal involvement causing respiratory obstruction. The prognosis is probably more dependent on the associated alcoholism.

The differential diagnosis includes obesity, steroid adiposity, hamartomatous polyposis, adiposis dolorosa (Dercum's disease: multiple painful lipomas) and lipomas. There is also one reported case of spontaneous transformation of Madelung's disease into liposarcoma. From the radiological point of view, this can be problematic because of difficulties in distinguishing between lipoma and well-differentiated liposarcoma⁽²⁾.

The exact cause of Madelung's disease remains unknown, but several theories have been proposed. The condition may also relate to another type of an enzyme defect, or a change in the surface of cells, that prevents the breakdown of fat. Some study suggests that the disease is an endocrine disorder due to inability to properly metabolize fat in affected individuals. One published data suggest that children with similar findings might have an underlying mitochondrial dysfunction⁽²⁾. There have been some cases reported among women as well as in nonalcoholic males and females. Alcohol consumption may play an important role in any of these potential causes. Blood studies tend to be quite normal. CT scan and MRI demonstrate the pres-

ence of the fatty masses that helpful in diagnosis. However, biopsy of a fatty mass with underlying muscle tissue, and the identification of specific pathology, is significant in confirming a diagnosis⁽⁸⁾.

The most effective treatment for Madelung's disease is surgery (surgical excision and/or liposuction). Liposuction has gained popularity in more recent years due to its minimal scarring, less invasive, technically easier, and better suited for individuals with a higher surgical or anesthetic risk but its limitation for inadequate aspiration of lipoma. Some researchers believe it is unnecessary to take surgical risk because the condition is usually benign. The surgical excision should be limited to those with airway compression or severe cosmetic deformities. Reportedly, it is rarely possible to remove the lipomas completely. Some studies have reported successful treatment with salbutamol, which increases the breakdown of lipids (lipolysis). Abstaining from alcohol intake, weight loss, and correction of any associated metabolic/endocrine abnormalities are recommended ⁽¹⁾.

Conclusion

Madelung's disease is a rare benign slowly progressive disorder but associated with a significant morbidity and mortality, particular respiratory obstruction. Surgical treatment should be performed only in case of airway compression or severe cosmetic deformities. Abstinence from ethanol ingestion and corrected metabolic disorder could relief the affection.

References

1. National Center for Advancing Translational Sciences (NCATS). National Institutes of Health (NIH). Genetic and Rare Diseases Information Center. Madelung disease. Available from: <http://rarediseases.info.nih.gov/gard/6957/madelung-disease/resources/1> (http://rarediseases.info.nih.gov/benign_symmetrical_lipomatosis)
2. Gutzeit A, Binkert C, Schmidt S, Jandali A, Mutschler J, Hergan K, et al. Growing fatty mass in the back: diagnosis of a multiple symmetric lipomatosis (Madelung's disease) in association with chronic alcoholism. *Skeletal Radiology* April 2012, Volume 41, Issue 4, pp 489-490. Available from: <http://link.springer.com/article/10.1007%2Fs00256-011-1280-6>
3. MedicineNet.com. <http://www.medterms.com/script/main/art.asp?articlekey=9399>
4. Ampollini L, M.D., Carbognani P, M.D., Ph.D. Madelung's Disease N Engl J Med 2011; 364:465 February 3, 2011 DOI: 10.1056/NEJMcm1003531
5. Bulum T, Duvnjak L, Car N, Metelko Z. MADELUNG'S DISEASE: CASE REPORT AND REVIEW OF THE LITERATURE. Vuk Vrhovac University Clinic, Zagreb, Croatia. *Diabetologia Croatica* 36-2, 2007
6. บริ๊ด เงาเทพพฤฒาราม. พป. Madelung's Disease (Multiple Symmetric Lipomatosis). J Prapokkla Hospital Clin Med Educat Center. Vol. 25 No. 2 Apr.-Jun. 2008
7. Herbst K, PH.D., M.D. Madelung's disease <http://www.lipomadoc.org/madelungs-disease.html>
8. J:\benign symmetrical lipomatosis\MSL, Multiple Symmetrical Lipomatosis, also known as Benign Symmetric Lipomatosis or Madelung's Disease and Lanois-Bensaude Syndrome-Cushing's Help and Support.mht, Available from: <http://www.cushings-help.com/madelung.htm>



Cerebral Hemorrhage and Femoral Neck Fracture as Initial Presentations of Hepatocellular Carcinoma

Patanee O'Charoen, MD.

Division of Radiology, Bangkok Metropolitan Administration General Hospital, Department of Medical Services, Bangkok Metropolitan Administration, Pomprap, Pomprapsattrupai, Bangkok 10110, Thailand

Abstract

Hepatocellular carcinoma (HCC) is the most common primary liver tumor and one of the most common causes of cancer-related death in Thailand, particular in male. Extrahepatic metastases are common but usually diagnosed after detection of HCC. These reported cases presented with cerebral hemorrhage and femoral neck fracture which are rare initial presentations of HCC.

Introduction

Hepatocellular carcinoma (HCC) is the most common primary liver tumor and one of the most common causes of cancer-related death worldwide, particular among males in Asia-Pacific region including Thailand.¹⁻⁵ This may be related to high prevalence of hepatitis B virus and hepatitis C virus infections in this region.⁶ HCC is a devastating tumor known for its propensity to directly invade the portal and hepatic veins, but lymphatic and distant metastases are not rare, especially in tumors greater than 5 cm.⁷ Extrahepatic metastases are seen in 13-64%, and common metastatic sites are lungs,

lymph nodes, bones and adrenal glands, respectively.⁸⁻¹¹ Brain metastasis from HCC is extremely rare with a reported frequency ranging from 0.2-2.2%, with utterly poor prognosis.¹²⁻¹⁵ Bone metastasis is commonly seen in the vertebrae.^{9,16,17} It is usually diagnosed after detection of HCC, and rarely developed pathological fracture as the first clinical manifestation.¹⁷⁻²¹

Case reports

Case I : Thai male presented with left hemiparesis. CT scan of the brain revealed a 4 cm round

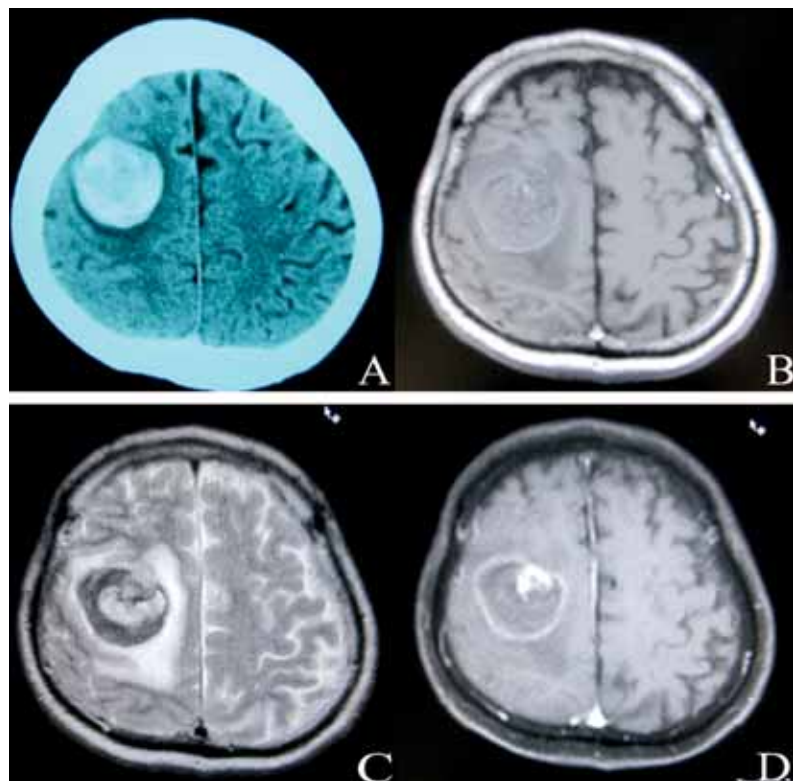


Fig 1. Axial CT scan of the brain (A) revealed a 4 cm round hyperdense lesion at right high frontal lobe. The lesion showed mostly iso SI on T1-weighted image (B), mixed SI on T2-weighted image (C) and enhancement after gadolinium administration (D). Perilesional edema is evident.

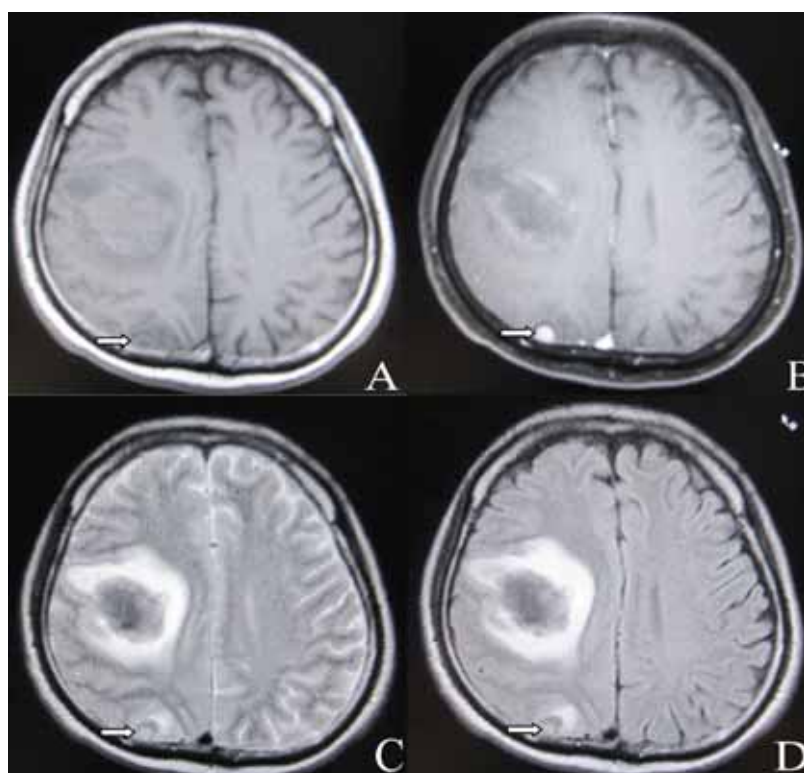


Fig 2. Axial T1-weighted image (A), post gadolinium T1-weighted image with fat saturation (B), T2- weight image (C), and FLAIR (D) demonstrated a 0.8 cm round lesion at posterior aspect of right parietal lobe (arrows) showing same SI as the large lesion in right frontal lobe with homogeneous enhancement and surrounding edema.

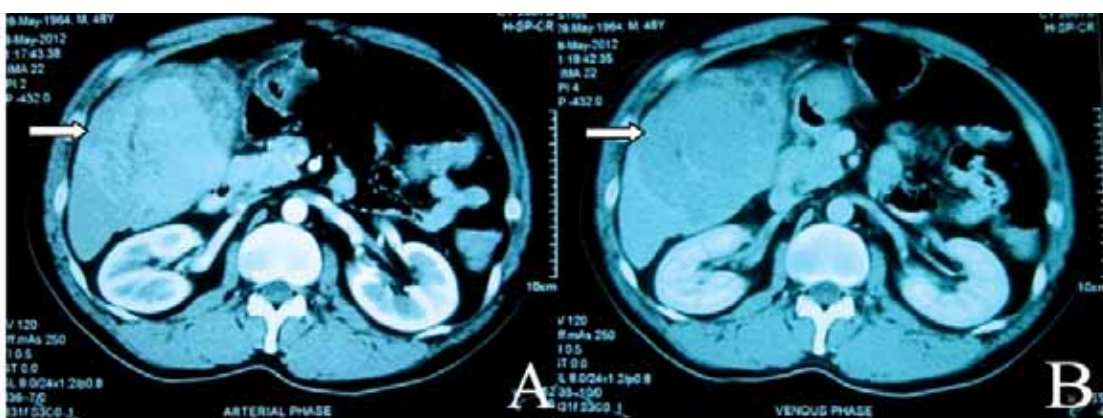


Fig 3. Post-contrasted CT scan of the abdomen, arterial phase (A) and venous phase (B) revealed a large mass at right hepatic lobe showing arterial enhancement and rapid washout (arrows).

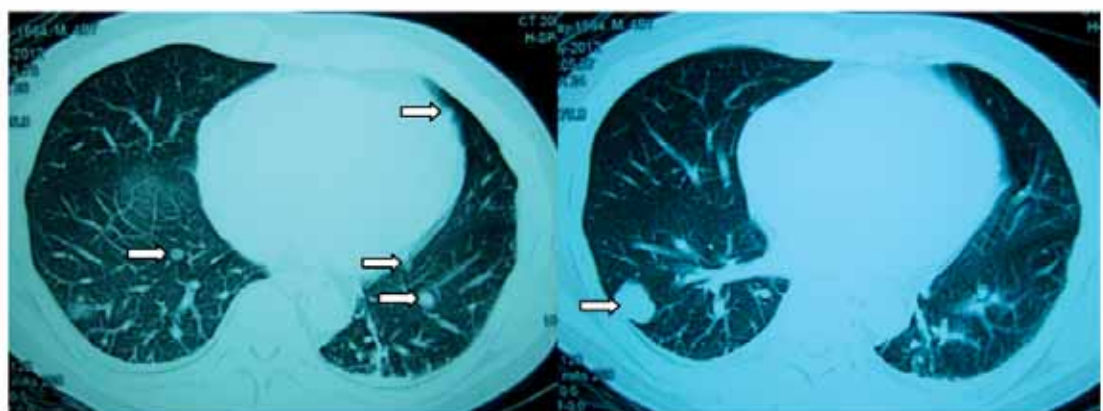


Fig 4. CT scan of the chest showed multiple nodules in both lungs (arrows).

hyperdense lesion with perilesional edema at right high frontal lobe consistent with hemorrhage (Fig 1A). MRI of the brain (Fig 1B-D) showed a 4x3.3 cm lesion at right high frontal lobe showing slightly low signal intensity (SI) on T1-weighted image, dark SI on T2-weighted image, FLAIR and gradient echo image with areas of high SI at anteromedial aspect, rim enhancement and small area of enhancement at anterior aspect. Marked surrounding edema was observed causing effacement of adjacent cortical sulci and midline shift to the left about 0.4 cm. There was a 0.8 cm round lesion at posterior aspect of right parietal lobe showing same SI with intense homogeneous enhancement and mild sur-

rounding edema (Fig 2). These two lesions were considered hemorrhagic metastases.

Laboratory findings showed positive HBsAg, Anti HBs, Anti HBc, Anti HCV, and negative HBeAg. Tumor markers were as following : AFP 5268 (0-7.02) ng/ml, PSA 0.51 (0.59-2.0) ng/ml, CA19-9 102.40 (0-37) U/ml, CA125 84.41 (0-35) U/ml, CEA 4.62 (0-4.6) ng/ml.

CT scan of the abdomen revealed multiple hepatic masses showing arterial enhancement and rapid washout. The largest mass was in right hepatic lobe (Fig 3). CT scan of the chest showed multiple nodules in both lungs consistent with pulmonary metastases (Fig 4).



Fig 5. Plain radiograph of right hip revealed osteolytic lesion at femoral neck with pathologic fracture (arrow).

Right frontal parasagittal craniotomy with clot and tumor removal was performed. Pathological and immunohistochemical report showed metastatic adenocarcinoma and the most possible diagnosis was HCC. Patient received whole brain radiation after surgery and the patient died a few months later.

Case II : A 55-year-old, Thai male presented with right hip pain after sound at right hip while wearing slacks for 2 weeks. He has underlying diabetes mellitus and hypertension. Plain radiograph of right hip revealed osteolytic lesion at femoral neck with pathologic fracture (Fig 5). Hemiarthroplasty of right hip was performed and pathology revealed anaplastic cells in organoid patterns, suggesting HCC.

Laboratory findings revealed RBC 2.53x1,000,000/mm³, Hb 8.1 g/dl, Hct 23.2%, WBC 12.8 x1,000/mm³ (neutrophil 78.1%, lymphocyte 10.9%, monocyte 9.2%, eosinophil 0.9%, basophil 0.9%), platelet count 641,000/mm³, total protein 7.0 (6-8

g/dl, albumin 3.0 (3.5-5.6) g/dl, globulin 4.0 (1.3-3) g/dl, total bilirubin 1.44 (0-1.5) mg/dl, direct bilirubin 0.27 (0-0.5) mg/dl, indirect bilirubin 1.17 (0-1) mg/dl, AST 72 (0-35) U/L, ALT 23 (0-43) U/L, alkaline phosphatase 406 (39-117) U/L, Anti HIV-non reactive, CEA 9.04 (0-4.6) ng/ml, CA 19-9 152 (0-37) U/ml, AFP 70.24 (0-7.02) ng/ml, PSA 0.334 (0.75-3.1) ng/ml.

He developed ascites and right leg edema after operation. Ultrasonography of abdomen was performed and revealed heterogeneously increased parenchymal echo of the liver with a 6.4x4.9x4.8 cm hyperechoic mass with central low echo at left hepatic lobe (Fig 6) and ascites. CT scan of whole abdomen demonstrated hepatic cirrhosis with a 5.8x4.3 cm mass with central necrosis at left lobe (Fig 7). Right portal vein thrombosis with cavernous transformation was observed. Moderate ascites and minimal right pleural effusion were seen.

Patient readmitted with anemia, abdominal distension, infected wound and electrolyte imbalance, and died two months after surgery.

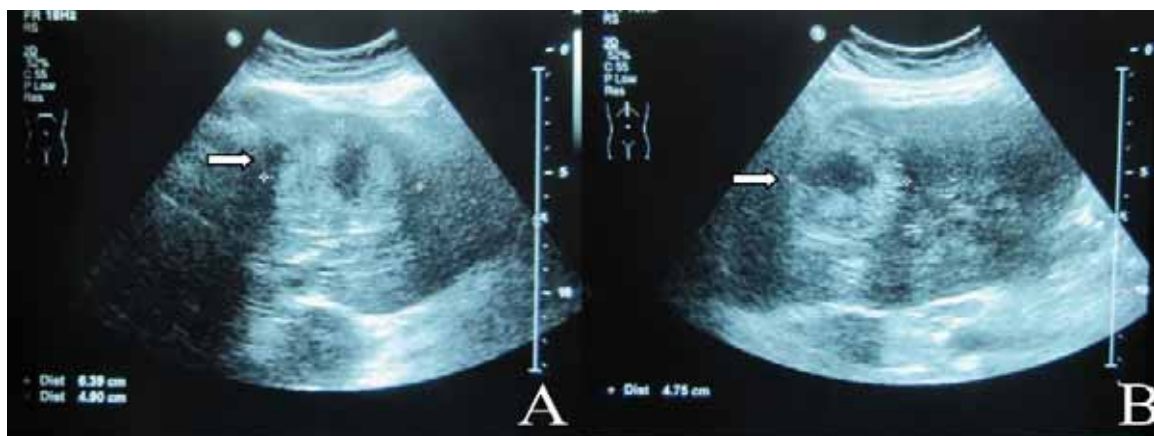


Fig 6. Ultrasonography of abdomen, axial (A) and sagittal (B) showed heterogeneously increased parenchymal echo of the liver with a 6.4x4.9x4.8 cm hyperechoic mass with central low echo at left hepatic lobe (arrow)

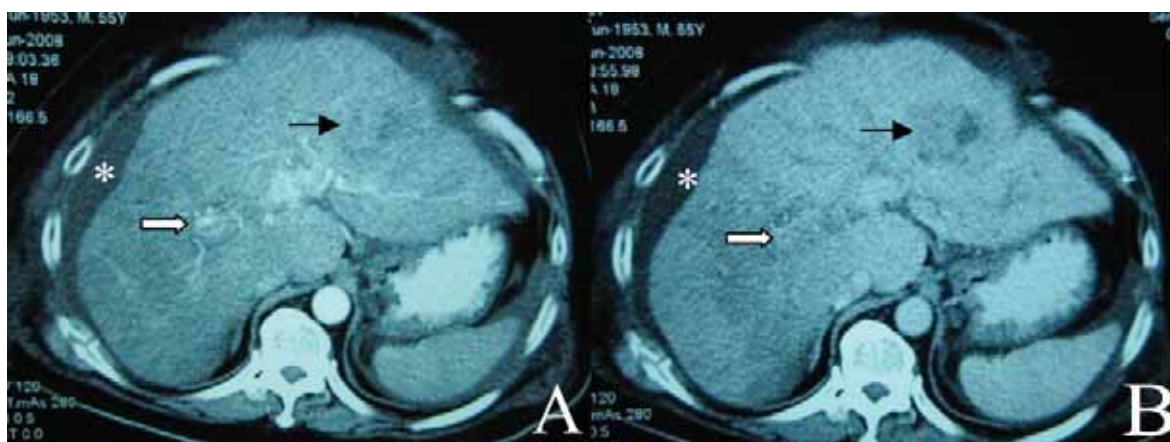


Fig 7. Post-contrasted CT scan of abdomen, arterial phase (A) and venous phase (B) revealed a mass at left hepatic lobe showing arterial enhancement with rapid washout and central necrosis (black arrows). Right portal vein thrombosis with cavernous transformation is shown (white arrows) with heterogeneous enhancement of hepatic parenchyma. Ascites is visualized (*).

Discussion

HCC is still a fatal disease possibly associated with the advanced stage at which the disease is usually diagnosed.^{4,11} HCC spreads locally and metastasizes distally by hematogenous and lymphatic routes. Common metastatic sites are lungs, regional lymph nodes, bones and adrenal glands. Brain and bone metastases as the initial manifestations are extremely rare.

Most of the brain lesions showed hyperdensity on non-contrasted computed tomography and homogeneous enhancement after contrast material administration, with perifocal edema. Some presented with intracerebral hemorrhage and some had skull involvement.^{14,22} The reported Case I manifested with intracerebral hemorrhage with perifocal edema, without skull involvement.

There was no survival difference according to

gender, age, control of HCC, liver function, levels of AFP, CEA and CA19-9, hepatitis virus B infection, intracranial hemorrhage, location and number of brain lesions, and interval between diagnosis of HCC and brain metastasis.¹² Bone metastases from HCC ranged from 3% to 20%.¹⁷ The incidence of HCC with bone metastasis at the time of initial diagnosis was around 5%.²⁰ The most common sites of bone metastases were the vertebra, followed by the pelvis, rib and skull.¹⁷ All the lesions were osteolytic type.^{8,9,17-21} The reported Case II presented with osteolytic lesion at femoral neck and pathological fracture.

In conclusion, brain metastases from HCC are fairly rare and it is even rare to find them as initial manifestation of HCC. Although bone metastasis is not uncommon but it is also rare to find bone metastasis as the first overt manifestation of HCC. The reported cases presented with cerebral hemorrhage and fracture femoral neck as initial manifestations of HCCs, thus, patients present with osteolytic bone lesions or hemorrhagic brain metastases, HCC should be included in the differential diagnosis, particular in Thai male.

References

1. Jemal A, Ward E, Hao Y, Thun M. Trends in the leading causes of death in the United States, 1970- 2002. *JAMA* 2005 Sep;294(10):1255-9.
2. Bosch FX, Ribes J, Diaz M, Cleries R. Primary liver cancer: worldwide incidence and trends. *Gastroenterology* 2004 Nov;127(5 suppl):S5-S16.
3. Srivatanakul P, Sontipong S. Incidence of liver cancer in Thailand 1979. *Thai Cancer J* 1979;8:127-34.
4. Kassianides C, Kew MC. The clinical manifestations and natural history of hepatocellular carcinoma. *Gastroenterol Clin N Am* 1987 Dec;16(4):553-62.
5. Jemal A, Bray F, Center MM, Ferlay J, Ward E, Forman D. Global cancer statistics. *CA Cancer J Clin* 2011 Mar-Apr;61(2):69-90.
6. Perz JF, Armstrong GL, Farrington LA, Hutin YJ, Bell BP. The contributions of hepatitis B and hepatitis C virus infections to cirrhosis and primary liver cancer worldwide. *J Hepatol* 2006 Oct;45(4):529-38.
7. Yuki K, Hirohashi S, Sakamoto M, Kanai T, Shimosato Y. Growth and spread of hepatocellular carcinoma. *Cancer* 1990 Nov;66(10):2174-9.
8. Sneag DB, Krajewski K, Giardino A, O'Regan KN, Shinagare AB, Jagannathan JP, Ramaiya N. Extrahepatic spread of hepatocellular carcinoma: Spectrum of imaging findings. *AJR* 2011 Oct;197(4):W658-64.
9. Katyal S, Oliver JH 3rd, Peterson MS, Ferris JV, Carr BS, Baron RL. Extrahepatic metastasis of hepatocellular carcinoma. *Radiology* 2000 Sep;216(3):698-703.
10. Tang ZY. Hepatocellular carcinoma-cause, treatment and metastasis. *World J Gastroenterol* 2001 Aug;7(4):445-54.
11. Sithinamsuwan P, Peratvisuth T, Tanomkiat W, Apakupakul N, Tongyoo S. Review of 336 patients with hepatocellular carcinoma at Songklanagarind Hospital. *World J Gastroenterol* 2000 June;6(3):339-43.
12. Jiang XB, Ke C, Zhang GH, Zhang XH, Sai K, Chen ZP, Mou YG. Brain metastases from hepatocellular carcinoma: clinical features and prognostic factors. *BMC Cancer* 2012 Feb;12:49.
13. Kim M, Na DL, Park SH, Jeon BS, Rah JK. Nervous system involvement by metastatic hepatocellular carcinoma. *J Neurooncol* 1998 Jan;36(1):85-90.
14. Choi HJ, Cho BC, Sohn JH, Shin SJ, Kim SH, Kim JH, Yoo NC. Brain metastases from hepatocellular carcinoma: prognostic factors and outcome: brain metastasis from HCC. *J Neurooncol* 2009 Feb;91(3):307-13.
15. Uchino K, Tateishi R, Shiina S, Kanda M, Masuzaki R, Kondo Y, Goto T, Ornata M, Yoshida H, Koike K. Hepatocellular carcinoma with extrahepatic metastasis: Clinical features and prognostic factors. *Cancer* 2011 Oct;117(19):4475-83.
16. Natsuizaka M, Omusa T, Akaike T, et al. Clinical features of hepatocellular carcinoma with extrahepatic metastases. *J Gastroenterol Hepatol* 2005 Nov;20(11):1781-7.

17. Fukutomi M, Yokota M, Chuman H, Harada H, Zaitsu Y, Funakoshi A, Wakasugi H, Iguchi H. Increased incidence of bone metastases in hepatocellular carcinoma. *Eur J Gastroenterol Hepatol* 2001 Sep;13(9):1083-8.
18. Barai S, Bandopadhyaya G, Chumber S, Haloi A, Seith A, Dhanapathi H, Kumar R, Malhotra A. Hepatocellular carcinoma presenting with pathological fracture of vertebra: report of a case. *Eur J Radiology Extra* 2004 Aug;51(2):73-6.
19. Golimbu C, Firooznia H, Rafii M. Hepatocellular carcinoma with skeletal metastasis. *Radiology* 1985 Mar; 154(3):617-8.
20. Liaw CC, Ng kT, Chen TJ, Liaw YF. Hepatocellular carcinoma presenting as bone metastasis. *Cancer* 1989 Oct 15;64(8):1753-7.
21. Raoul JL, Le Simple T, Le Prisé E, Meunier B, Ben Hassel M, Bretagne JF. Bone metastasis revealing hepatocellular carcinoma: a report of three cases with a long clinical course. *Am J Gastroenterol* 1995 Jul;90(7):1162-4.
22. Yen FS, Wu JC, Lai CR, Sheng WY, Kuo BI, Chen TZ, Tsay SH, Lee SD. Clinical and radiological pictures of hepatocellular carcinoma with intracranial metastasis. *J Gastroenterol Hepatol* 1995; 10:413-8



Reports of Four Cases of Hypertrophic Olivary Degeneration in King-Chulalongkorn Memorial Hospital from August 2010 to November 2011

Pra Urusopone M.D., Sasitorn Petcharunpaisan M.D., Sukalaya Lerdum M.D.

Department of Radiology, King-Chulalongkorn Memorial Hospital, Bangkok, Thailand

Abstract

We report four cases of hypertrophic olivary degeneration (HOD), the first three cases after pontine hemorrhage from cavernous malformation, arteriovenous malformation (AVM) and hypertension and the latter one after surgery for removal of Non-Hodgkin lymphoma (NHL) involving dentate nucleus. The magnetic resonance (MR) features of all cases and diffuse tensor imaging (DTI) with fiber tractography findings in one case are described as well as discussion and review literature of this uncommon condition are performed.

Keywords: Hypertrophic olivary degeneration, Dentato-rubral-olivary pathway.

Introduction

Hypertrophic olivary degeneration (HOD) was first described by Oppentieim in 1887.⁽¹⁾ It is a transsynaptic degeneration after injury to the neuronal connections in the dentatorubral olivary pathway or Guillain-Mollaret triangle (GMT) and is regarded as a unique morphologic type of neuronal degeneration because of hypertrophy rather than atrophy of the affected neurons within the inferior olivary nucleus (ION).⁽²⁾

Clinically patients may develop signature syndrome: palatomyoclonus or cyclic jerk at the soft palate, dentatorubral tremor or ocular nystagmus⁽³⁾

The MR imaging features are enlarged size and increased signal intensity (SI) of the ION on T2- weighted image (T2 WI). On DTI there was a

report of decreased volume and the fractional anisotropy (FA) value of the central tegmental tract at the same side of the affected ION by R. Shah et al in Oct 2010.⁽⁴⁾ Another report on 2011 also demonstrated dynamic changes of signal intensity and DTI parameters in all anatomic components of the affected GMT.⁽⁵⁾

For radiologists, familiarity with the characteristic features and understanding the pathophysiology of this degeneration will protect them not to misinterpret this condition as other lesions such as infarction, tumor or demyelinating diseases. In addition, recognition and prompt diagnosis of this condition lead to the appropriate counseling and treatment for the patients who may develop delayed symptoms.

Results

Case 1 :

History : A 32 year old woman with history of bleeding cavernous hemangioma at right sided pons on January 1998. She had undergone suboccipital craniectomy with removal of blood clot. Post operation she had developed right lateral rectus and facial palsy. She had lost follow up since 2003.

On October 2010, she went to the hospital because of vertigo and diplopia. On neurologic examination, she still had right sixth and seventh cranial nerve palsy. Left torsional nystagmus was

also detected. No cerebellar sign or palatomimic clonus was observed.

Imaging : MRI of the brain showed a well defined oval shaped low SI on T1WI and hyper SI on T2 WI with hemosiderin rim at right lateral aspect of dorsal pons with minimal enhancement at the medial part, representing the prior residual bleeding cavernous hemangioma. (Fig.1) The right inferior olfactory nucleus (ION) revealed iso SI on T1WI and hyper SI on T2WI and FLAIR without restricted diffusion or contrast enhancement, compatible with HOD. There was also left cerebellar atrophy. (Fig. 2)

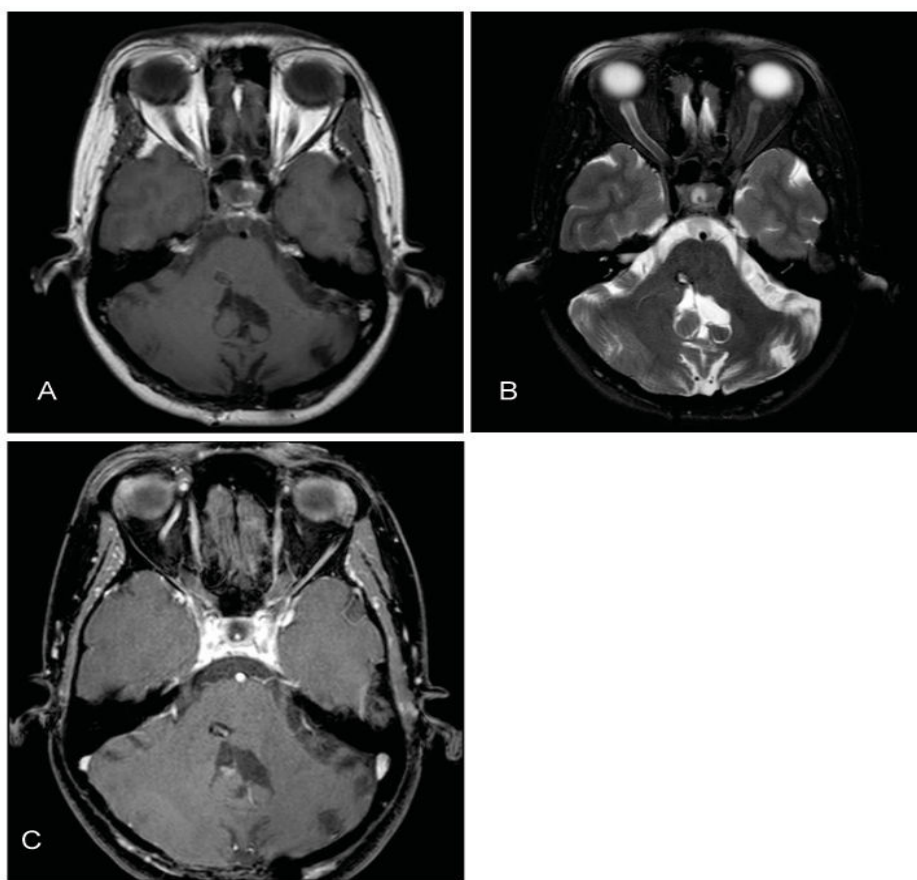


Fig.1 A) T1WI reveals : a well defined hypo SI with hyper SI rim at right sided dorsal pons.
B) T2WI : There is also a hemosiderin rim around the hyper SI lesion.
C) T1WI with contrast shows enhancement at medial part of the lesion.
The findings are compatible with previous bleeding cavernous angioma.

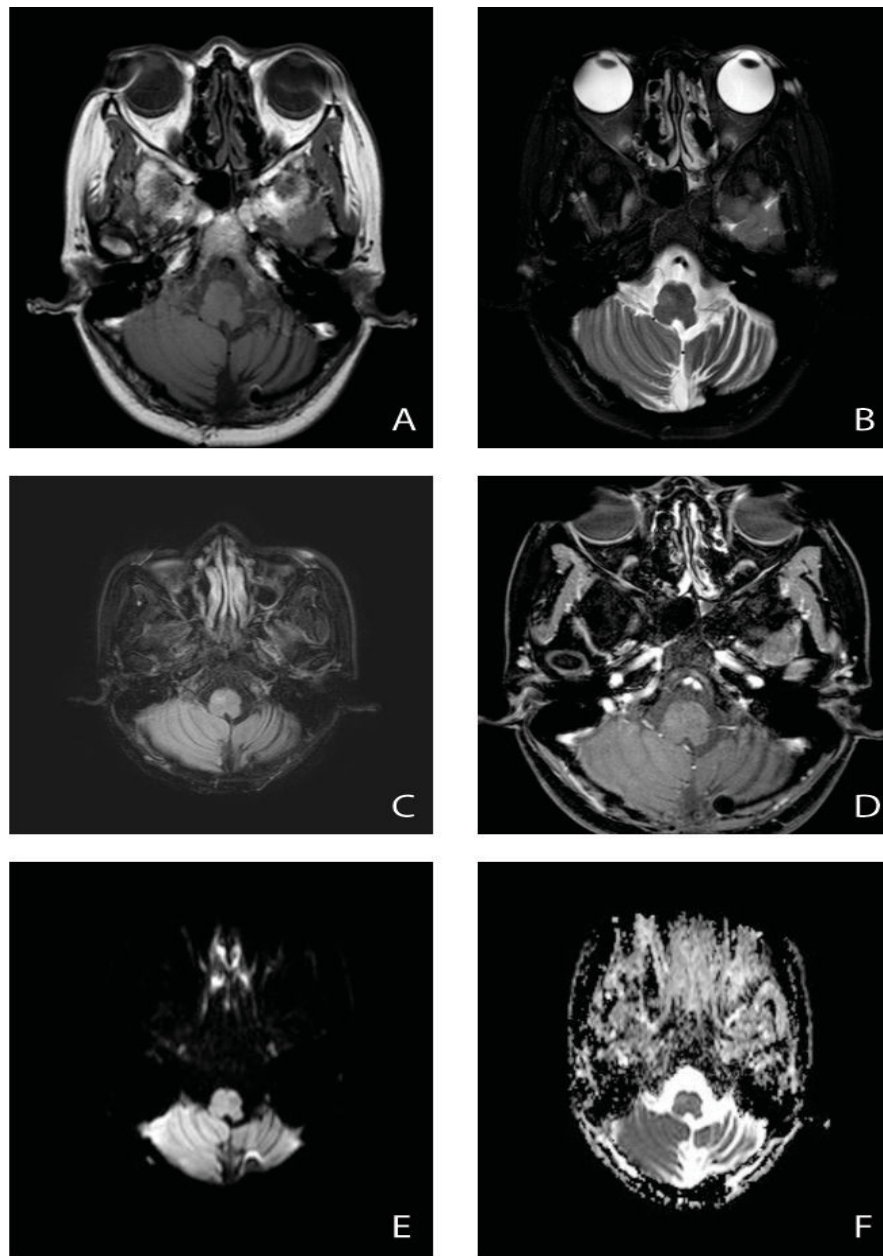


Fig.2 A-F : T1WI, T2WI, FLAIR, T1WI with CE,DWI and ADC reveal an iso SI lesion on T1WI, hyper SI on T2WI and FLAIR without contrast enhancement at right inferior olive. This lesion shows no restrict diffusion or enlargement, so HOD is compatible. There is also evidence of left cerebellar atrophy.

Case 2 :

History : A 30 year old man presenting with diplopia for 2 years after history of intracranial bleeding. On neurologic examination he had bilateral horizontal rotary nystagmus. No ataxia or palatotomyoclonus was observed.

Imaging : MRI revealed a serpigenous flow void lesion at left sided pons and pontomedullary region and a well defined lobulated lesion with hypo

SI on T1WI, mixed hyper and hypo SI on T2WI and blooming SI on GRE T2*WI at left dorsal pons extending to left sided tegmentum of midbrain. DSA findings also demonstrated multiple feeding arteries and draining veins which are highly suggestive of AVM with previous bleeding. There was also evidence of left HOD, showing enlarged size of ION with iso SI on T1WI and hyper SI on T2WI. (Fig. 3)

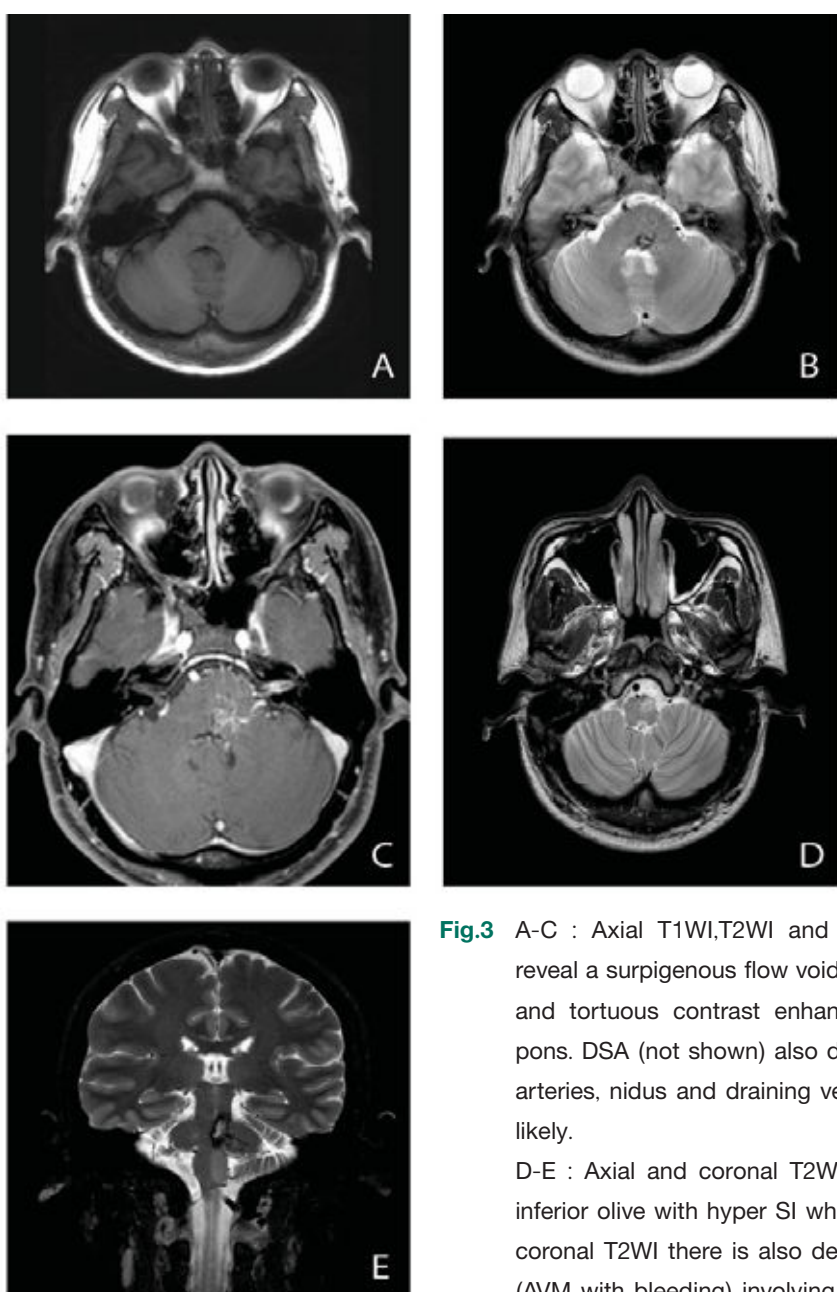


Fig.3 A-C : Axial T1WI,T2WI and T1WI with contrast studies reveal a serpigenous flow void lesions with hemosiderin rim and tortuous contrast enhancement at left sided dorsal pons. DSA (not shown) also demonstrates multiple feeding arteries, nidus and draining veins, so AVM with bleeding is likely.

D-E : Axial and coronal T2WI reveal enlarged size of left inferior olive with hyper SI which is suggestive of HOD. At coronal T2WI there is also demonstrated an inciting lesion (AVM with bleeding) involving left central tegmental tract.

Case 3 :

History : A 75 year old woman with history of a right cerebellar mass detected on December 2009. The patient had had right suboccipital craniectomy with removal tumor. Post operation there had been hematoma at surgical bed. Pathologic result had concluded of NHL. So the patient had been treated by whole brain radiation. During follow up, the patient developed right facial palsy and right pronator drop without palatomysoclonus.

Imaging : First MRI on August 2010 had shown gliotic change at right cerebellum passing through right dentate nucleus without leptomeningeal enhancement. So post operative change without recurrent tumor had been concluded. There had been enlarged size of left ION with iso SI on T1WI and hyper SI on T2W, showing no restricted diffusion or contrast enhancement. (Fig. 4) Second MR findings of left ION on January 2011 were the same to the first study. So left HOD was diagnosed. (Fig. 5)



Fig.4 Case 3: First MRI : A-B) Axial T1WI and T1WI with contrast : Evidence of slitlike hypo SI on T1WI without contrast contrast enhancement at right dentate nucleus is detected. C)Coronal GRE T2*WI also reveals hyper SI with blooming artifact . These findings are suggestive of encephalomalacia with previous bleeding .

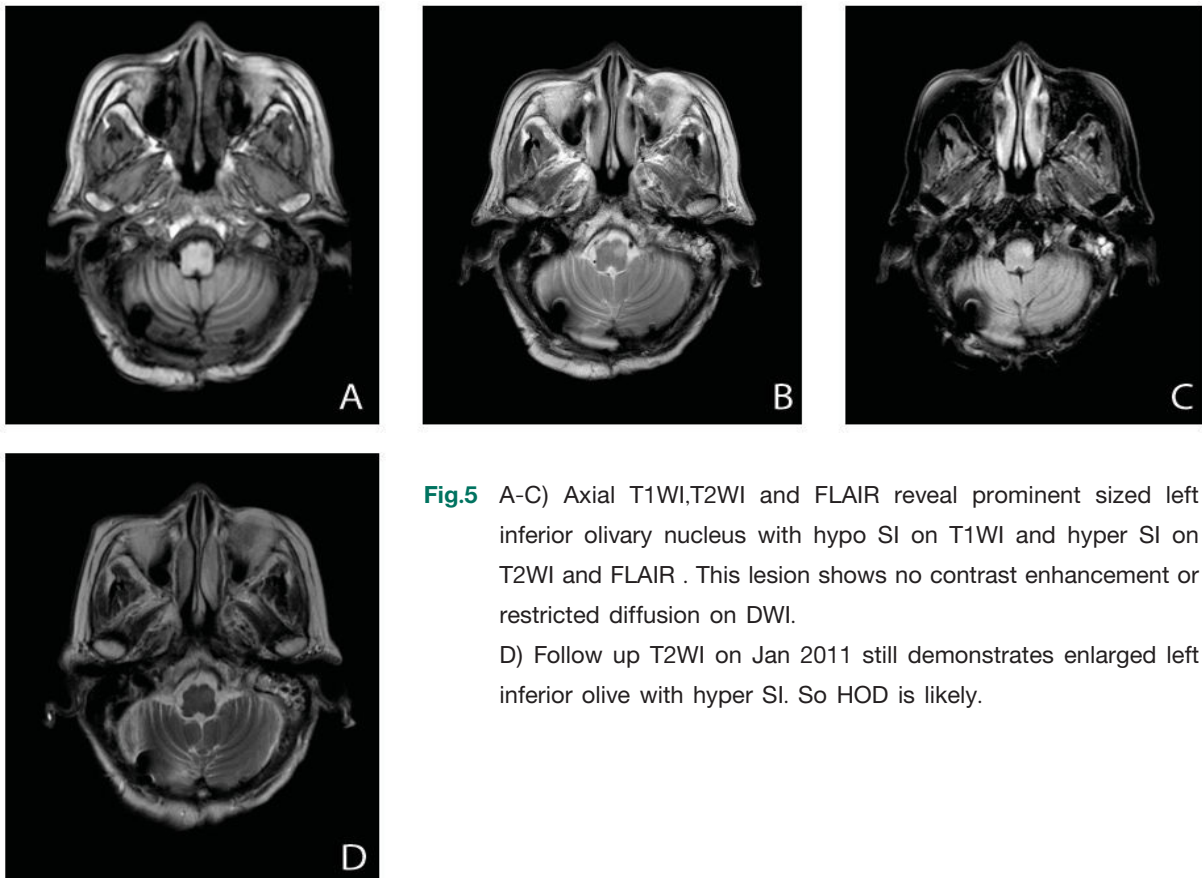


Fig.5 A-C) Axial T1WI, T2WI and FLAIR reveal prominent sized left inferior olivary nucleus with hypo SI on T1WI and hyper SI on T2WI and FLAIR. This lesion shows no contrast enhancement or restricted diffusion on DWI.
D) Follow up T2WI on Jan 2011 still demonstrates enlarged left inferior olive with hyper SI. So HOD is likely.

Case 4 :

History : A female , 64 year of age, with history of hypertensive pontine hemorrhage and a small right parasagittal meningioma two years ago. She had undergone craniectomy with removal the meningioma on February, 2010. Five months later, she presented with pontine hemorrhage again.

Imaging : CT findings on September, 2010 showed a hematoma at pons. (Fig.6) MRI on November 2011 revealed an evidence of hemosiderin deposit along transverse pontocerebellar fibers and dorsal part of pons which was compatible with prior pontine hemorrhage. Prominent size of left ION and signal intensity change representing HOD was also found (Fig.7)

DTI and fiber tractography were performed by placing regions of interest (ROI) on axial slices at five levels. The first level at upper part of midbrain was used for ROI of both red nuclei and then fiber tractography were generated . Evidence of relatively thin left central tegmental tract was detected. (Fig.8) The second level at upper part of pons was used for ROI of both superior cerebellar peduncles. The third to fifth level were at pons through the fifth nerve entry zone for both central tegmental tracts, at medulla through the inferior cerebellar peduncle for both ION and at pons through the middle cerebellar peduncle for both dentate nuclei respectively. (Fig.9) The average FA and apparent diffusion

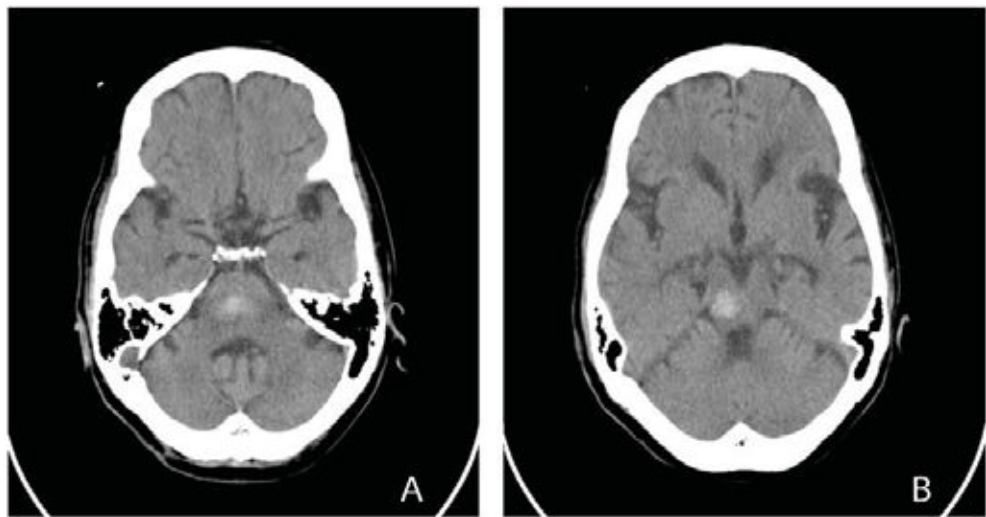


Fig.6 Case 4 A-B) Axial NCECT reveals a hematoma at dorsal pons and right sided midbrain

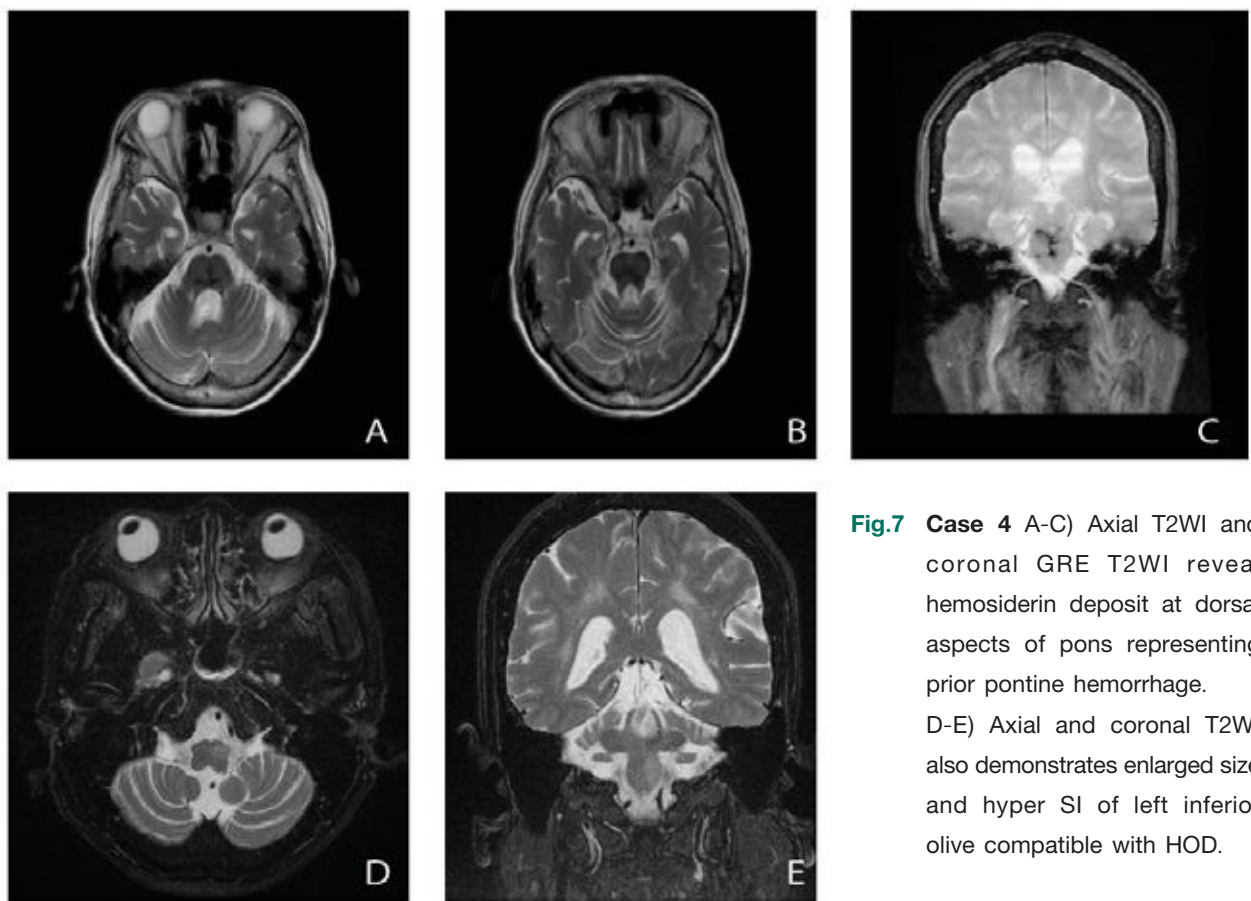


Fig.7 Case 4 A-C) Axial T2WI and coronal GRE T2WI reveal hemosiderin deposit at dorsal aspects of pons representing prior pontine hemorrhage.
D-E) Axial and coronal T2WI also demonstrates enlarged size and hyper SI of left inferior olive compatible with HOD.

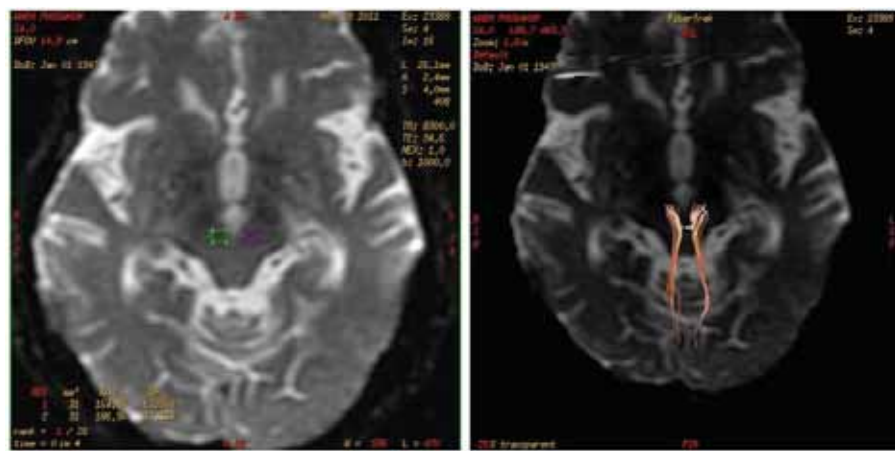


Fig.8 Fiber tractography performed by placing region of interest on both red nuclei . The study shows relatively thin left central tegmental tract.

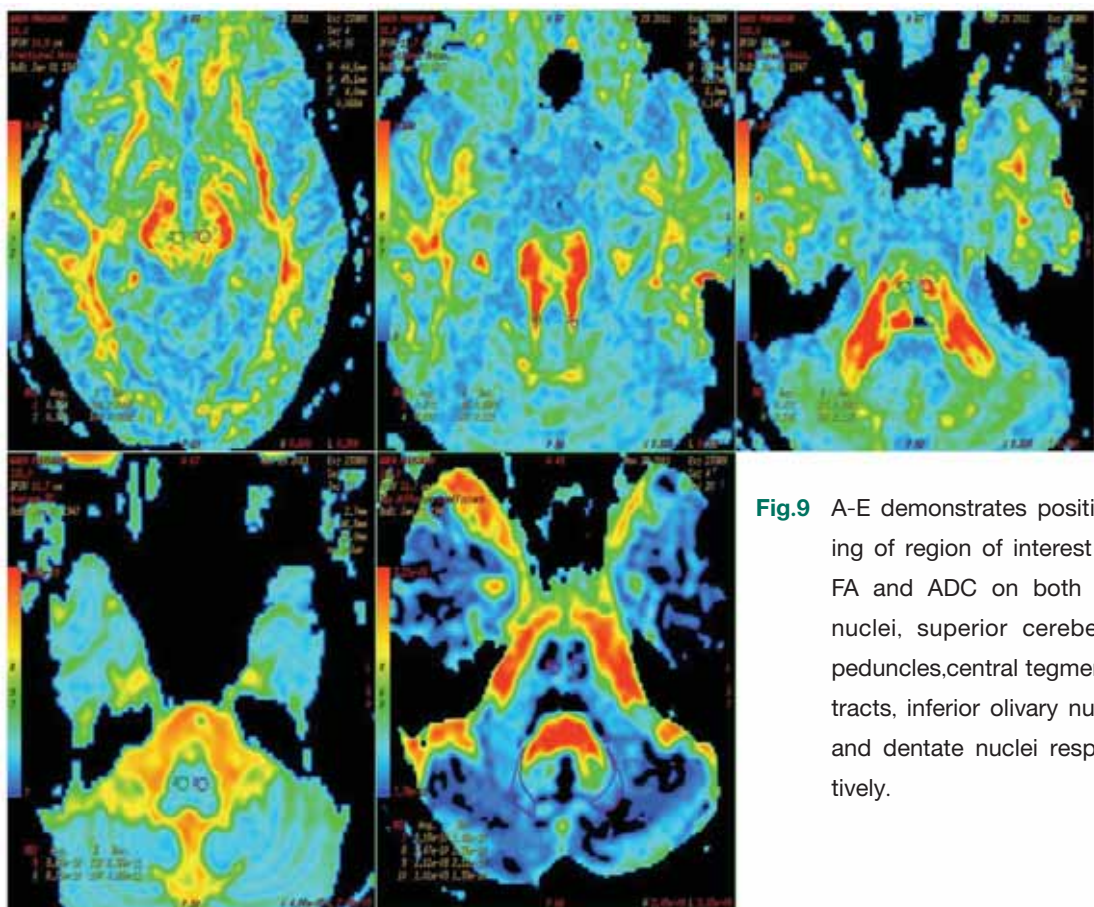


Fig.9 A-E demonstrates positioning of region of interest for FA and ADC on both red nuclei, superior cerebellar peduncles, central tegmental tracts, inferior olfactory nuclei and dentate nuclei respectively.

coefficient (ADC) values of five levels were calculated and summarized as table I.

Demographics and clinical profiles of all patients with HOD are summarized as table II.

Table I

	Average FA		Average ADC	
	RT	LT (lesion)	RT	LT (lesion)
Red nucleus	0.331	0.354 (106%)	8.67	7.42 (85%)
Superior cerebellar puduncle	0.637	0.375 (59%)	1.12	1.56 (138%)
Central tegmental tract	0.597	0.433 (72%)	7.58	8.64 (114%)
Inferior olivary nucleus	0.243	0.122 (50%)	8.19	9.88 (120%)
Dentate nucleus	0.234	0.261 (111.5 %)	9.76	9.23 (94.5 %)

Table II

Patient no.	Age/Sex	Inciting lesion and cause	Palatal tremor	Time of MRI after inciting lesion	Location of HOD	Hypertrophy in ION
1	32/F	Carverous hemangioma with bleeding at Right sided pons	absent	13 years	right	absent
2	30/M	AVM at Left sided pons and pontomedullary region	absent	2 years	left	present
3	75/F	Removal of Right cerebellar Non-Hodgkin lymphoma	absent	1 year/ 8 months and 2 years	left	present
4	64/F	Two episodes of hypertensive hemorrhage at 2 years and 2 months before	absent	2 years of first episode or 2 months of recent bleeding	left	present

Discussion

HOD is a unique type of transsynaptic degeneration with hypertrophy of the affected ION. It represents to the end result of disruption of the components in GMT pathways.^(6,7) Common causes include bleeding injury (hypertensive, cavernous malformation or trauma), neoplasm and demyelination.⁽⁸⁾ This triangle was described by Guillain and Mollaret in 1931.⁽⁶⁾ It consists of three anatomical structures: the ipsilateral dentate nucleus in cerebellum, the contralateral red nucleus in the midbrain and ION in the medulla.

The afferent pathway originates in the contralateral dentate nucleus, passes over the superior cerebellar peduncle, crosses the midline through the inferior colliculi, enters the ipsilateral red nucleus and descends through the central tegmental tract to the ION. The efferent fibers from ION exits out of the hilus medially, crosses the midline and con-

nects to the contralateral dentate nucleus through the contralateral inferior cerebellar peduncle : the olivocerebellar tract. (Fig. 10)⁽⁶⁾ Although the pathway has been described as a triangle, HOD is only the result of the disruption of the afferent fibers, less likely of the efferent ones.⁽⁹⁾

Knowledge of the components of the GMT is essential for understanding how the disruption can influence the ION. Three possible patterns of HOD are described. First the ipsilateral HOD occurs if the lesion involves the red nucleus or central tegmental tract. Secondly, when the lesion is at the dentate nucleus or the superior cerebellar peduncle, the contralateral HOD develops. Finally bilateral HOD appear in a paramedian lesion affecting both the central tegmental tract and the superior cerebellar peduncle or at the level of brachium conjunctivum where the decussation of bilateral GMT locates.

The major pathologic change of HOD includes

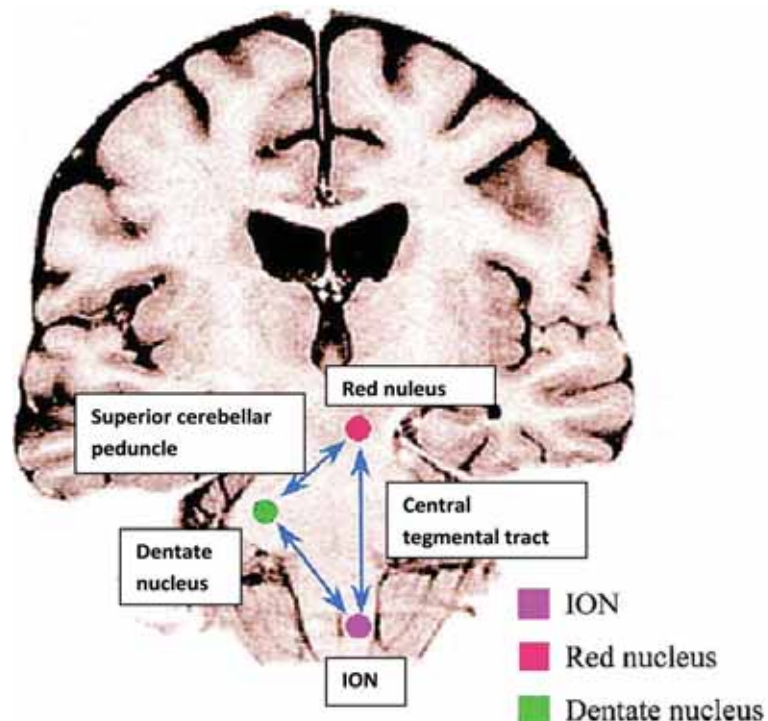


Fig.10 Diaphragm of dentatorubral-olivary pathway or Guillain-Mollaret triangle

Table III Goto and Kaneko findings of HOD

	Pathologic stage	Timing	Pathologic findings
I	No change	24 hours	-
II	Olivary amiculum	2-7 days or more	Degeneration of amiculum olive
III	Mild olivary hypertrophy	3 weeks	Mild enlarged olive ,neuronal hypertrophy no gliotic reaction
IV	Maximal olivary enlargement	8.5 months	Hypertrophied neuron and astrocytes
V	Olivary pseudohypertrophy	> or =9.5 months	Neuronal dissolution and gemistocytic astrocyte
VI	Olivary atrophy	Several years	Neuronal disappearance and degeneration of amiculum olive

vacuolar degeneration of the enlarged neurons, hypertrophy of the astrocytes and gliosis. The spectrum and predictable temporal microscopic changes in HOD was documented and categorized into six stages by Goto and coworker in 1981 and assessed correlation with MRI findings in 1994 by Mika Kitajima et al as summarized in table III.⁽¹⁰⁾

Three distinct MR stages and temporal evolution of the histopathology of HOD abnormalities have been demonstrated by Birbamer et al and Mayank Goyal and co workers.⁽¹¹⁾

Stage 1: Increased SI on T2WI and Proton Density without hypertrophy of the olive which occurs at 1-6 months after onset.

This finding may relate to the 3rd to 4th classified by Goto in which gliosis and increased water content are associated with demyelination and vacuolization.

Stage 2: Hypertrophy and increased SI on T2WI which ends up as resolution of hypertrophy at 3-4 years after onset.

This stage is most likely the result of neuronal and astrocytic hypertrophic precursors to cell death (stage 4th-5th of Goto et al)

Stage 3: Persistence of increased SI leading to atrophy of olive (stage 6th of Goto et al)

About DTI and fiber tractography studies, normal white matter anatomy in the brain stem has been described by several authors on MRI 1.5 and 3T system. The central tegmental tracts are symmetrical running in a superior-inferior directions.^(12,13)

Decreased central tegmental tract volume away from the site of affected ION without deviation, deformation or interruption of tract in HOD has been reported.⁽⁴⁾ Dynamic change of signal and DTI parameters of all anatomical components in the GMT of HOD have also been studied which have shown the statistic significant increase in ADC of affected ION and other regions in GMT, excluding the inciting lesion.⁽⁵⁾

For our four cases, the remote inciting lesion, affected GMT, ION lesion, time evolution, possible pathologic classification by Goto et al and MRI stages are defined and summarized at Table IV.

All of the findings are compatible with previous reports of the causes of HOD (remote inciting lesion), pattern of pathway, disruption and temporal evolution with MRI findings.

Table IV

Case No.	Remote inciting lesion	Affected GMT	ION lesion/ hypertrophy	Time evaluation	Pathologic stage	MRI stage
1	Cavernous hemangioma at Right sided dorsal pons with prior hemorrhage on 1998	Right CTT	Right/ absent	13 years	6	3
2	AVM at Left sided pons and pontomedullary junction and multistage hemorrhage at Left sided pons and Left tegmentum of mid brain	Left CTT	Left/ present	2 years	5	2
3	Post operative hematoma after removal NHL at Right dentate nucleus	Left GMT	Left/ present	13 months	5	2
4	Repeated hypertensive pontine hemorrhage	Left CTT	Left/ present	2 years of first episode and 2 months of recent bleeding	5	2

GMT=Guillain-Mollaret triangle, ION=inferior olivary nucleus, CTT= central tegmental tract, AVM = arteriovenous malformation, NHL= non Hodgkin lymphoma

About the first patient, there was also left cerebellar atrophy, likely to be a crossed cerebellar diachisis. (CCD)⁽¹⁴⁾. This lesion resulted from an interruption of the cerebro pontine cerebellar tract . This tract receives axons from extensive areas of the cerebrum, passes through the cerebral peduncles, enters to the ipsilateral pontine nuclei and then runs to the contralateral cerebellum via the middle cerebellar peduncle. (Fig.11)⁽¹⁵⁾

In our patient, the old bleeding site also involved right middle cerebellar peduncle. So we postulated that this lesion might be from degeneration via right pontocerebellar tract. However, there was another report of cavernous angioma at left tectum of midbrain with left HOD and right cerebellar atrophy by Yunichi Komabe et al in 1997.⁽¹⁶⁾ Of their patient the lesion did not involve the ponto-cerebel-

lar tract, so they postulated that it was caused by interruption of GMT.

Of the DTI study in the forth case, our findings of decreased DTI volume of the left central tegmental tract (affected tract) were the same as the case report in October 2010.(4) Decreased FA and increased ADC of affected left ION were also observed identical to the study of Alp. Dricer et al⁽⁵⁾

Increased ADC of left central tegmental tract and right dentate nucleus relatively to the contralateral side were also detected which the findings were the same as formentioned report, represent progressive demyelinative lesion of left GMT tract. We also detected increased ADC of left superior cerebellar peduncle and right red nucleus relatively to the contralateral side. This might be from recent bleeding involving left superior cerebellar peduncle

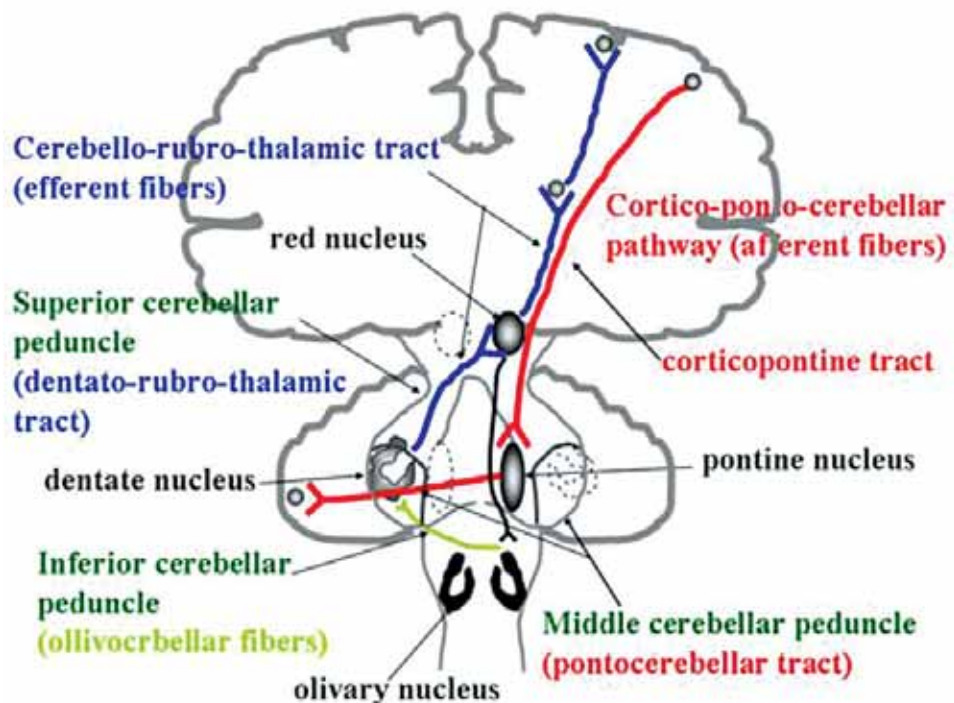


Fig.11 Diagram of corticopontocerebellar tract

which caused the degeneration of the components of right GMT tract (red nucleus). We postulated that there might be right HOD in the future.

However the study of DTI was limited because no control study of compatible white matter tract was available for comparison.

Conclusion

Hypertrophic olivary degeneration is a unique pathology with characteristic imaging manifestations. This process should be concerned when there is a non enhancing enlargement of the inferior olivary nucleus with T2 hyper signal intensity. Although these findings are non specific and can be seen in

a wide variety of lesions including demyelination, infection, inflammation, infarction and tumor, lack of contrast enhancement, no restricted diffusion and evidence of an remote inciting lesion in the contralateral cerebellum or ipsilateral brainstem should lead to the diagnosis of HOD.

In addition to conventional MRI features, DTI and fiber tractography can demonstrate the disruption pathways of HOD and are useful for confirm diagnosis. Moreover, DTI parameters may reflect the temporal spatial progression of transneuronal degeneration in HOD. So further study of DTI in this rare condition needs to be performed.

References

- 1) Oppenheim H. Uber olivary degeneration bei atherosclerotic der basalen Hirnnervation. Berl Klin Wochenscher 1887;34: 638-9.
- 2) Duchen LW. General pathology of neurons and neuroglia. In : Greenfield H, Corsellis JAN, Duchen LW, eds. Neuropathology 4th ed. New York, NY: Wiley, 1984;18-9.
- 3) Noriko Salamon-Murayama N, Russel EJ, Rabin BM. Case 17 :hypertrophic olivary degeneration secondary to pontine hemorrhage .Radiology 1999;213:814-7.
- 4) R.Shah, J.Market, A.K.Bag, J.K.Cure. Diffusion Tensor Imagine in Hypertrophic Olivary Degeneration. AJNR Am J Neuroradiol 2010;31:1729-31.
- 5) Alp Dincer, Onur Ozyurt, Dilava Kaya, et al. Diffusion Tensor Imaging of Guillain-Mollaret Triangle in Patients with Hypertrophic Olivary degeneration. J Neuroimaging 2011;21:145-51.
- 6) Goyal M, Versnick E, Tuite P, et al . Hypertrophic olivary degeneration : metaanalysis of the temporal evolution of MR findings. Am J Neuroradiol 2000;21:1073-7.
- 7) Kitajima M, Yukunori K, Shimomura O, et al. Hypertrophic olivary degeneration; MR imaging and pathologic findings. Radiology 1994;192:539-43.
- 8) Lorraine Ash, Ashok Srinivasan : Case of the Season : Hypertrophic Olivary degeneration. Seminars in Roentgenology 2008;02:171-2.
- 9) T Krings, H Foltys, I G Meister, J Reul . Hypertrophic olivary degeneration following pontine hemorrhage: hypertensive crisis or cavernous hemangioma bleeding? J. Neurol Neurosurg Psychiatry 2003;74:797-9.
- 10) Mika Kitajima, Yukunori Korogi, Osamu Shimoura, et al. Hypertrophic Olivary degeneration : MR imaging and pathologic findings. Radiology 1994;192:539-43.
- 11) Mayank Goyal, Eric Versnick, Paul Tuite, Jean Saint Cyr, et al . Hypertrophic Olivary degeneration : Metaanalysis of the Temporal Evolution of MR findings. AJNR Am J Neuroradiol 2000;21:1073-7.
- 12) Nagae-Poetscher LM, Jiang H, Wakana S, et al. High resolution diffusion tensor imaging of the brain at 3T. AJNR Am J Neuroradiol 2004;25:1325-30.
- 13) Salamon N, Sicotte N, Alger G, et al. Analysis of the brain-stem white-matter tracts with diffusion tensor imaging. Neuroradiology 2005;47:895-902.
- 14) Brodal A. Cerebrocerebellar pathways : Anatomical data and some functional implications. Acta Neurol Scan Suppl 1972;51:153
- 15) B.M. Rabin, D.J.Hebel, N. Salamon-Murayama, E.J. Russel. Distal Neuronal Degeneration Caused by Intracranial Lesions AJR 1998;171:95-102.
- 16) Yuichi Kamaba, Tatsuya Nomoto, Shin Kitamura and Akiro Terashi. Cavernous Angioma with Olivary Hypertrophy and Contralateral Cerebellar Diaschisis. Internal Medicine 1997;36(7):504-7.



Case Report

Blunt Traumatic Diaphragmatic Hernia: Case Report

Siwipan Changtham, MD.

Department of Radiology, Buddachinnaraj Hospital, Muang, Phitsanulok, Thailand. 65000

Case Report

A 55-year old man visited the orthopedic OPD due to tenderness and swelling at left ankle from a motorcycle accident, 3 hours before. Left medial malleolus fracture was diagnosed. A short leg cast was performed by orthopedist. During the wait to receive his medicines, he had sudden onset of chest discomfort, pain at left lower chest and left upper abdomen. He was sent to the ER department. He had blood pressure of 110/75 mmHg, pulse rate of 64 beats/min, respiratory rate of 20 breaths/min and oxygen saturation of 97%. A physical examination found mild pale conjunctiva, tender at left chest wall, equal breath sounds. Mild tenderness at LUQ was also noted without guarding or rebound tenderness.

Chest film showed air-fluid level within left hemithorax and mild shifting of mediastinum to the right. A CT chest including upper abdomen with contrast study was performed. Discontinuity of left hemidiaphragm with herniation of stomach and duodenum into left hemithorax was seen. Splenic laceration and minimal left hemothorax were also noted.

He was admitted at the traumatic surgery ward for an exploratory laparotomy. Rupture of left hemidiaphragm, approximately 10 cm in diameter, with herniation of stomach, duodenum and omentum into left thorax was found. Left hemothorax and splenic contusion were also found. Repair to left diaphragm with interrupted non-absorbable sutures was performed. No evidence of complication was detected.

Discussion

Diaphragmatic hernia is a herniation of abdominal structures into the thoracic cavity through a defect on the diaphragm.¹ It can be broadly classified as acquired or congenital.² Traumatic diaphragmatic hernia, acquired diaphragmatic hernia, is rare and often overlooked complication of penetrating and blunt trauma.³ It is present in 1-6% of major thoracic injuries.⁴ The common causes of traumatic diaphragmatic hernia are depending on the geographic location and socioeconomic status of trauma patients.⁵

In blunt traumatic diaphragmatic rupture, motor vehicle accident is the most common cause, followed by falls and crush injuries.⁶⁻⁸ Mechanisms

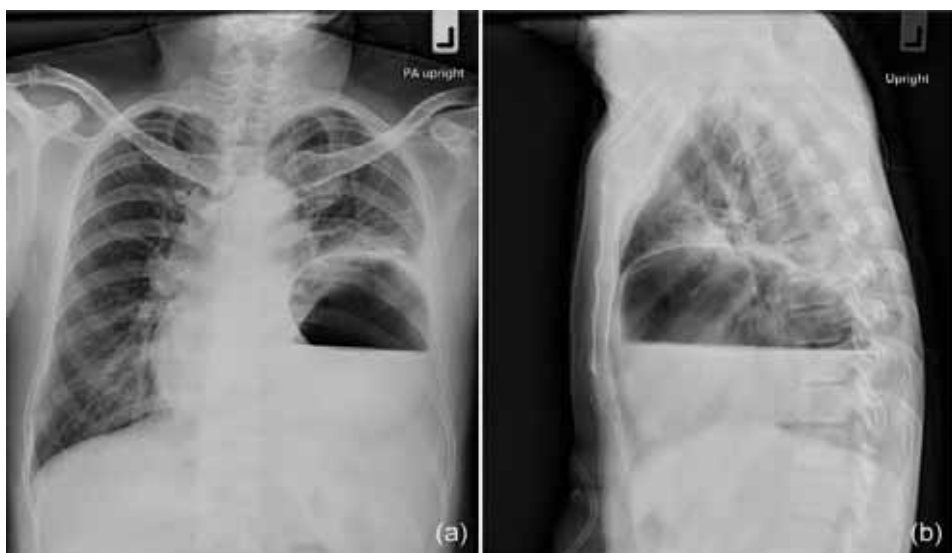


Fig 1. Chest radiographs in PA upright (a) and left lateral views (b) reveal air-fluid level within the left hemithorax. Mild shifting of the mediastinum to the right is noted.

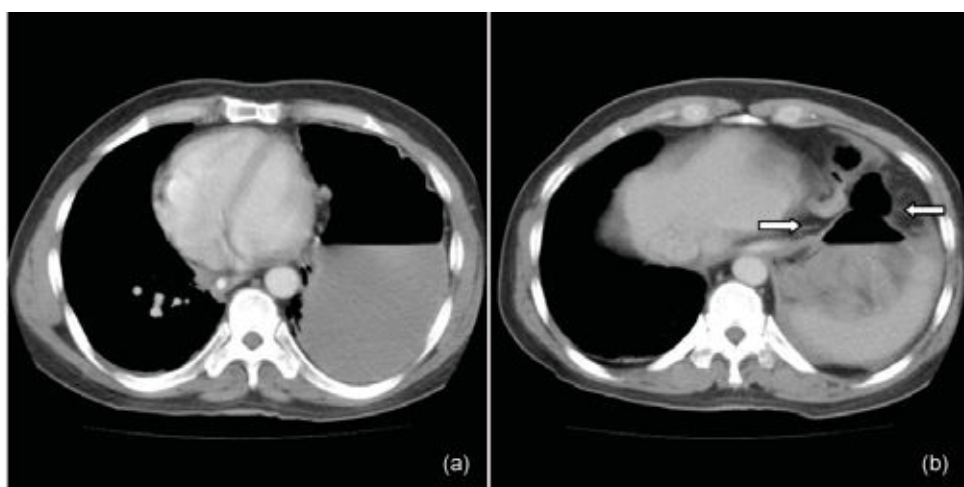


Fig 2. Axial contrast-enhanced CT images: (a) The stomach is in left hemithorax and in a dependent position. Contact of the stomach and the posterior thoracic wall is noted. (dependent viscera sign). (b) The waist like contraction of the stomach is seen at the level of left hemidiaphragm (The collar sign; white arrow).

of blunt diaphragmatic injury include a sudden increase in transdiaphragmatic pressure caused by direct frontal impact, distortion of the chest wall with resultant avulsion of the diaphragmatic attachments and direct penetration by rib fragments.⁹ The left-sided injury is significant predominantly, up to 95%, while right-sided injury is less common from protective effect of liver.¹⁰⁻¹²

The stomach is the most common herniated organ in left-sided diaphragmatic rupture, followed by colon.¹³ The liver, kidney, spleen and small intestine may also migrate within thorax.¹ The diaphragm is rarely injured alone, with an associated injury rate approaching 100%, both intra-abdominal injuries and extra-abdominal injuries.¹⁴ Common intra-abdominal injuries are spleen and liver.^{8,13} Extra-abdominal

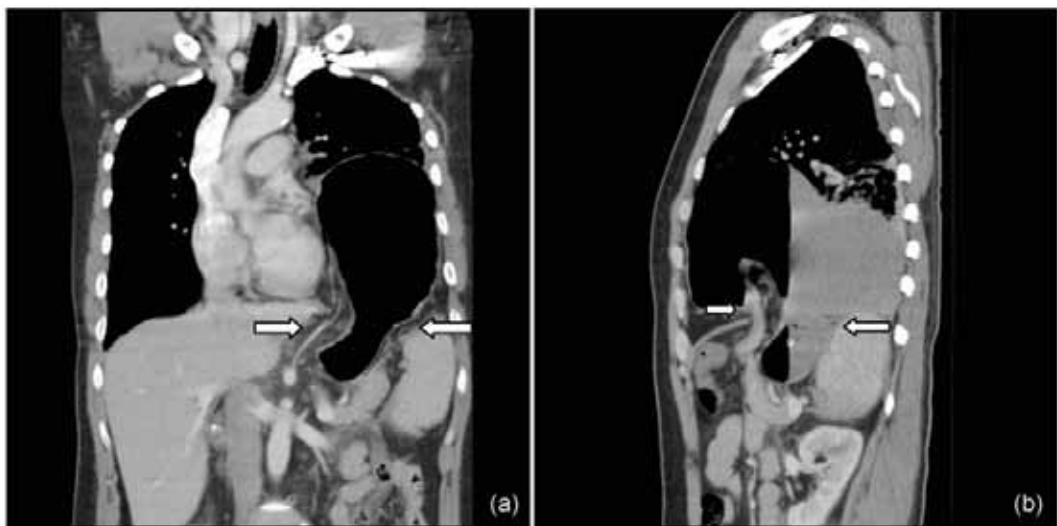


Fig.3 Contrast-enhanced CT images with coronal (a) and sagittal (b) show a focal defect of the left hemidiaphragm (segmental diaphragmatic defect sign; white arrow). Herniation of the stomach through this defect into left hemithorax is noted with the waist like contraction of the stomach at the level of diaphragm (The collar sign).

injuries are hemothorax, lung injury, fracture and head injury.^{6,8,13}

Clinical presentation of diaphragmatic rupture was described in 3 phases.¹⁵ The acute phase is at the time of injury. Acute phase may be asymptomatic or present with chest pain, abdominal pain, respiratory distress or shock.¹⁶ Dyspnea and chest pain were the most common presenting complaint.¹⁷ The delayed phase is associated with transient herniation of viscera that could be absence or intermittent non specific symptoms. The obstruction phase is complication of a long standing herniation, manifesting as obstruction, strangulation and rupture.

Chest film, direct peritoneal lavage, fluoroscopy, upper GI studies, ultrasound, CT scan, MRI, Liver-spleen scintigraphy, peritoneo-scintigraphic establish the diagnosis, however, lack both sensitivity and specificity.¹⁸

Chest film is basic screening for thoraco-abdominal injury. The specific radiographic signs of

blunt diaphragmatic rupture include intrathoracic location of abdominal viscera, with or without a site of focal constriction (collar sign) and clear demonstration of a nasogastric tube tip above the left hemidiaphragm.¹⁹ Chest film at the time of admission may be diagnostic traumatic diaphragmatic injury, 27 to 62% of left side injury and 33% of right side injury.⁹ So, chest film obtained at admission and repeated soon after are more valuable in suggestive the diagnosis of rupture of the diaphragm, especially left-sided injury.²⁰

Ultrasound uses for evaluation of the blunt traumatic patient. It can be performed bed side and can suggest diaphragmatic rupture during FAST examination.²¹ However, diagnosis of diaphragmatic hernia by ultrasound is difficult because of gas-filled intestinal loops, aerate lungs and acoustic shadowing from the ribs.¹

Barium studies are also used for diagnosis of traumatic diaphragmatic injury in non-acute setting.

to confirm herniation of stomach and intestine.^{13,22}

CT is the imaging modality of choice in severe blunt abdominal trauma and has a sensitivity of 61-71% and a specificity of 87-100% for diagnosis of acute traumatic diaphragmatic rupture.²³ The multidetector CT with multiplanar reformatted images improves sensitivity and specificity of diagnosis. CT sign of diaphragmatic rupture can divide to direct sign and indirect sign. The direct signs are segmental diaphragmatic defect, dangling sign and absent diaphragm.⁵ The indirect signs related to herniation and loss of border between thorax and abdomen are herniation through a defect, hump sign, band sign, dependent viscera sign, sinus cutoff sign, abdominal content peripheral to the diaphragm or lung, elevated abdominal organs, abdominal fluid abutting a thoracic structure, abdominal viscera abutting thoracic fluid or a thorax organ, pneumothorax and pneumoperitoneum, hemothorax and hemoperitoneum.

MRI is not suitable in most acute traumatic cases, however, it may use in selected traumatic diaphragmatic hernia patients, especially in chronic complicated cases.¹ MRI imaging with multiplanar capability will clearly reveal the normal diaphragm and the hernia orifice as a diaphragmatic discontinuity on sagittal and coronal images.

The traditional method of treating blunt traumatic diaphragmatic injuries is open surgical repair.¹⁴ Acute left-sided traumatic diaphragmatic rupture is best approached through abdomen, although the chest approach adding laparotomy should be performed when necessary. Acute right-sided and chronic traumatic diaphragmatic rupture should be approached through the chest.²⁴

The mortality rate in blunt diaphragmatic rupture vary from 7-42%, associated with concurrent

injuries rather than the diaphragm rupture itself.^{6,25} Mortality factors are age, high injury severity score, shock and bilateral diaphragmatic injury.^{6,16}

Conclusion

Blunt traumatic diaphragmatic rupture can present with associated injuries. In cases of blunt thoracoabdominal injury, delayed clinical presentation of chest pain should be re-evaluated. Chest film is a basic imaging modality and can be used to make a diagnosis in these cases. A CT was performed to confirm diagnosis and showed associated splenic injury. However, it should be remembered that there is a high suspicious index of diaphragmatic injury in cases of thoracoabdominal trauma.

References

1. Eren S, Kantarci M, Okur A. Imaging of diaphragmatic rupture after trauma. Clin rad 2006; 61:467-77.
2. Sandstorm CK, Stern EJ. Diaphragmatic Hernias: A Spectrum of Radiographic Appearances. Curr Probl Diagn Radiol 2011;40:95-115.
3. Wardi G, Lasoff D, Cobb A, Hayden S. Traumatic diaphragmatic hernia. J Emerg Med 2014;46:80-2.
4. Eckstein M, Henderson SO. Thoracic trauma. In: Marx J, Robert H. Walls R. et. Al., eds. Rosen's emergency medicine: concepts and clinical practice. Philadelphia: Mosby Elsevier;2009; 387-413.
5. Desir A, Ghaye B. CT of Blunt Diaphragmatic Rupture. RadioGraphics 2012;32:477-98.
6. Kuo I, Liao C, Hsin M, Kang S, et al. Blunt diaphragmatic rupture - a rare but challenging entity in thoracolabdominal trauma. Am J Emerg Med 2012;30:919-24.
7. Meyers BF, McCabe CJ. Traumatic Diaphragmatic Hernia Occult Marker of Serious Injury. Ann Surg 1993;218(6):783-90.
8. Al-Refaiea RE, Awad E, Mokbel EM. Blunt traumatic diaphragmatic rupture: a retrospective observational

study of 46 patients. *Interact Cardiovasc Thorac Surg* 2009;9:45-9.

9. Killeen KL, Shanmuganathan K, and Mirvis SE. Imaging of Traumatic Diaphragmatic Injuries. *Seminars in Ultrasound, CT and MRI* 2002;23:184-92.
10. Wiencek RG, Wilsong R, Steiger Z. Acute injuries of the diaphragm: an analysis of 165 cases. *J Thorac Cardiovasc Surg* 1986;92(6):989-93.
11. Kerney PA, Rouhana SW, Burney RE. Blunt rupture of the diaphragm: Mechanism, diagnosis, and treatment. *Ann Emerg Med* 1989;18:1326-30.
12. Heiberg E, Wolverson MK, Hurd RN, Jagannadharao, et al. CT recognition of traumatic rupture of the diaphragm. *AJR* 1980;135:369-72.
13. Simpson J, Lobo DN, Shah AB, Rowlands BJ. Traumatic diaphragmatic rupture: associated injuries and outcome. *Ann R Coll Surg Engl* 2000;82:97-100.
14. Bosanquet D, Farboud A, Luckraz H. A review diaphragmatic injury. *Respiratory medicine CME* 2009;2:1-6.
15. Rashid F, Chakrabarty MM, Singh R, Iftikhar SY. A review on delayed presentation of diaphragmatic rupture. *World Journal of Emergency Surgery* 2009;4:32.
16. Soundappan SV, Holland AJ, Cass DT, Farrow GB. Blunt traumatic diaphragmatic injuries in children. *Injury, Int. J. Care Injured* 2005;36:51-4.
17. Peer SM, Devaraddeppa PM, Buggi S. Traumatic diaphragmatic hernia-our experience. *Inter J Surg* 2009;7:547-9.
18. Athanassiadi K, Kalavrouziotis G, Athanassiou M, Vernikos P, et al. Blunt diaphragmatic rupture. *Eur J cardio Thorac Sur* 1999;15:469-74.
19. Sliker CW. Imaging of diaphragm injuries. *Radiol clin N Am* 2006;44:199-211.
20. Gelman R., Mirvis SE, Gens D. Diaphragmatic rupture due to blunt trauma: sensitivity of plain radiograph. *AJR* 1991;156:51-7.
21. Blaivas M, Brannam L, Hawkins M, Lyon M, et al.. Bedside emergency ultrasonographic diagnosis of diaphragmatic rupture in blunt abdominal trauma; *Am J Emerg Med* 2004;22:601-4.
22. Shackleton KL, Stewart ET, Taylor AJ. Traumatic diaphragmatic injuries: Spectrum of radiographic findings. *RadioGraphics* 1998;18:49-59.
23. Bergin D, Ennis R, Keogh C, Fenlon HM, et al.. The dependent viscera sign in CT diagnosis of blunt traumatic diaphragmatic rupture. *AJR* 2001;177:1137-40.
24. Haciibrahimoglu G, Solak O, Olcmen A, Bedirhan MA, et al.. Management of Traumatic Diaphragmatic Rupture. *Surg Today* 2004;34:111-4.
25. Bergeron E, Clas D, Ratte S, Beauchamp G, et al.. Impact of deferred treatment of blunt diaphragmatic rupture: A 15-Year experience in six trauma centers in Quebec. *J Trauma Inj Infect Crit Care* 2002;52(4):633-40.



Tumefactive Multiple Sclerosis Clinically Mimicking Acute Stroke and Lesional Migration Along the Biopsy Tract: A Case Report

Oranan Tritanon, MD.¹, Arunee Singhnaeh, MD.^{2*}, Jiraporn Laothamatus, MD.^{1,3},
Atthaporn Boongird, MD.⁴, Disya Ratanakorn, MD.⁵, Prawat Nitiyanant, MD.²

¹ Division of Diagnostic Neuroradiology, Department of Diagnostic and Therapeutic Radiology,

² Department of Pathology, ³ Advanced Diagnostic Imaging Center,

⁴ Division of Neurosurgery, Department of Surgery, ⁵ Division of Neurology, Department of Internal Medicine,

Faculty of Medicine Ramathibodi Hospital, Mahidol University, Bangkok, Thailand

Abstract

Tumefactive multiple sclerosis is a form of demyelinating disease which patient can present with acute stroke. We reported a case of a 49-year-old woman with well controlled hypertension, who presented with right hemiplegia 15 hours prior to admission. The initial diagnosis of acute stroke was made. Emergency computed tomography showed hypodense lesion at the left lentiform nucleus and posterior limb of the left internal capsule. The magnetic resonance imaging (MRI) study showed hyperintense FLAIR lesion in the left lentiform nucleus, left internal capsule, left thalamus, and periventricular area of the left frontoparietal region, some areas of restricted diffusion and inhomogeneous enhancement. The MR spectroscopy (MRS) of the lesion showed increased choline peak, decreased creatine and NAA peaks, and maximal choline to creatine ratio 2.25. Her symptoms deteriorated with progressive headache and motor aphasia. The follow up MRI showed extension of the inhomogeneous enhancing lesion along the biopsy tract at the left frontal lobe with the enhancing and MR spectra pattern similar to the lesion.

The craniotomy with left frontal lesion excision included the mass and the biopsy tract was done. The lesion showed acute and chronic inflammatory cell infiltration with macrophages, necrotic tissue and reactive gliosis. The further pathological worked up demonstrated foci of demyelination with relative axonal preservation, numerous CD68+ macrophages with intracyto-plasmic Luxol fast blue(+) myelin debris. Perivascular and parenchymal CD3+ T-cells were identified, especially in demyelinating foci. These findings supported the diagnosis of tumefactive multiple sclerosis.

Her conditions were improved after treating with pulse methylprednisolone and intravenous immunoglobulin (IVIG). Follow up MRI study 4 months after treatment revealed almost resolution of the preexisting inhomogeneous enhancing lesion.

* Corresponding author: Arunee Singhnaeh, email: arueed@gmail.com

Introduction

Tumefactive multiple sclerosis is often described as atypical feature of multiple sclerosis that is larger than 2 cm, mass effect, oedema and/or ring enhancement, which clinically and radiographically mimicking stroke, intracranial tumor and infection^(1,2). We reported a case of biopsy-proven tumefactive MS patient that clinically mimicking acute stroke and radiographically mimicking intracranial lymphoma that challenged neurologist and radiologist.

Case reports

A 49-year old woman with well controlled hypertension presented with acute right upper and

lower extremities weakness 15 hours prior to hospitalization. Physical examination showed right hemiparesis, right facial palsy upper motor neuron type, positive right Babinski reflex, positive jaw jerk reflex, and motor power grade I on the right extremities.

CT scan of the brain at emergency room showed hypodense lesion at the left lentiform nucleus and posterior limb of the left internal capsule (Fig 1A).

First MRI of the brain in two days later disclosed the lesion seen as hyperintense T2W and FLAIR in the left lentiform nucleus, genu & posterior limb of the left internal capsule, left thalamus, left corona radiata, left cerebral peduncle and periven-

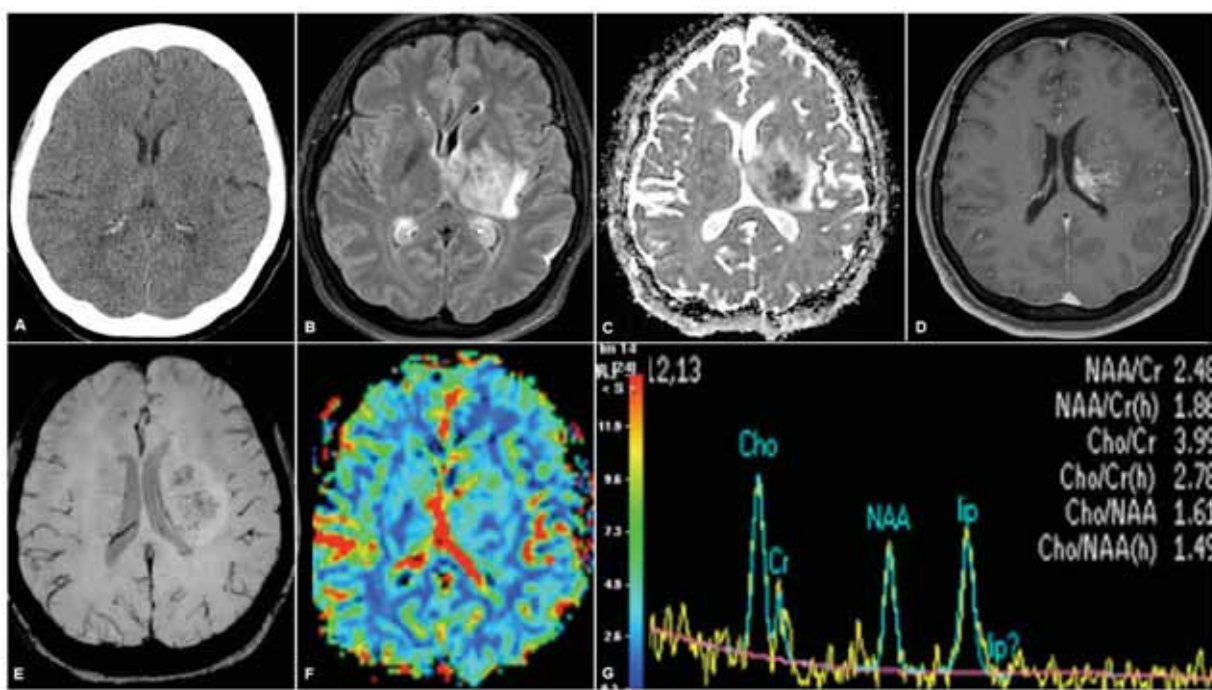


Fig 1. (A) Non contrast CT scan at initial presentation showed hypodense lesion at the left lentiform nucleus and posterior limb of the left internal capsule. (B) FLAIR MRI showed hyperintense at the left lentiform nucleus, genu & posterior limb of the left internal capsule, left thalamus and left external capsule. (C) ADC showed the area of restricted diffusion within the lesion. (D) Gd-THRIVE showed inhomogeneous enhancing and non-enhancing areas. (E) SWI showed prominent parallel venules within the lesion. (F) Perfusion images revealed increased CBF of the lesion. (G) MRS revealed increased choline peak, decreased creatine and NAA peaks.

tricular area of the left frontoparietal region with prominent perivenular space within the lesion (Fig 1B). The area of restricted diffusion within the lesion was detected (Fig 1C). The inhomogeneous enhancing and non-enhancing areas on axial Gd-THRIVE were noted, which demonstrated intense patchy enhancement at the periventricular area (Fig 1D). In SWI, there were prominent parallel venules within the lesion radial to the body of left lateral ventricle (Fig 1E). Also, there were the increased cerebral blood flow (CBF) and cerebral blood volume (CBV) of the lesion in MR perfusion (Fig 1F). There was increased choline peak, decreased creatine and NAA peaks, maximal choline to creatine ratio 2.25, maximal choline to NAA ratio 1.61 on MR spectra using multivoxel, 2000/ 144 TR/ TE) (Fig 1).

First biopsy obtained from the left thalamus revealed perivascular acute and chronic inflammatory cell infiltration in the background of reactive gliosis. Inflammation/infectious process were suspected (Fig. 2). Special stains for acid fast bacilli and fungi showed negative findings.

Two week later, the patient had progressive headache and motor aphasia. The 2nd MRI showed

an increased enhancing area within the preexisting lesion (Fig 3). Also seen was an extension of the enhancing lesion along the biopsy tract at the left frontal lobe with the enhancing and MR spectra pattern similar to the lesion (Fig 4, 5).

The 2nd biopsy obtained from the left frontal lobe and tissue from biopsy tract also showed similar pathologic findings that were acute and chronic inflammatory cell infiltration along perivascular area in background of gliosis and numerous foamy histiocytes.

Because of suspicious of neoplastic process and deterioration of clinical conditions, the craniotomy with left frontal lesion removal of the mass and biopsy tract was done. The lesion showed more acute and chronic inflammatory cell infiltration with marked increased macrophages, necrotic tissue and reactive gliosis (Fig. 6). The further pathological worked up demonstrated foci of demyelination with relative axonal preservation, numerous CD68+ macrophages with intracyto-plasmic Luxol fast blue(+) myelin debris. (Fig 7) Perivascular and parenchymal CD3+ T-cells were identified especially in demyelinating foci. These findings supported the diagnosis

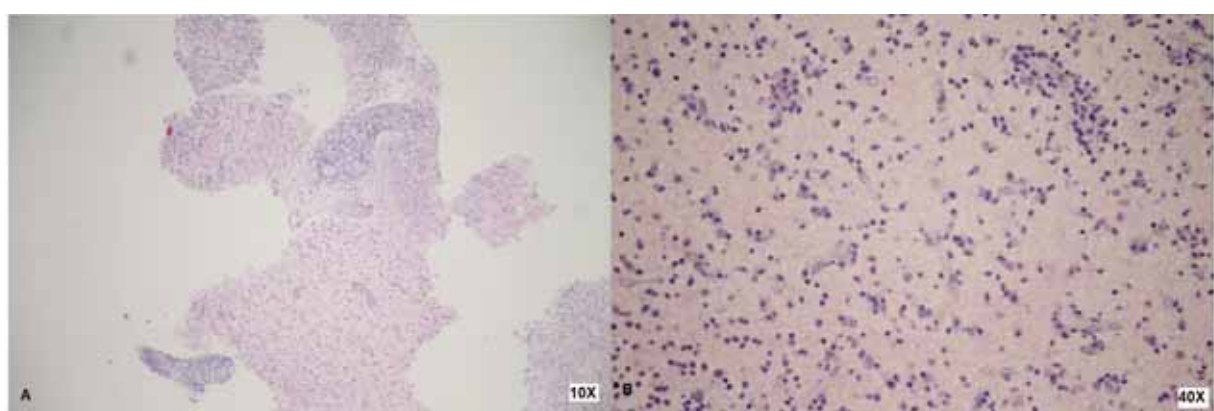


Fig 2. (A,B) Perivascular and intraparenchymal acute and chronic inflammatory cell infiltration

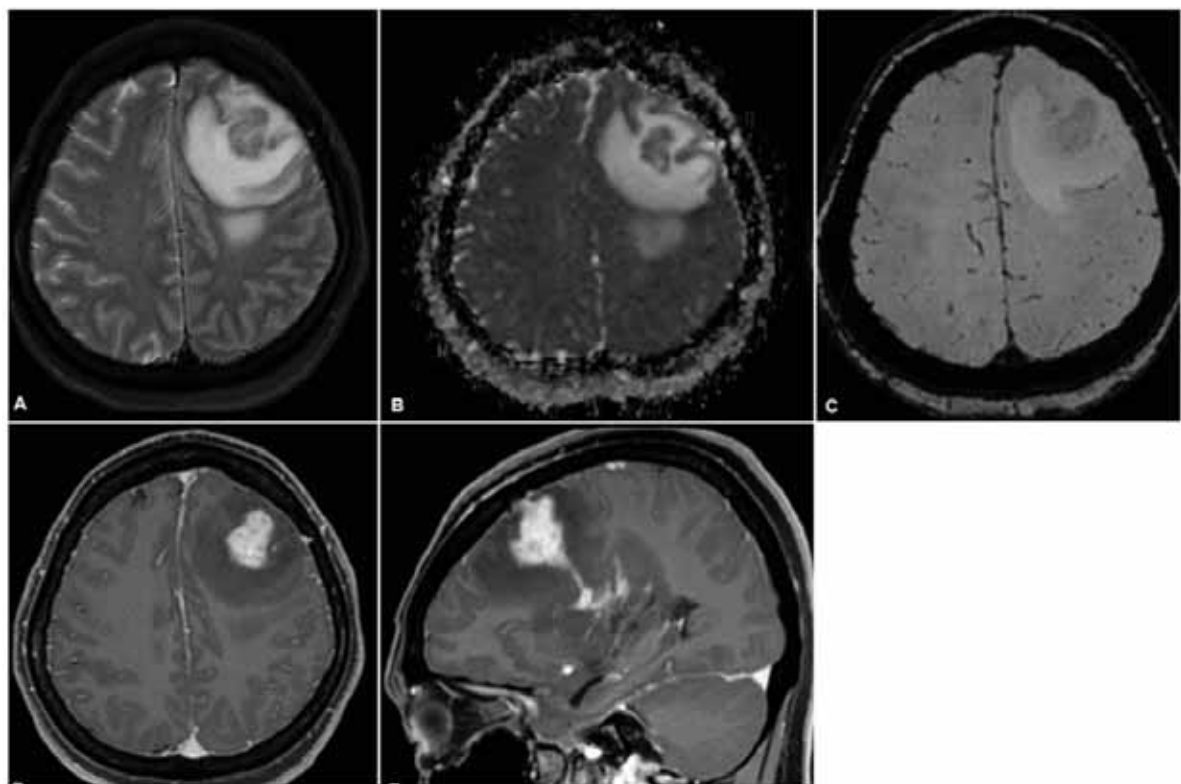


Fig 3. Two weeks later, follow up MRI of the brain

(A) FLAIR MRI revealed increased hyperintense area of the preexisting lesion. (B) Gd-THRIVE showed increased enhancing area within the preexisting lesion

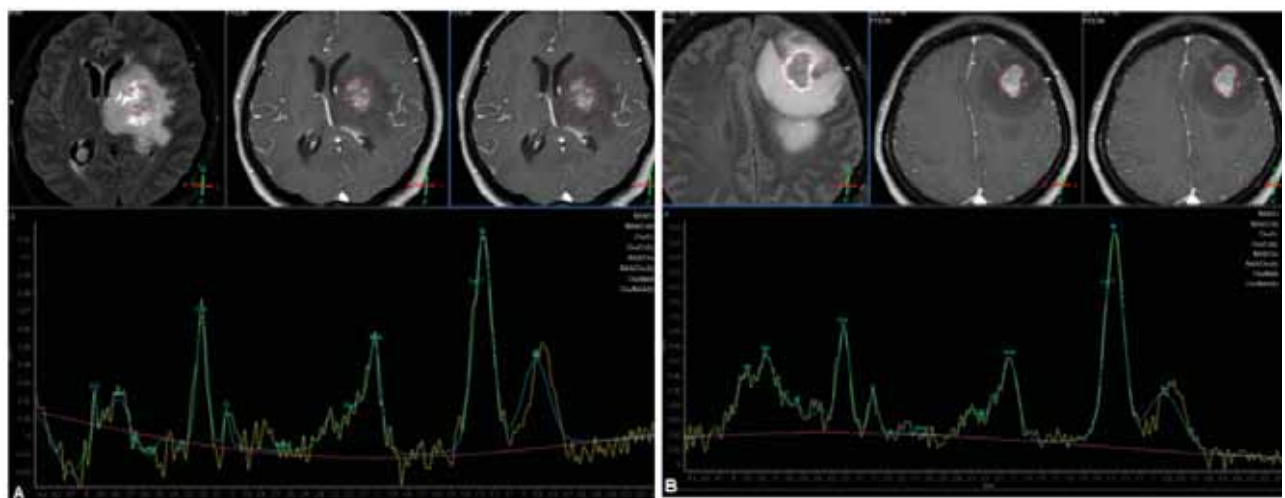


Fig 5. (A, B) MRS showed similar pattern of the lesion along the biopsy tract at the left frontal lobe and the left lentiform nucleus

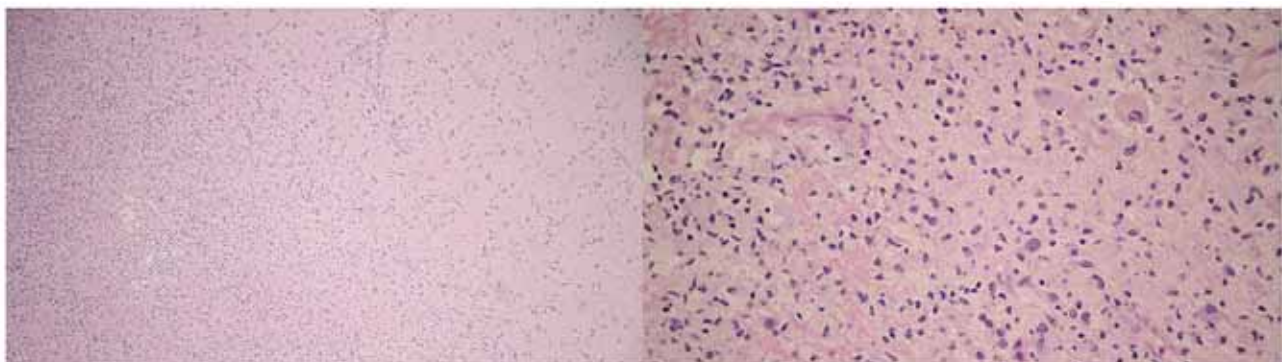


Fig 6. More acute and chronic inflammation with numerous macrophage infiltrations

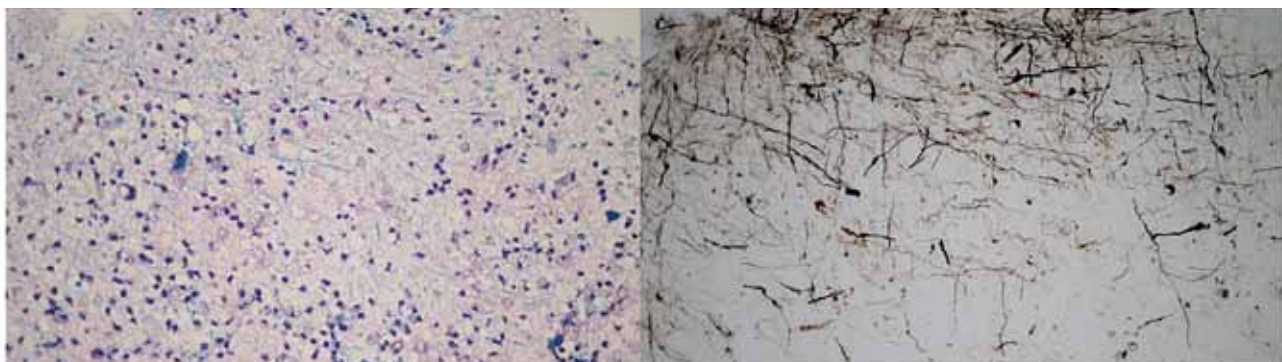


Fig 7. Luxol fast blue PAS and Bielschowsky staining show demyelination with axonal preservation

of tumefactive multiple sclerosis.

Her clinical improved after treatment with pulse methylprednisolone and intravenous immunoglobulin (IVIG). Follow up MRI studies 4 months after treatment revealed almost resolution of the pre-existing inhomogeneous enhancing lesion that known as tumefactive multiple sclerosis.

Discussion

Multiple sclerosis is an inflammatory demyelinating condition attacking the myelin that causes absence of proteolipid protein in area of demyelination⁽³⁾. Tumefactive MS is atypical feature of multiple sclerosis that sometimes mimic intracranial tumor

such as lymphoma or glioblastoma multiforme (GBM)⁽³⁾. In our case, there were some characters on MR perfusion and MR spectroscopy which showed markedly increased CBF and CBV, increased choline peak, choline to NAA and choline to creatine ratio. These findings made the difficulty to exclude high grade brain tumor. However prominent venules in SWI and dilated perivenular space on T2W in our case were the clues for diagnosis of tumefactive MS, that represented inflammatory activity and perivenular lymphocytic cuffing^(4,5).

Interestingly, there was an extension of the demyelinating lesion along the biopsy tract which sometimes confused with the tumor seeding. The

pathological-proven this migratory lesion along the biopsy tract confirmed the same demyelination as the basal ganglion & thalamic lesion. These findings may be explained by the activation of immune & inflammatory process along the biopsy tract.

Conclusion

Tumefactive multiple sclerosis is “tumor-like” lesion and radiologically mimicking tumors, which can infiltrates along the biopsy tract confusing with tumor seeding. Prominent venules in SWI and dilated perivenular space on T2W are helpful signs for diagnosis. Biopsy is required, if there are atypical clinical presentations and MR imaging. Luxol fast blue PAS and Bielschowsky stains should be considered if tumefactive multiple sclerosis is suspected.

References

1. Lucchinetti CF, Gavrilova RH, Metz I, Parisi JE, Scheithauer BW, Weigand S. Clinical and radiographic spectrum of pathologically confirmed tumefactive multiple sclerosis. *Brain* 2008;131:1759-75.
2. Yacoub HA, Al-Qudahl ZA, Lee HJ, Baisre A, Souayah N. Tumefactive multiple sclerosis presenting as acute ischemic stroke. *Journal of Vascular and Interventional Neurology* 2011;4(2):21-3.
3. Trapp BD, Peterson J, Ransohoff RM, Rudick R, Mörk S, Bö L. Axonal transection in the lesions of multiple sclerosis. *The New England Journal of Medicine* 1998; 338(5): 278-85.
4. Ge Y, Law M, Herbert J, Grossman RI. Prominent perivenular spaces in multiple sclerosis as a sign of perivascular inflammation in primary demyelination. *AJNR* 2005; 26:2316-9.
5. Given CA, Stevens BS, Lee C. The MRI appearance of tumefactive demyelinating lesions. *AJR* 2004;182:195-9.



Reversible Cerebral Vasoconstriction Syndrome: A Commonly Missed Diagnosis in Acute Severe Headaches

Siriporn Hirunpat, MD., Nuttha Sanghan, MD., Adchara Wan-ai, MD.,

Natee Ina, MD., Pornrujgee Hirunpat, MD.

Department of Radiology, Faculty of Medicine, Prince of Songkla University

Hat-Yai, Songkhla, Thailand 90110

Abstract

Summary: In spite of the recent acceptance to be a common cause of acute severe headaches, reversible cerebral vasoconstriction syndrome (RCVS) is still commonly missed.

The syndrome is characterized by acute severe headaches due to the vasoconstriction of the cerebral arteries, which eventually resolve spontaneously. We present a reported case of RCVS with a typical magnetic resonance angiography (MRA) appearance and a review of the literature.

* Corresponding author: Hirunpat S, MD., Email: hirsirip@hotmail.com

Case report

A 38-year-old man presented with the sudden onset of a severe headache, the feeling of almost syncope (presyncope) and dizziness. The patient was previously healthy and had no underlying disease. On clinical examination, the patient had full consciousness with a blood pressure of 130/80 mm Hg. No evidence of neurological deficit was found and all basic investigations revealed normal results. He was sent for an MRI and MRA in order to search for the cause of his acute severe headache, such as ruptured aneurysm, and to exclude the possibility of minor stroke.

MRI and MRA studies were performed with a 3-Tesla imaging unit (Archieva-X series, Phillips Healthcare, Best, the Netherlands). The results were reported as normal by a radiologist. Therefore, chronic stress and migraine were diagnosed as the causes of his symptoms by the clinician.

Later consultation with a neuro-radiologist, multiple scatter foci of tiny high signal intensities on SET2w and FLAIR within the subcortical white matter of both frontal and left parietal lobes were detected (Fig.1). Although these lesions are commonly seen as part of normal aging, or due to underlying small vessel disease such as DM or HT, other causes, such as migraines, vascular dissection, anoxia or vasculopathy, should be of concern when detected in younger patients that do not have a definite underlying disease like in this case.

The MRA study of intracranial arteries was first performed using the 3-dimensional time-of-flight (3D TOF) technique (FA=20°, TR ~ 25 msec, TE 3.45 msec, matrix size 500x287, FOV=139x139 mm) and the post processing, by maximum intensity projection (MIP) technique, revealed segmental narrowing and dilatation along the wall of the M2 segment of the left middle cerebral artery (MCA)

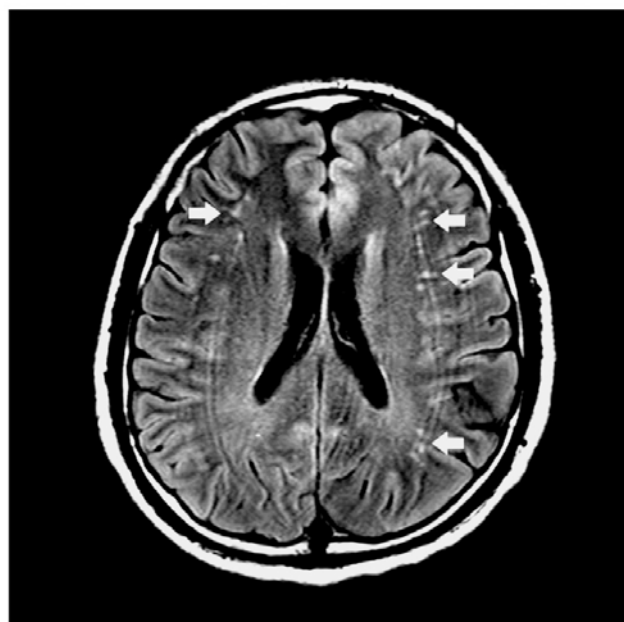


Fig 1. Axial FLAIR MR image revealed multiple scatter foci of tiny high signal intensities within the subcortical white matter of both frontal and left parietal lobes (arrows).

and the A2 segments of both anterior cerebral arteries (ACA), which resembled sausages on a string (Fig. 2).

With regard to the possibility of artifacts mimicking a lesion, on the following day the patient underwent a second MRA study which incorporated a number of MRA techniques, such as 3DTOF (FA=20°, TR ~ 25 msec, TE 3.45 msec, matrix size 328x572, FOV=152x152mm), 3D PC (venc 45 cm/sec, TR=6.63 msec, TE=3.69 msec, matrix size 272x272, FOV=134x134 mm) and post contrast enhanced MRA (FA=30°, TR=4.86 msec, TE 1.67 msec, matrix size 250x400, FOV=200x200 mm). Persisting

irregularities along the wall of the M2 segment of the left MCA and the A2 segments of both ACAs were noted in all the studies (Fig 3) and a non-specific cause of vasculopathy was suggested.

Since no definite cause of vasculopathy or vasculitis could be found upon further investigations, the patient was diagnosed as a complicated migraine. Symptomatic treatments were provided. Follow-up MRA studies at about 6 weeks and the following year (Fig. 4a&4b) revealed a full recovery of the vasoconstriction and RCVS was diagnosed. The patient also recently had a 3-year clinical follow-up. His severe headache has not returned and he is fine.

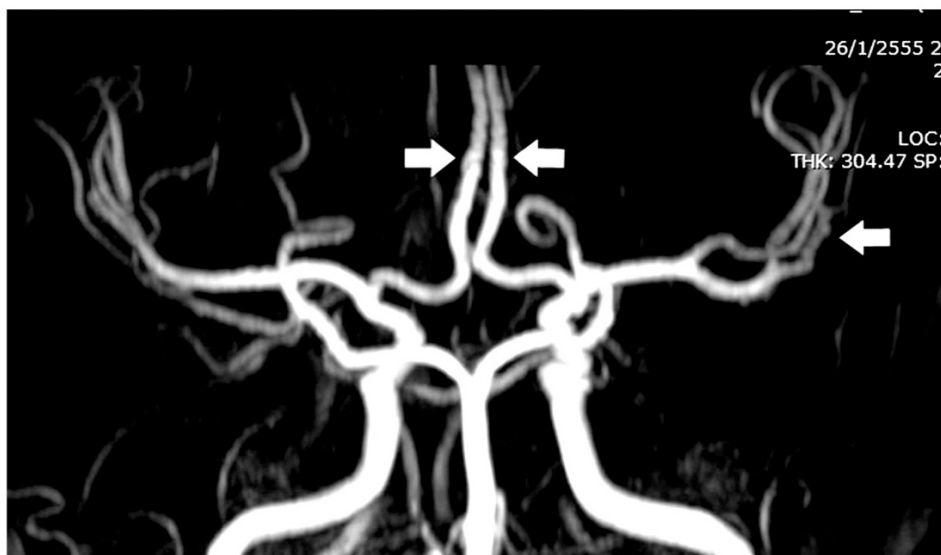


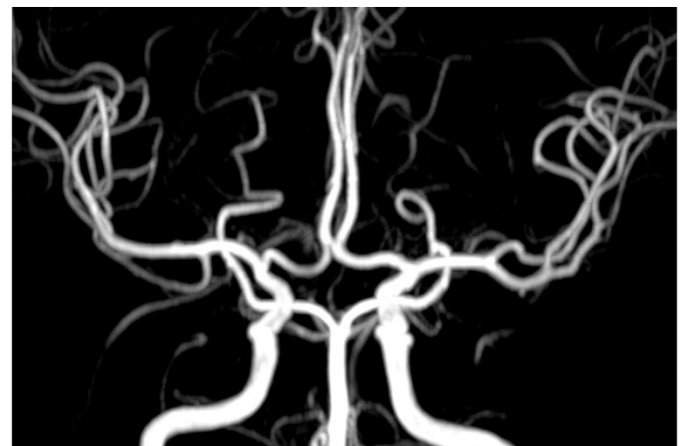
Fig 2. 3D TOF MRA (FA=20°, TR ~ 25 msec, TE 3.45 msec, matrix size 500x287, FOV=139x139 mm) The post processing by MIP revealed segmental narrowing & dilatation along the wall of the M2 segment of the left MCA and the A2 segments of both ACAs, like sausages on a string appearance (arrows).



Fig 3. 3D TOF MRA (FA=20°, TR ~ 25 msec, TE 3.45 msec, matrix size 328x572, FOV=152x152mm) on the following day. Persisting irregularities along the wall of the M2 segment of the left MCA and the A2 segments of both ACAs were noted (arrows).



a.



b.

Fig 4. 3D TOF MRA at 6 weeks (a) and 1 year (b) revealed a full recovery of the vasoconstriction.

Discussion

Reversible cerebral vasoconstriction syndrome (RCVS) is characterized by acute severe headache due to the constriction of the cerebral arteries which will eventually resolve spontaneously. It was first described by Call et al. in 1988⁽¹⁾, followed by Calabrese et al. in 1993.⁽²⁾ The acute severe headache was often described as a “thunderclap in nature” because of the sudden excruciating pain reaching its maximal intensity within 1 minute, like a “clap of thunder” mimicking that of a ruptured aneurysm. Screaming, crying, agitation, confusion and collapse are also common. Associated with photophobia, nausea/vomiting and focal neurological deficit secondary to ischemia or hemorrhage can sometimes occur. Most thunderclap headaches are as short as a few minutes; however, some have been reported to last as long as several days. A single attack is possible, but usually patients have a mean of 4 attacks during 1-4 weeks.⁽³⁾

RCVS affects females more than males, with the variable frequency for females between 64-92%,⁽⁴⁾ and the mean age of onset is around 42 years.^(5,6)

Diagnosis requires the demonstration of segmental narrowing and dilatation along the walls of the affected cerebral arteries, which resemble a “string of beads” or “sausages on a string” on an angiography, and complete resolution on a repeated angiography, within 3 months after onset.⁽⁷⁾

RCVS is a unifying term proposed in 2007 by Calabrese et al.⁽⁸⁾ which encompasses a group of recurrent headache syndromes, including Call-Fleming syndrome, benign angiopathy of the CNS, post-partum angiopathy, drug induced arteritis, migraineous vasospasm, migraine angiitis, primary (or idiopathic) thunderclap headache with reversible vasospasm, fatal vasospasm in migrainous infarc-

tion, drug induced cerebral vasculopathy, and CNS pseudovasculitis.^(7,9,10) Since then, reports of the condition have been accumulating rapidly. In spite of the unknown exact incidence, it has been postulated that RCVS is under-recognized and is a common cause of acute severe headache.⁽¹¹⁻¹⁴⁾

RCVS can occur spontaneously (idiopathic) or be secondary to a precipitating factor. The proportion of spontaneous cases has varied depending on the studied populations, from 37% in a French study⁽⁵⁾ to 96% in a Taiwanese cohort.⁽⁹⁾ Precipitating factors include postpartum state, migraine history and exposure to vasoactive substances, such as cannabis, cocaine, ecstasy, amphetamines, binge drinking, selective serotonin reuptake inhibitors, triptans, nasal decongestants, ergotamine tartrate, LSD (lysergic acid diethylamide), methergine, bromocriptine, nicotine patches, ginseng and caffeine.^(7,15,16) Other causes such as hypercalcemia, pheochromocytoma, exertion, and sexual activity also have been described to be related with this syndrome.^(7,13,17) The syndrome may occur after a few days of exposure or after several months of regular or irregular exposure in normal or excessive doses. Post-partum RCVS has been described to start in two-thirds of cases during the first week after delivery, usually after a normal pregnancy. In 50-70% of cases it is associated with the intake of vasoconstrictors, mostly ergots used to treat post-partum hemorrhage or to inhibit lactation.⁽⁷⁾

Despite recently accepted to be a common cause of acute severe headaches, RCVS is still commonly missed due to its recent description in literature. Furthermore, the degree of vasoconstriction may be too subtle to be definitely detected, or the detected lesion may be missed classified as vasculitis or other causes of vasculopathy.

RCVS is likely to be one of the most common vasculopathies that is confused with vasculitis. Vasculopathy is any disorder of blood vessels while vasculitis implies inflammation of blood vessels. Distinguishing RCVS from vasculitis seen in primary angiitis of the CNS (PACNS), which often requires brain biopsy for definite diagnosis, is very important for determining the appropriate treatment. Treatment for PACNS is much more aggressive, often including steroids and immunosuppressive agents with substantial adverse effects. By contrast with RCVS, PACNS usually has an insidious onset. Headaches are frequent but not of the thunderclap type and are followed by a stepwise deterioration. MRI scans are abnormal in most cases and show several small deep or superficial infarcts of different ages with or without white matter abnormalities. CSF analysis also shows an inflammatory reaction. Angiography is frequently normal in PACNS, whereas, by definition, it is always abnormal in RCVS (except when done early).⁽³⁾ Some features suggest PACNS, irregular eccentric and asymmetrical narrowing or several occlusions on angiograms and contrast enhancement of the vessel wall in MRI.^(18,19) When the clinicians remain unsure of the diagnosis, waiting for a few days might be best. RCVS should stabilize, improve quickly and resolution of vasoconstriction, whereas arterial irregularities in PACNS do not improve rapidly.⁽⁶⁾ Response to intra-arterial nimodipine has been proposed as a differential diagnosis test that remains to be validated; the drug immediately normalized arterial abnormalities in a few cases of RCVS, but is not expected to change the lesions in PACNS.^(20,21)

The diagnosis of RCVS does not require aggressive brain biopsy but can be suggested by the following triad:

1. Appropriate clinical history (acute severe or thunderclap headache)

2. Eventual resolution of angiographic vasoconstriction (within 3 months)

3. Absence of inflammatory/infection etiology.

The sensitivity and specificity of various imaging modalities for RCVS have not been established but cerebral angiogram is generally accepted to be the gold standard for the diagnosis. Since angiography is not a convenient tool for frequent follow-up, CTA or

MRA could be good alternative options. CTA and MRA also have been reported to be valuable tools for clinical evaluation and risk assessment in patients with RCVS.^(17,22,23)

The large amount of bony artifacts from the skull base interfering with the arteries around the Circle of Willis causes the more popularly used MRA than CTA in our institution. Furthermore, MRI, which is generally more sensitive to brain lesions than CT, can be performed in the same setting.

MRI in RCVS can be normal, but may also show small ischemic/infarcts lesions, especially in the posterior circulation and watershed areas.^(3,6,15)

The incidences of infarcts vary between 4-39%.^(3,6,24)

The MRI brain scan of this 38-year-old patient without underlying disease revealed multiple scatter foci of tiny high signal intensities on T2w and FLAIR within the watershed ischemic distributions of the subcortical white matter of both frontal and left parietal lobes. Although similar multiple scatter foci of high signal intensities are commonly seen in the elderly, as part of normal aging, other causes of small vessel disease, such as DM, HT, migraine, vascular dissection, anoxia or other non-specific causes of vasculopathy, should be of concern in younger patients, like in this case.

Vasoconstriction in RCVS is most common in large- and medium-sized vessels.⁽²⁵⁾ Although an MRA can demonstrate vasoconstriction in the proximal parts of the cerebral arteries, a normal MRA does not rule out the diagnosis. In a series of 44 RCVS patients, 6 had a normal MRA while with the cerebral angiography there were signs of vasoconstriction.⁽²⁶⁾ Vasoconstriction can persist for weeks after the resolution of the headaches⁽³⁾ but resolution of vasoconstriction is expected in all patients at repeat angiography within 3 months. In our patient, complete resolution of vasoconstriction was seen at 6 weeks; the patient recovered fully without any specific treatment. Follow-up MRA at 1 year, which was conducted in order to write this report, revealed no evidence of vasoconstriction.

The exact cause of RCVS is still unknown. The sympathetic nervous system may play a role in the pathogenesis of this headache since this headache has been reported to be associated with multiple factors elevating the sympathetic tone, such as adrenergic drugs and physical stress.⁽²⁷⁾ Furthermore, proximal parts of the intracranial vessels are also strongly innervated by sympathetic afferents, which modulate vascular tone.

RCVS and posterior reversible encephalopathy syndrome (PRES) are frequently associated. Reversible brain edema occurs about 8-38% of RCVS.^(3,16,28) Moreover, a multifocal cerebral vasoconstriction has been noted in more than 85% of patients with PRES whenever the investigation included angiography. This vasoconstriction was shown to be reversible on follow-up MRA.⁽³⁾ PRES can complicate toxæmia of pregnancy, immunosuppressive treatment after transplantation, chemotherapy, autoimmune diseases, hypertension and septic shock, all of which are associated with endothelial

damage or activation. It was thought to be caused by severe hypertension, leading to altered cerebral autoregulation with hyperperfusion and vasogenic edema. However, a quarter of the patients with PRES are normotensive. A more recent view is that endothelial dysfunction of any cause can affect the regulation of cerebral arterial tone and trigger vasoconstriction with subsequent hypoperfusion, and breakdown of the blood-brain barrier and vasogenic edema.^(3,7,29)

Intracranial hemorrhage, especially cortical subarachnoid hemorrhage (SAH), has been reported to accompany RCVS.^(26,28,30-32) Up to 34% of patients with RCVS developed intracranial hemorrhage⁽²⁸⁾ and the most common intracranial hemorrhage was tiny localized cortical subarachnoid hemorrhage, unilateral or bilateral, which was seen as much as 22-50% in patients with RCVS.^(28,31)

Vasoconstriction as a result of subarachnoid hemorrhage is well-known, but vasoconstriction as the cause of subarachnoid hemorrhage is rather difficult to believe without question. Ducros et al. hypothesized an interesting concept, in an opposite way to the others, that arterial abnormalities first involve small distal arteries and then progress toward medium-and large-sized vessels, which could explain the high rate of normal early angiogram (up to 33%). Moreover, marked vasoconstriction could persist for weeks after headache resolution, suggesting that vasoconstriction was not the direct cause of the headache.

Segmental vasodilatation is likely to play an important role in the initial stage of RCVS, triggering thunderclap headaches by abruptly stretching the vessel walls and causing hemorrhage by small vessel rupture or reperfusion injury. In the second stage, vasoconstriction of the second and first

segments of the major cerebral arteries becomes the major problem causing ischemia or mainly watershed infarction.^(3,23)

RCVS also has been recently included as a possible cause of spontaneous subarachnoid hemorrhage, especially for tiny localized cortical subarachnoid hemorrhage situated far from the Circle of Willis, which is usually easy to distinguish from aneurysmal subarachnoid hemorrhage. Besides RCVS, small convexity bleeding can occur in amyloid angiopathy.

A retrospective study suggested that RCVS appears to be a common cause of convexity subarachnoid hemorrhage in patients aged 60 years or younger, whereas amyloid angiopathy is frequent in those older than 60 years.⁽³³⁾

In spite of possible serious complications, the rate of permanent neurological disability is low.⁽¹⁴⁾ Most patients do well and recover completely without neurological sequelae, especially in the spontaneous cases.^(13,14,24) Migraine history, post-partum status and cannabis use have been observed to be more related with stroke and poor outcome.^(13,23) Recurrence of the syndrome is possible. The rate is unknown but is probably low.⁽³⁾

There is no established therapy in RCVS. Good outcomes have been reported with symptomatic treatment, the discontinuation of any possibly related substances or triggers, and rest for a few days to a few weeks according to the severity of the headaches.^(7,34) Benzodiazepine to relieve anxiety, which is common and could be an aggravating factor, is recommended in some institutions.⁽³⁾ In most cases, headaches and angiographic abnormalities resolve within days or weeks. Because of the similarities with post subarachnoid hemorrhage-related vasospasm, calcium channel blockers are

widely used in the treatment of RCVS. Nimodipine has been shown to terminate the headache within 48 hours in 63-84% of patients^(3,5,9,14,35,36), in spite of no outcome benefit over symptomatic alone in a large case series report.⁽⁶⁾ Short-term high dose glucocorticoids had been recommended because of radiological similarities with vasculitic disorders and experimental evidence that glucocorticoids reduce vasoconstriction.^(18,37) However, they have recently been shown to be an independent predictor of poor outcome and should be avoided.^(6,14) The use of intravenous magnesium sulfate in patients with post-partum RCVS also has been reported to produce good results.⁽²⁴⁾

Conclusions

RCVS is still under-recognized. The primary diagnostic dilemma is distinguishing RCVS from primary CNS arteritis and RCVS should be included in the differential diagnosis as a possible cause of tiny cortical subarachnoid hemorrhage. Complete resolution of vasoconstriction of cerebral arteries in 3 months without evidence of inflammatory/infection etiology should suggest the diagnosis.

Acknowledgments

Special thanks to Mr. Trevor T. Pearson for proof reading and editing assistance.

References

1. Call GK, Fleming MC, Sealfon S, Levine H, Kistler JP, Fisher CM. Reversible cerebral segmental vasoconstriction. *Stroke* 1988;19:1159-70.
2. Calabrese LH, Gragg LA, Furlan AJ. Benign angiopathy: a distinct subset of angiographically defined primary angiitis of the central nervous system. *J Rheumatol* 1993;20: 2046-50.

3. Ducros A. Reversible cerebral vasoconstriction syndrome. *Lancet Neurol* 2012;11:906-917.
4. Velez A, McKinney J. Reversible Cerebral Vasoconstriction Syndrome: A Review of Recent Research. *Current Neurology and Neuroscience Reports* 2012;13:1-5.
5. Ducros A, Boukobza M, Porcher R, Sarov M, Valade D, Bousser M. The clinical and radiological spectrum of reversible cerebral vasoconstriction syndrome: a prospective series of 67 patients. *Brain* 2007;130:3091-101.
6. Singhal A, Hajj-Ali R, Topcuoglu M, Fok J, Bena J, Yang D, et al. Reversible cerebral vasoconstriction syndromes: analysis of 139 cases. *Arch Neurol* 2011;68:1005-12.
7. Ducros A, Bousser MG. Reversible cerebral vasoconstriction syndrome. *Pract Neurol* 2009;9:256-67.
8. Calabrese LH, Dodick DW, Schwedt TJ, Singhal AB. Narrative Review: Reversible Cerebral Vasoconstriction Syndromes. *Annals of Internal Medicine* 2007;146:34-44.
9. Chen SP, Fuh JL, Lirng JF, Chang FC, Wang SJ. Recurrent primary thunderclap headache and benign CNS angiopathy: spectra of the same disorder? *Neurology* 2006;67:2164-9.
10. Chen SP, Fuh JL, Wang SJ. Reversible cerebral vasoconstriction syndrome: current and future perspectives. *Expert Rev Neurother* 2011;11:1265-76.
11. Chen S, Fuh J, Wang S. Reversible cerebral vasoconstriction syndrome: an under-recognized clinical emergency. *Ther Adv Neurol Disord* 2010;3:161-71.
12. Headache Classification Committee of the International Headache Society. The International Classification of Headache Disorders, 3rd edition (beta version). *Cephalalgia* 2013;33:629-808.
13. Cheng Y-C, Kuo K-H, Lai T-H. A common cause of sudden and thunderclap headaches: reversible cerebral vasoconstriction syndrome. *J Headache Pain* 2014;15:13.
14. Tan LH, Flower O. Reversible Cerebral Vasoconstriction Syndrome: An Important Cause of Acute Severe Headache. *Emergency Medicine International* 2012;2012:8.
15. Koopman K, Teune LK, ter Laan M, Uyttenboogaart M, Vroomen PC, De Keyser J, et al. An often unrecognized cause of thunderclap headache: reversible cerebral vasoconstriction syndrome. *J Headache Pain* 2008;9:389-91.
16. Hijikata Y, Watanabe H, Ito M, Yoneyama N, Atsuta N, Sobue G. Reversible cerebral vasoconstriction syndrome (RCVS) triggered by nicotine patches. *Rinsho Shinkeigaku* 2013;53:721-3.
17. Marder CP, Donohue MM, Weinstein JR, Fink KR. Multimodal Imaging of Reversible Cerebral Vasoconstriction Syndrome: A Series of 6 Cases. *American Journal of Neuroradiology* 2012;33:1403-11.
18. Hajj-Ali RA, Furlan A, Abou-Chebel A, Calabrese LH. Benign angiopathy of the central nervous system: Cohort of 16 patients with clinical course and long-term followup. *Arthritis Care & Research* 2002;47:662-9.
19. Mandell DM, Matouk CC, Farb RI, Krings T, Agid R, terBrugge K, et al. Vessel Wall MRI to Differentiate Between Reversible Cerebral Vasoconstriction Syndrome and Central Nervous System Vasculitis: Preliminary Results. *Stroke* 2012;43:860-2.
20. Elstner M, Linn J, Muller-Schunk S, Straube A. Reversible cerebral vasoconstriction syndrome: a complicated clinical course treated with intra-arterial application of nimodipine. *Cephalgia* 2009;29:677-82.
21. Linn J, Fesl G, Ottomeyer C, Straube A, Dichgans M, Bruckmann H, et al. Intra-arterial application of nimodipine in reversible cerebral vasoconstriction syndrome: a diagnostic tool in select cases? *Cephalgia* 2011;31:1074-81.
22. Chen SP, Fuh JL, Wang SJ, Chang FC, Lirng JF, Fang YC, et al. Magnetic resonance angiography in reversible cerebral vasoconstriction syndromes. *Ann Neurol* 2010;67:648-56.
23. Marder CP, Donohue MM, Weinstein JR, Fink KR. Multimodal imaging of reversible cerebral vasoconstriction syndrome: a series of 6 cases. *AJNR Am J Neuroradiol* 2012;33:1403-10.
24. Sattar A, Manousakis G, Jensen MB. Systematic review of reversible cerebral vasoconstriction syndrome. *Expert Rev Cardiovasc Ther* 2010;8:1417-21.
25. Saini M, Jeerakathil T, Butcher K. Reversible cerebral vasoconstriction syndrome. *Neurol India* 2009;57:63-5.
26. Ducros A, Boukobza M, Porcher R, Sarov M, Valade D, Bousser MG. The clinical and radiological spectrum of reversible cerebral vasoconstriction syndrome. A prospective series of 67 patients. *Brain* 2007;130:3091-101.
27. Lu SR, Liao YC, Fuh JL, Lirng JF, Wang SJ. Nimodipine for treatment of primary thunderclap headache. *Neurology* 2004;62:1414-6.

28. Ducros A, Fiedler U, Porcher R, Boukobza M, Staff C, Bousser MG. Hemorrhagic manifestations of reversible cerebral vasoconstriction syndrome: frequency, features, and risk factors. *Stroke* 2010;41:2505-11.
29. Bartynski WS, Boardman JF. Catheter angiography, MR angiography, and MR perfusion in posterior reversible encephalopathy syndrome. *AJNR Am J Neuroradiol* 2008;29:447-55.
30. Edlow B, Kasner S, Hurst R, Weigle J, Levine J. Reversible Cerebral Vasoconstriction Syndrome Associated with Subarachnoid Hemorrhage. *Neurocritical Care* 2007;7:203-10.
31. Muehlschlegel S, Kursun O, Topcuoglu MA, Fok J, Singhal AB. Differentiating reversible cerebral vasoconstriction syndrome with subarachnoid hemorrhage from other causes of subarachnoid hemorrhage. *JAMA Neurology* 2013;70:1254-60.
32. Ducros A, Boukobza M, Porcher R, Sarov M, Valade D, Bousser M-G. The clinical and radiological spectrum of reversible cerebral vasoconstriction syndrome. A prospective series of 67 patients. *Brain* 2007;130:3091-101.
33. Kumar S, Goddeau RP, Selim MH, Thomas A, Schlaug G, Alhazzani A, et al. Atraumatic convexal subarachnoid hemorrhage: Clinical presentation, imaging patterns, and etiologies. *Neurology* 2010;74:893-9.
34. Singhal A, Bernstein R. Postpartum angiopathy and other cerebral vasoconstriction syndromes. *Neurocritical Care* 2005;3:91-7.
35. Dodick D. Reversible Segmental Cerebral Vasoconstriction (Call-Fleming Syndrome): the Role of Calcium Antagonists. *Cephalgia* 2003;23:163-5.
36. Lu S-R, Liao Y-C, Fuh J-L, Lin J-F, Wang S-J. Nimodipine for treatment of primary thunderclap headache. *Neurology* 2004;62:1414-6.
37. Werring DJ. Reversible Cerebral Vasoconstriction Syndrome and Intracranial Hemorrhage: Some Answers, Many Questions. *Stroke* 2010;41:2455-6.



Kartagener's Syndrome: A Case Report in the Samutsakhon Hospital

**Luckana Girapongsa¹, Thanapat Puangpatch²,
Orawan Autravisitkul¹, Pariyanoot Deesuwun¹**

¹ Department of Radiology, Samutsakhon Hospital, Thailand.

² Department of Medicine, Samutsakhon Hospital, Samutsakhon, Thailand.

Abstract

Kartagener's syndrome is an autosomal recessive disorder.¹ It is characterized by the triad of situs inversus, bronchiectasis and sinusitis. Basic problem is defective movement of the cilia.³ Recognition in this condition keeps prevention for unnecessary investigation. We have presented a case of "Kartagener's syndrome" in the Samutsakhon hospital.

Keyword: Kartagener's syndrome, primary ciliary dyskinesia, situs inversus.

Introduction

Kartagener's syndrome is a rare autosomal recessive disorder syndrome with an estimated incidence about 1: 20,000- 30,000.² Male and female are effected equally.^{6,11}

Manes Kartagener, a pulmonologist in Zurich, described an unusual triad of situs inversus, bronchiectasis and sinusitis in four patients and became known as Kartagener's syndrome in 1933.⁸ Actually, it was firstly described in literature by Sievert in 1904 who reported the case of a 21-years-old man in whom the three elements of syndrome were presented.⁶ Our case was diagnosed as Kartagener's syndrome.

Case report

History

A 29 -years-old female presented with dyspnea for 3 hours. She asked for emergency medical service for taking her from home to the Samutsakorn hospital. Her past medical history showed that she was used to be treated as pulmonary TB from another hospital since many years.

The vital sign; T 36.5°C, PR 140/ min, RR 40 / min, BP 109/44 mmHg. The physical examination revealed crepitation and rhonchi at both lungs. The other physical examinations are within normal limit.

The CBC; Hemoglobin 9.7 g/ dl (anisocytosis 1+ and ovalocyte 1 +), WBC 15,800 cell / uL (neu-



Figure 1. The chest radiography revealed alveolar infiltration at RUL (arrow).
Bilateral bronchiectasis and dextro-cardia were seen.



Figure 2. CT of the chest (coronal view), there were left position of the liver and right position of the spleen / stomach. Dextrocardia was noted.

trophil 89.3%, lymphocyte 7.9%, monocyte 2.1%) and platelet count 753,000 cell/ μ L. His laboratory investigation including kidney and liver function test were within normal limited.

She performed the radiography of the chest. The chest study revealed alveolar infiltration at RUL with diffuse bronchiectasis at both lungs. Right side of the cardiac apex is noted.

Then she performed the computed tomography of the chest. The computed tomographic findings revealed right position of the cardiac apex / the anatomic left atrium / left ventricle, the right-sided of the aortic knob including descending aorta, the right upper quadrant position of the stomach / spleen, the left upper quadrant position of the liver / gallbladder, left -sided trilobed lung and right-sided bilobed lung which were mirror-image to situs solitus representing situs inversus totalis.

There were multi-focal alveolar infiltrations with nodules at the apico-posterior segment of RUL, the superior segment / the anterior basal segment / lateral basal segment of RLL with some tree-in bud appearance; representing multi-focal pneumonia. There were cystic bronchiectasis with partial atelectasis at LUL and the medial basal segment of LLL.

Additional radiography of the para-nasal sinuses was also performed. The study revealed opacification of the right maxillary sinus and mucoperiosteal thickening of the left maxillary sinus representing sinusitis.

Thus, Kartagener's syndrome was diagnosed clinically. She was admitted and treated with intravenous antibiotics and bronchodilators. The majority of symptoms improved and was discharged with oral antibiotics.



Figure 3. CT of the chest (axial view), there were alveolar infiltration at posterior segment of RUL and the superior segment of RLL. Right side aortic arch and descending aorta were noted.

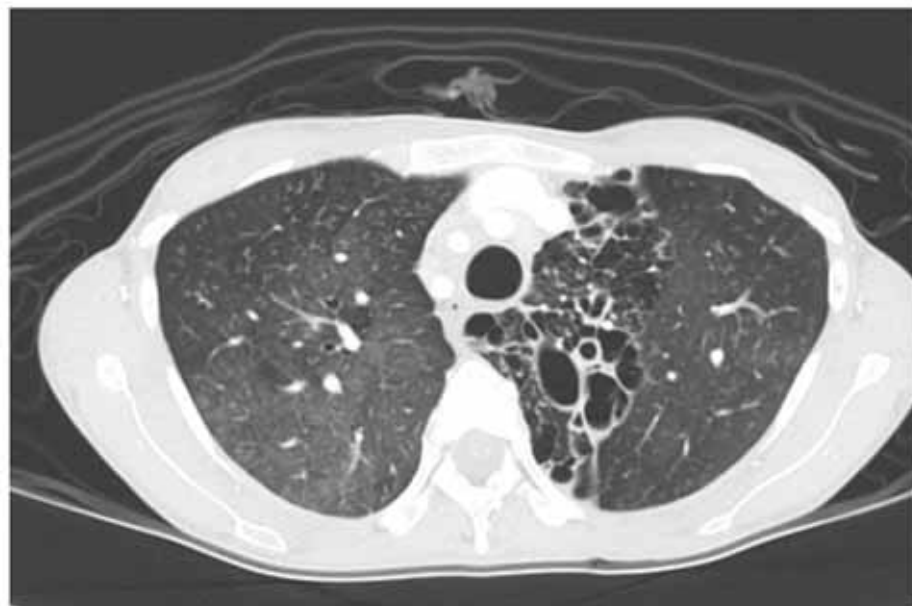


Figure 4. CT of the chest (axial view and lung window) There were cystic bronchiectasis at LUL.



Figure 5. The paranasal sinuses study were opacification of the right maxillary sinus and mucoperiosteal thickening of the left maxillary sinus.

Discussion

Kartagener's syndrome is recognized as the clinical variant of the primary ciliary dyskinesia (PCD) and occurs about 50 % of PCD. The primary ciliary dyskinesia is autosomal recessive disorder characterized by inefficient or absent mucociliary clearance.⁵

The pathology is based on the ultra structural defects of the cilia. Cilia can be structurally divided into subcomponents that include a basal body, transitional zone, axoneme, ciliary membrane and ciliary tip.¹⁰ Cilia can either be motile (in air ways, brain, fallopian tube, sperm, embryonic node) or non-motile (in kidney tubule, bile duct, pancreatic duct, eye, ear, bone cartilage and fibroblast).¹⁰ Normally in most motile cilia, the core or axoneme of the cilia consists of a 9+2 microtubule structure with a ring of nine microtubules doublets surrounding a central pair of single microtubule. The nine microtubule doublets are studded with dynein arms that contain adenosine triphosphatase and act as molecular motor to effect the sliding of the peripheral micro-

tubule pairs relative to one another.^{2,5} The 9+0 axonemes that are found in most of non-motile cilia lack the two central microtubules and lack of dynein arms.¹⁰

Most of the disease results from mutations identified to date involve two genes such as genes encoding for the dynein axonal intermediate chain 1 (DNAL1) and the dynein axonemal heavy chain 5 (DNAH 5).⁵ Since dynein is one of key intracellular molecular motors, the absence of dynein arms is responsible for the impaired motility of the cilia and sperm.⁷

The clinical features depend on the involved systems. In the upper respiratory tract, rhino-sinusitis and otitis media are cardinal features of disease and responsible for much of the morbidity associated with PCD in early childhood. Nasal congestion and rhinorhea are very common.⁵ In the lower respiratory tract, most patients report a chronic and productive cough as a prominent symptom because cough compensates for lack of effective mucociliary clearance and impaired muco-ciliary clearance

lead to recurrent episode of pneumonia or bronchitis.⁵ Bronchiectasis does not present at birth but may develop early sometimes as early as in childhood.² Bronchiectasis is an acquired condition. Involved bronchi are dilated, inflamed and easily collapsible resulting in airflow obstruction and impaired clearance of secretion. Insufficient clearance of secretion causes colonization and infection with pathogen organisms contributing to common purulent expectoration in patients with bronchiectasis resulting in further bronchial injury and vicious cycle of bronchial damage, bronchial dilatation, impaired clearance of secretions, recurrent infection and more bronchial damage.⁶ The most common respiratory pathogens are *Haeophilus influenza*, *Streptococcus pneumonia*.⁴

Laterality defects, cilia on the embryonic node play critical role in left-right patterning during early development.⁵ *Situs inversus totalis*, heterotaxy with or without congenital cardiovascular abnormality are observed. In other organ, such as in the genito-urinary tract, male fertility is common and reflects defects in sperm tail axonems. In the central nervous systems, hypothetically due to impaired CSF flow secondary to dysfunction motile cilia that line the ventricular ependymal cells may be linked with hydrocephalus. In the eye, some may develop with retinitis pigmentosa.⁵

Diagnosis of Kartagener's syndrome is usually achieved by clinical features and radiological images.⁶ Other investigations are also helpful such as quantitative decreased in number of dynein arm and subjective abnormality in other ciliary components on electrom microscopy.⁹

Treatment is aimed to relieved symptoms and prevents complications. Early recognition of the disease and prompt antibiotic treatment are the key to

minimize the irreversible lung damage. Physiotherapy with postural drainage and cessation of smoking are also important.⁴ Coughing should not be suppressed since it acts as a substitute for mucociliary clearance.⁴ Prophylactic measures such as appropriate immunization particular influenza vaccines and pneumococcal vaccine are mainstay.⁶

The prognosis is generally considered favorable and life expectancy is usually normal.^{6,8} There will have progressively greater impact in health in the second half of life producing significant morbidity and restriction of life style. But there is a clinical case demonstrated a non-progressive course of the bronchiectasis indicates that is a complex inter-relationship between genetic variation and an appropriate non-specific treatment.⁸ Early diagnosis and hence earlier treatment may improve symptoms and the impact of the condition.⁷

Conclusion

Kartagener's syndrome is the clinical variant of the primary ciliary dyskinesia (PCD) and consists of *situs inversus*, bronchiectasis and sinusitis. Basic pathology is defect of the cilia causing impair mucociliary clearance. Prognosis is good. Early recognition in this disease can improve symptoms and may prevent progressive course.

References

1. Kartagener M, Horlancher A, *Situs vuscerum inversus* and polyposisnais in eniem Falle familliaerer Brouchiectasin . Beitr Klin Tub 1936;87:331-3.
2. Bivaliya M, Sadatia V, Vekariya R, Jani D. Kartagener's syndrome. A Rare Case. NJIRM 2012;3(4):139-41.
3. Mahsud I, Din S. Kartagener 's syndrome. Glomal Journal of Medical Science 2006;4(2):79-81.
4. Dabni AS, Chaudhri SR, Thorat PB, Pandya HB, Shah MC, Meswani UN, Vaghela PR. Kartagener's syndrome:

A Triad of Bronchiectasis, Situs inversus and Chronic Sinusitis . JIACM 2005;6(3):241-3.

5. Masumi Akita. Primary Ciliary Dyskinesia/Kartagener Syndrome - Clinical and Genetic Aspects. Approaches to Bronchitis, 2011. (cited 2014 Jan 20) InTech, Available from:<http://www.intechopen.com/books/approaches-to-bronchitis/primary-ciliary-dyskinesia-kartagener-syndrome-clinical-and-genetic-aspect>.

6. Casonova MS, Tuji FM, Yoo HJ, Hainter-Neto F. Kartagener 's syndrome. Dentmaxillofac Radiology 2006;35(5): 386-9.

7. McManus IC, Mitchison HM, Chung EM, Stubbing GF, Martin N. Primary ciliary dyskinesia (Siewert's / Kartagener's syndrome): BMC pulmonary medicine 2003;3:4.

8. Serapinas D, Staikuniene J, Barkauskiene D, Jackute J, Sakalauskas R. An unusual regression of the symptoms of Kartagener's syndrome. Arch Bronconeumol 2013;49(1): 28-30.

9. Teknos TN, Metson R, Chasse T, Belecia G, Dickersin GR. New development in the diagnosis of Kartagener's syndrome. Otolaryngol Head Neck Surg 1977;116(1): 68-74.

10. Fliegauf M, Benzing T, Omran H. When cilia go bad: cilia defects and ciliopathies. Nat Rev Mol Cell Bio 2007; 8(11):880-91.

11. Homma S, Kawabata M, Kishi K, Tsuboi E, Narui K, Saiki S et al. Bronchiolitis in Kartagener 's syndrome. Eur Respir J 1999;14:1332-9.



The Committee of Royal College of Radiologists of Thailand and Radiological Society of Thailand

Apr 2013-Mar 2015

President:	Jiraporn	Laothamatas
Vice-president:	Wilaiporn	Bhothisuwan
Secretariat General:	Chamaree	Chuapetcharasopon
Vice-secretary General:	Nitra	Piyavisetpat
Treasurer:	Krisdee	Prabhassawat
Academic president:	Anchalee	Churojana
House Master & Social Programme:	Chantima	Rongviriyapanich
Secretary:	Alongkorn	Kiatdilokrath
Registrar:	Sutipong	Jongjirasiri
Committee:	Poonsook	Jitnuson
	Pongdej	Pongsuwan
	Sukalaya	Lerdlum
	Panruethai	Trinavarat

The Journal of the Royal College of Radiologists & Radiological Society of Thailand

(2013 - 2015)

Editor:	Anchalee Churojana	
Co-Editor:	Jiraporn Laothamatas	
Editorial board:	Walailak Chaiyasoot Wanvarang Teerasamit Numphung Numkarunarunrote Bundit Chaopathomkul Sukalaya Lerdlum Kaan Tangtiang Wanabee Meennuch Charoonsak Somboonporn Jiraporn Srinakarin Jaturat Kanpittaya Wiwatana Tanomkiat Nantaka Kiranantawat Sutipong Jongjirasiri Pakorn Jiarakongmun Samart Rajchadara Janjira Petsuksiri	Chantima Rongviriyapanich Nitra Piyavisetpat Monravee Tumkosit Panruethai Trinavarat Pisit Wattanaruangkowit Wichet Piyawang Anuchit Ruamthanthong Kamolwan Jungmeechoke Jureerat Thammaroj Juntima Euathrongchit Siriporn Hirunpat Bussanee Wibulpolprasert Rathachai Kaewlai Ratana Kuntiranon Mantana Dhanachai Kobkun Muangsomboon
Emeritus Editors:	Poonsook Jitnuson	

Office:

The Royal college of Radiologists & Radiological society of Thailand. 9th Floor,
Royal Golden Jubilee Building, 2 Soi Soonvijai, Petchburi Road, Bangkok, 10320
Tel 02-716-5963, Fax 02-716-5964
E-mail pusjeckchon@hotmail.com.

Instructions for Authors

1. The Asean Journal of Radiology publishes the papers on Radiological Sciences, such as research work, reviews articles case reports, innovations in medical Sciences related to all branches of Radiology, and letters to the editor. The aforementioned materials can be written in English only.
2. The authors have to submit 2 copies of the manuscript and a CD :to Assoc. Prof. Sirintara Singhara Na Ayudya, Department of Radiology, Faculty of medicine, Ramathibodi hospital 270, Rama VI Road, Toong Phayathai, Ratchathewi, Bangkok, 10400. Tel 02-2011259#110, Fax 02-2011297, E-mail Sirintarapongpech2@hotmail.com
3. The original copy to be submitted must be typed in a double space on one of the page 8.5"x11" (A4) paper.
4. The format of the article must include:
 - a. Title page and address of the author (s)
 - b. Abstract (Objective, Methods, Results and conclusion)
 - c. Introduction
 - d. Material and Method
 - e. Results and discussion
 - f. Acknowledgment (if any)
 - g. References (Follow the Vancouver style)
5. We will provide 5 copies of reprints for the author (s) an article for publication in the Asean Journal.
6. The illustrations and table must be clearly prepared with legends in English as they are the art works to be reproduced
7. The authors are responsible for the contents of the article as to its facts and findings.
8. Ethics

Paper reporting studies which might be interpreted as human experimentation (e.g. controlled trials) should conform to the standards of the Declaration of Helsinki (see British Medical Journal 1964;2:177) and should indicate that, approval that such studies may proceed, has been granted by the local or hospital Ethics Committee.

When reporting experiments on animal indicate whether the institution's or the National Research Council's guide for, or any national law on, the care and use of laboratory animals was followed.